2012

Design and Evaluation of a Marine Scrubber System

Louise S. Ayre
West Virginia University

Design and Evaluation of a Marine Scrubber System

By Louise S. Ayre

Thesis submitted to the College of Engineering and Mineral Resources at West Virginia University in partial fulfillment of the requirements for the degree of

Master of Science
in
Mechanical Engineering

Nigel Clark, Ph.D., Chair
Gregory Thompson, Ph.D.
Scott Wayne, Ph.D.

Mechanical and Aerospace Engineering Department
Morgantown, West Virginia
2012

Keywords: Diesel, Marine, NO_X, Scrubber, Absorption

Abstract

West Virginia University

Louise S. Ayre

Increasingly stringent oxides of nitrogen (NO_X) emissions regulations for diesel marine engines are resulting in the development of newer engines with inherent NO_X emissions reduction technologies. With typical useful service lives over 20 years, older diesel marine engines are producing disproportionate amounts of NO_X emissions when compared with their newer counterparts. The development of retrofit exhaust aftertreatment technologies would therefore aid in reducing the total NO_X emissions from these engines.

A marine scrubber system for the reduction of NO_X emissions from diesel marine engines was designed, constructed, and evaluated. This work focused on gathering data for the design of a marine scrubber system specifically for use with marine harbor craft. The operation of the marine scrubber system was based on and designed using NO_X absorption theory. The system consisted of a continuously regenerating diesel particulate filter and diesel oxidation catalyst for oxidation of nitric oxide to nitrogen dioxide, a heat exchanger for exhaust gas temperature reduction, a scrubber unit for NO_X gas absorption, and a liquor pump for liquor recirculation.

The system was tested with a 1992 Mack E7 engine over two test cycles, a High Flow cycle and Low Flow cycle. The High Flow cycle was used to represent marine harbor craft operation. Over this cycle the system was able to reduce engine NO_X emissions by an average of 41.2%. The Low Flow cycle was developed to investigate the operating parameters of the scrubber unit. Over the Low Flow cycle the system was able to reduce engine NO_X emissions by an average of 59.9%. The collection of data from this system facilitated parameter estimation and therefore future optimization of marine scrubber system design and control decisions.

Acknowledgements

I would like to thank my advisor Dr. Nigel Clark for hiring me as a graduate student, the wise words of wisdom, encouragement, and support. You have been an excellent advisor. I truly appreciate this learning opportunity; I feel that it has helped me grow into a better engineer. I would like to thank my other committee members Dr. Scott Wayne and Dr. Gregory Thompson for their time and input. I would like to thank the other graduate student who worked on the Scrubber project with me, Derek Johnson. Thank you for your hard work and answers to countless questions. I would like to thank David McKain for his assistance and helping to keep the Scrubber project on track.

I would like to thank everyone at MJ Bradley & Associates for supporting this research. Thank you in particular to Thomas Balon and Paul Moynihan for your work and guidance. I would like to thank the State of Texas, Texas Environmental Research Consortium, and Texas Commission on Environmental Quality for funding and supporting the Scrubber project.

I would like to thank everyone who helped with the Scrubber project at the WVU Westover Laboratory. Thank you Chris Beers, Ron Jarrett, and Chris Rowe for all of the help. You were always happy to lend a hand whenever I needed it. I would like to thank Jason England for his assistance during fabrication and testing. The time and effort that you put into this project was greatly appreciated.

I would like to thank the people at the EERL who helped with this project. Thank you Richard Atkinson for your witty insight and technical advice. Thank you Brad Ralston for your assistance during testing. Thank you Zac Luzader all of your technical assistance.

I would like to thank my family for all of the support and long-distance advice. I would like to thank James Perry and Nathan Music. Your friendship has made my time at WVU fun and enjoyable. I would like to thank Toby Radcliff for always understanding and for his untiring support. You keep me focused on my goals and make me smile every day.

Table of Contents

Table of Tables

Table of Figures

Nomenclature and Abbreviations

[A*]	Liquid Phase Saturation Concentration of the Solute Gas (mol/L)
$[NO_X]$	NO_X concentration recorded during the test (ppm)
$[NO_X]_{adj}$	Adjusted NO_X concentration (ppm)
a_p	Area of packing (m^2/m^3)
atm	Atmosphere
CO	Carbon monoxide
CO_2	Carbon dioxide
cS	Centistokes
C_S	C-factor, given by Equation 5.6
d	Diameter of packing (m)
D	Diffusivity (m^2/s)
F_p	Packing factor (m^{-1})
g	Acceleration due to gravity (m/s^2)
g	Gram
G_m	Gas mass flow rate (kg/s)
G_{op}	Volumetric gas flow rate per unit area (m/s)
H	Enthalpy (J/kg)
H1	Scrubber packed bed height 1 (0.864m)
H2	Scrubber packed bed height 2 (1.804m)
H3	Scrubber packed bed height 3 (2.794m)
Ha	Hatta number (-)
HC	Hydrocarbons
H_L	Height of one transfer unit based on liquid phase resistance
hp	Horsepower
h_{PB}	Required packed bed for desired NO_X reduction (m)
J	Joule
K	Kelvin
k_1	First order rate constant (s^{-1})
k_2	Second order rate constant (m^3.kmol/s)
k_G	Gas side mass transfer coefficient (kmol/m^2.s.kPa)
K_G	Overall mass transfer resistance based on the liquid phase (kmol/s.m^3)
K_{G2}	Gas phase equilibrium constant for N_2O_4 (kN/m^2)
K_{G3}	Gas phase equilibrium constant for N_2O_3 (kN/m^2)

k_H	Henry's Law Coefficient (m^3Pa/kmol)
$k_{H,AvgBase}$	baseline NO_X humidity correction factor for a specific mode and test (-)
$k_{H,MT}$	NO_X humidity correction factor specific to a test and mode (-)
k_L	Liquid side mass transfer coefficient (kmol/m^2.s.kPa)
K_L	Overall mass transfer resistance based on the gas phase (kmol/s.m^3)
kW	Kilowatt
l	Liquid hold up in the scrubber per unit volume of packing (-)
L	Liter
L	Superficial liquid velocity (m/s)
Liquor	Liquid stream that circulates through a scrubber
L_m	Liquor mass flow rate (kg/s)
L_{min}	Minimum liquid wetting rate (m^3/h.m^2)
LNT	Lean NO_X Trap
m	Meter
M	Molar concentration in the liquid phase (mol/L)
mmt	Million metric tonne
mol	Mole
n	Number of iterations completed by Simulink model
N_A	The rate of absorption of species A
NAAQS	National Ambient Air Quality Standards
nm	Nanometer
NO	Nitric oxide
NO_2	Nitrogen dioxide
NO_X	Oxides of nitrogen
OKP	Overall kinetic parameter (kmol/m^2.s.kPa)
OxR	Oxidation ratio (%)
p	Pressure(kPa)
P^*	Effective partial pressure (kPa)
Pa	Pascal
p_i	Partial pressure of gas species i (kPa)
PM	Particulate matter
P_m	Power consumption per unit mass of gas
ppm	Parts per million
R	Ideal gas constant (J/mol.K)
$\overline{R_A}$	Average rate of absorption of species A (kmol/m^2.s)

R_i	Rate of absorption of species i (kmol/m^2.s)
Re_L	Reynolds number liquid phase (-)
RPM	Revolutions per minute
s	Second
Sc_G	Schmidt number for the gas phase (-)
Sc_L	Schmidt number for the liquid phase (-)
SCR	Selective Catalytic Reduction
SO_X	Oxides of sulfur
T	Temperature (K)
U.S. EPA	United States Environmental Protection Agency
V	Superficial velocity (m/s)
X	Mole fraction of NO_X in the liquid phase (-)
Y	Mole fraction of NO_X in the gas phase (-)
γ	Y-axis value of the generalized Eckert pressure drop correlation
δ	Film thickness parameter
E	Void fraction of the packing (-)
μ	Viscosity (Pa.s)
ν	Kinematic viscosity (cS)
ρ	Density (kg/m^3)
φ	Controlling mechanism ratio

Superscripts

*	At flooding
$\ominus$	Reference parameter
phys	Considering physical absorption only, (i.e. no chemical reactions)

Subscripts

1	Scrubber inlet
2	Scrubber exit
A	Solute species A
b	Composition in bulk of phase
e	At equilibrium
G	Gas
g	Gas phase
i	Gas phase species

L	Liquid
l	Liquid phase
R	Reaction

1 Introduction

Diesel engines are well known for their longevity, high torque output, and reliability. They are therefore used for a wide variety of applications, including both on-road and off-road applications. Diesel engines are also more efficient than gasoline engines of a similar power rating[(1)]. A major disadvantage of diesel engines is that the control of their oxides of nitrogen (NO_X) and particulate matter (PM) emissions is more difficult than controlling those of similarly sized spark ignited engines[(2)].

With typical useful service lives over 20 years it is becoming increasingly apparent that older diesel marine engines are contributing disproportionate amounts of NO_X emissions when compared with newer engines that have been developed with inherent NO_X reduction technologies[(3)]. NO_X emissions regulations are becoming more stringent for both older and newer engines as these gases have negative environmental and health impacts.

2 Objective

The objective of this work was to assemble and utilize existing theory to design, construct, and evaluate a wet scrubber system that reduces NO_X emissions from diesel marine engines by more than 40% over a test cycle that is representative of diesel marine engine operation. This work had a specific focus on marine harbor craft. Limited real-world data has been published on the application of wet scrubbers to large applications, like the treatment of diesel marine engine emissions. The collection of data from a wet scrubber fed with diesel exhaust gas facilitated parameter estimation and will therefore aid in the future optimization of scrubber system design and control decisions.

3 Literature Review

3.1 Diesel Engine Emissions

The combustion process of diesel engines produces emissions that are harmful to the environment and contribute to human health problems; particularly cancer development and respiratory issues. These emissions arise from fuel impurities, nonstoichiometric combustion, high in-cylinder temperatures, and the dissociation of diatomic nitrogen. Diesel emissions species that exist in significant quantities in the exhaust and are considered to be harmful or contribute to climate change are: carbon dioxide (CO_2), carbon monoxide (CO), PM, hydrocarbons (HC), and NO_X. These emissions are considered to be primary pollutants as they are exhausted directly to the atmosphere[4].

3.1.1 Carbon Dioxide Emissions

Carbon dioxide is produced in the combustion of any hydrocarbon fuel and is a major component of diesel exhaust. Carbon dioxide emissions are considered by the United States Environmental Protection agency (U.S. EPA) to be likely contributing to climate change, they are therefore referred to as greenhouse gas emissions. In the upper atmosphere it behaves as a thermal radiation shield. It is able to raise the temperature of the earth by reducing the amount of thermal energy that escapes the earth's atmosphere[1]. Diesel engines produce lower levels of carbon dioxide emissions than gasoline engines of a similar size as they inherently use less fuel[2]. Reducing the amount of CO_2 produced during combustion is best achieved by increasing the thermal efficiency of an engine[1].

3.1.2 Carbon Monoxide Emissions

Carbon monoxide is a colorless gas that is without odor or taste. Above concentrations of 1200 ppm it is highly toxic to humans although it is still dangerous below this concentration, especially with prolonged exposure[5]. Carbon monoxide is generated by a diesel engine in a locally fuel-rich region of the combustion chamber; when there is not enough oxygen present to form CO_2 with all of the carbon atoms present. As diesel engines operate on a lean basis, their CO emissions are very low compared with spark ignited engines that run stoichiometrically[1].

3.1.3 Particulate Matter Emissions

Particulate emissions are carbon clusters or particles present in diesel exhaust. The size of these clusters vary across a broad range, although they typically range in size from 10 to 80 nm[1]. The surfaces of these carbon clusters may have HC and other fuel trace components adsorbed onto them. Soot in diesel exhaust is generated by fuel-rich zones present in the combustion cylinder where there is not enough oxygen present to convert the carbon in the fuel to CO_2.

About 75% of the particulate matter emissions come from the incomplete combustion of fuel and account for 0.2-0.5% of the fuel consumed. The remaining particulate matter emissions are generated from lubricating oil vaporizing and reacting during the combustion process[1].

Reducing particulate matter emissions can be achieved by controlling the engine operating conditions however this can have a negative impact on the level of other emissions generated. Particulate emissions may be reduced by increasing the time of combustion by altering the timing control and/or combustion chamber design. This allows for the soot to become better mixed with the oxygen and consequently reacts to form CO_2. This strategy, however, increases the amount of NO_X produced as the extended combustion creates higher in-cylinder temperatures which favor NO_X production. Increasing the fuel injection pressure can reduce PM and HC emissions as the fuel droplet size is reduced; although this increases in-cylinder temperatures and therefore the NO_X emissions. Generally a trade-off exists between generating PM and NO_X emissions. Often engine design and control alone cannot reduce PM emissions to acceptable levels and exhaust after treatment is required[1].

3.1.4 Hydrocarbon Emissions

Diesel engines have a high combustion efficiency of about 98%. Their HC emissions are about 25% that of gasoline engines. HC emissions occur from the incomplete combustion of fuel. This may arise from under-mixing where local areas within the combustion chamber that are too rich and do not have access to enough oxygen or areas that are too lean to combust completely. Areas that are too cool (e.g. near the cylinder wall, 'quench zone') will not combust completely. Over-mixing in the combustion chamber will also cause incomplete combustion as some of the fuel will mix with gas that has already been burnt. Deposits and oil films on the combustion chamber walls and crevice volumes also contribute to HC emissions in diesel engines[1].

3.1.5 Oxides of Nitrogen Emissions

In the environment, oxides of nitrogen exist in a number of different forms: NO, NO_2, NO_3, N_2O, N_2O_3, N_2O_4, and N_2O_5. NO_X gas reacts with ozone in the atmosphere to form photochemical smog[1,4]. Typically, more than 90% of NO_X emissions from diesel engines are nitric oxide (NO). This gas is immediately dangerous to humans above concentrations of 100 ppm. The majority of the remaining NO_X is comprised of nitrogen dioxide (NO_2) which is immediately dangerous to humans above 20 ppm. These emissions are particularly undesirable and therefore highly regulated. NO_X formation occurs from diatomic nitrogen in the intake air (or sometimes from the nitrogen present in the fuel) disassociating at high temperatures and reacting with oxygen or hydroxide. Temperature is the biggest influencing factor of NO_X production; significant levels of NO_X are generated above combustion temperatures of 2500 K. Other factors that influence NO_X generation are combustion time, pressure, and the air-to-fuel ratio. Extended combustion times generally create higher temperatures and thus more NO_X emissions.

Increasing the air-to-fuel ratio beyond the stoichiometric ratio provides excess oxygen for the nitrogen to react with, increasing NO_X emissions[(1)].

3.2 NO_X Production by Diesel Marine Engines

The main objective of this research was to reduce the amount of NO_X emissions from diesel marine engines, specifically harbor craft. Accordingly, NO_X production from these engines will be addressed in this section. Global NO_X emissions have increased over the past 20 years. In spite of NO_X control technologies improving over this time, the number of in-use engines and NO_X sources (like power stations) has increased. Aviation and shipping engines represent some of the most significant contributors to global NO_X emissions inventories, currently the quantity of these emissions are increasing[(6)].

Total NO_X emissions produced within the United States is currently decreasing as a result of increasingly stringent emissions regulations. It was estimated that total NO_X emissions produced by humans within the United States was 22.825 million metric tonnes (mmt) in 1990 and decreased to 17.032 mmt in 2005[(epa 1)]. In 2001 NO_X emissions produced by all mobile sources was estimated to be 11.757 mmt, 6% of which was estimated to come from marine sources. In 2030 NO_X emissions from mobile sources are expected to decrease to 5.452 mmt, of which NO_X emissions from marine sources are expected to represent 12%[(10)]. Global NO_X emissions from diesel marine engines may be separated by vessel type, this data is presented in Table 3.1 for the year of 1996. Category 2 engines that typically propel harbor craft vessels are estimated to contribute to 27% of the total NO_X emissions produced by commercial marine engines[(7)].

Table 3.1: Global NO_X Production by Vessel Type[(8)]

Vessel Type	Annual Global NO_x Production (mmt)
Bulk Carrier	2.36
Container	1.48
General Cargo	1.61
Liquid/Chemical/Oil Tanker	2.37
Passenger	0.26
Refrigerated Cargo	0.24
Roll-on/Roll-off	0.60

3.3 Emissions Control Standards

Increasing social awareness of the environment creates pressure for more stringent emissions standards to be enacted. As the global population increases so does the number of in-use engines that generate harmful emissions. Out of necessity emissions standards therefore become more stringent with time[(1)]. The United States Environmental Protection Agency (U.S. EPA) first began to regulate engine emissions in the late 1960's, by introducing standards for light-duty passenger vehicles. The first non-road heavy duty diesel emissions standards were introduced relatively recently in 1996[(9)].

The U.S. EPA regulates the emissions from diesel marine engines. These regulations are set according to the National Ambient Air Quality Standards (NAAQS) and cover PM, NO_X, SO_X, CO, ozone, and lead[(10)]. Lead and SO_X emissions from diesel marine harbor craft are reduced by mandating the use of lead free and low sulfur diesel fuel. The formation of ground level ozone caused by diesel marine harbor craft is reduced by regulation NO_X and HC emissions as these species react to from ground level ozone. New regulations only apply to new engines or remanufactured engines above 600 kW (800 hp). The most recent and stringent regulations for diesel marine engines to be introduced by the EPA are the Tier 3 and 4 emissions standards. For Category 2 engines, these standards will be phased in over the years 2013 through 2017 and are summarized in Table 3.2 and Table 3.3[(11)].

Table 3.2: Tier 3 Emissions Standards for Category 2 Engines[(11)]

Power (P) [hp]	Displacement (D) [liter/cylinder]	NOx+HC† [g/bhp-hr]	PM [g/bhp-hr]	Date
P < 4962	7 ≤ D < 15	4.62	0.10	2013
	15 ≤ D < 20	5.22	0.20[a]	2014
	20 ≤ D < 25	7.31	0.20	2014
	25 ≤ D < 30	8.20	0.20	2014

† Tier 3 NO_X+HC standards do not apply to 2682-4962 hp engines.
a - 0.25 g/bhp-hr for engines below 4425 hp.

Table 3.3: Tier 4 Emissions Standards for Category 2 Engines[11]

Power (P) [hp]	NOx [g/bhp-hr]	HC [g/bhp-hr]	PM [g/bhp-hr]	Date
P ≥ 4962	1.34	0.14	0.09[a]	2014[c]
	1.34	0.14	0.04	2016[b,c]
2683 ≤ P < 4962	1.34	0.14	0.03	2014[c,d]
1879 ≤ P < 2683	1.34	0.14	0.03	2016[c]
806 ≤ P < 1879	1.34	0.14	0.03	2017[d]

a - 0.19 g/bhp-hr for engines with 15-30 liter/cylinder displacement.

b - Optional compliance start dates can be used within these model years.

c - Option for Cat. 2: Tier 3 PM/NO_X+HC at 0.10/5.8 g/bhp-hr in 2012, and Tier 4 in 2015.

d - The Tier 3 PM standards continue to apply for these engines in model years 2014 and 2015 only.

3.4 Emissions Control Technologies

As NO_X emissions continue to rise, the need for control technologies becomes more apparent[4]. Harbor craft engines are often in use for more than 20 years. Considering that many engines currently being used today were produced at a time when there were no marine engine emissions regulations, retrofitting them with aftertreatment technologies has the potential to reduce NO_X emissions significantly. Major current exhaust aftertreatment options include lean NO_X traps (LNT), selective NO_X recirculation, selective catalytic reduction (SCR), hydrocarbon selective catalytic reduction, and wet NO_X scrubbers. Researchers of these technologies often find that reducing NO_X emissions by 20% is easily achieved but difficulty is experienced when attempting NO_X reduction above 50%.

There are three emissions control strategies available for diesel engines: fuel technologies, engine design techniques, and exhaust gas aftertreatment[2]. Exhaust aftertreatment technologies are necessary as it is currently not possible to produce engines and fuels that are able to meet current emission standards[1].

Researchers do not regard NO_X emissions reduction as a standalone issue; system integration for the reduction of multiple emissions species is often investigated. This is especially true for NO_X and PM emissions as their reduction often requires opposing strategies. Currently, some on-road engines use multiple technologies like LNTs or SCR with particulate traps to reduce both NO_X and PM emissions. It is expected that in the future marine emissions control will closely follow that of the on-road diesel engines. At present, SCR is the most popular control technology for on-road NO_X emissions[4].

3.5 Wet Scrubber Systems

Wet scrubber systems hold promise for diesel marine applications as water surrounding the vessel may be used as a cooling agent, they operate independently of the engine, and require a limited amount of input chemicals. Flue gas scrubbers have been used since 1935. They are primarily used to remove SO_X emissions from the flue gas and can have SO_X removal efficiencies of up to 98%[12]. Wet scrubber systems have been used to reduce NO_X emissions from stationary applications like chemical plants and power stations for decades. NO_X scrubber units consist of a packed tower, where a liquid stream enters through the top and contacts with a gas stream that flows counter currently. The liquid stream is referred to as the liquor. The packing in the tower is designed to maximize the interfacial surface area between the liquor and gas for NO_X absorption. When only water is used as the liquor for NO_X absorption two by-products are produced, nitric and nitrous acid[13].

Recently wet scrubber system technology has been applied to mobile applications. Krystallon[14] in collaboration with BP Marine, developed a wet scrubber for use with ocean going vessels. In-use testing demonstrated that 98% of the SO_X emissions can be reduced by this system. Due to the lower solubility of NO_X gas, the NO_X reduction capability of this scrubber is significantly lower[14]. The use of seawater and its electrolytes in the liquor of wet scrubber systems for marine applications has also been investigated. Acidic seawater oxidizes NO and enhances the NO_2 to NO ratio, thereby increasing overall NO_X absorption as NO_2 is more soluble than NO. NO_X reduction results were not reported for this study[15].

3.6 The NO_X Absorption Process

The NO_X absorption process is used in nitric acid production and for the reduction of NO_X emissions in flue gas. It is a particularly complex process for a number of reasons:

- NO_X gas contains multiple species that are oxygen and nitrogen based; including NO, NO_2, NO_3, N_2O, N_2O_3, N_2O_4, and N_2O_5.
- Equilibrium exists between many of these species in both the liquid and gas phases.
- NO_X absorption into water generates two acids, nitric acid and nitrous acid.
- The reactions that occur during the absorption process take place in both the liquid and gas phases; some reactions are reversible and some are irreversible.
- A chemical reaction immediately follows NO_X absorption and immediately precedes NO_X desorption.
- Current knowledge of equilibrium, solubility, diffusivity, and reaction rate constant data are incomplete[13,16]. Particularly for aqueous and mixed phase equilibriums.

NO_X gas absorption is a two phase, multi-component process that occurs with consecutive and simultaneous reactions. The process may therefore be referred to as a reactive absorption process. The design of a NO_X absorber

requires knowledge of species equilibrium, solubility, diffusivity, the reactions that take place, reaction rates, mass transfer, effects of temperature, and species concentration[17]. Extreme difficulty has been experienced by researchers attempting to obtain individual parameters involved in the absorption process. To overcome this, a combined absorption rate parameter has been developed; it is referred to as an overall kinetic parameter (OKP)[16].

In the NO_X absorption process, the gas side mass transfer resistance is much higher than the liquid side mass transfer resistance. The absorption of NO_X into water is therefore dependent upon the gas side mass transfer coefficient. Using the Gilliland and Sherwood correlation the gas side mass transfer coefficient for N_2O_4 is approximated to be 3.55×10^{-2} m/s[18]. When NO_X gas is absorbed into water two acids are produced, the rate of absorption decreases with an increase in acid concentration. Once the acid reaches a critical concentration no further NO_X will be absorbed into it[16].

3.6.1 NO_X Absorption Process Reactions

The NO_X absorption process consists of a system of reactions. Different reaction pathways may be taken depending on the NO_X species present in the exhaust gas. Most of the reactions are of complex orders with respect to the reactants and they are generally exothermic. When the concentration of the nitric acid in the water is below 34 wt% the following reactions dominate gas phase of the system[2]:

$$2NO + O_2 \rightarrow 2NO_2 \qquad \Delta H_R = \text{-114 kJ/mol} \qquad \text{Reaction 3.1}^{(17)}$$

$$2NO_2 \leftrightarrow N_2O_4 \qquad \Delta H_R = \text{-57.2 kJ/mol} \qquad \text{Reaction 3.2}^{(17)}$$

$$NO + NO_2 \leftrightarrow N_2O_3 \qquad \Delta H_R = \text{-39.9 kJ/mol} \qquad \text{Reaction 3.3}^{(17)}$$

$$3NO_2 + H_2O \rightarrow 2HNO_3 + NO \qquad \Delta H_R = \text{-35.4 kJ/mol} \qquad \text{Reaction 3.4}^{(17)}$$

Thomas and Vanderschuren[19] claim that nitrous acid is also created in the gas phase:

$$NO + NO_2 + H_2O \rightarrow 2HNO_2 \qquad \text{Reaction 3.5}^{(19)}$$

After a species of NO_X is absorbed into the liquid phase, it immediately reacts with water according to the following reactions:

$$2NO_2 + H_2O \rightarrow HNO_2 + HNO_3 \qquad \Delta H_R = \text{-10.72 kJ/mol} \qquad \text{Reaction 3.6}^{(17)}$$

$$N_2O_3 + H_2O \rightarrow 2HNO_2 \qquad \Delta H_R = \text{-3.99 kJ/mol} \qquad \text{Reaction 3.7}^{(17)}$$

$$N_2O_4 + H_2O \leftrightarrow HNO_3 + HNO_2$$ ΔH_R = -5.03 kJ/mol Reaction 3.8[17]

Reactions 3.2, 3.3, and 3.8 are equilibrium reactions and therefore are considered to be instantaneous. The gas phase production of HNO_3 according to Reaction 3.4 only occurs in significant quantity at high temperatures and high partial pressures[20].

3.6.2 Solubility of NO_X Species

Henry's Law coefficient describes the solubility of a species in water, it is usually determined via experimental methods. There is disagreement amongst published data for Henry's law coefficient for most NO_X gas species[21]. It is suggested that measurement is difficult because a chemical reaction with water follows the absorption of NO_X[13]. Also some methods used to determine solubility require knowledge of the diffusivity of the gas species in water and these values vary and are not often published[13]. Table 3.4 presents various Henry's law coefficients for NO, NO_2, N_2O_3, and N_2O_4 as determined by different authors.

Table 3.4: Henry's Law Constant for NO_X Species[22]

Substance	k_H (mol/L.atm)	Reference
NO	$1.4x10^{-3}$	Zafiriou & McFarland [1980]
	$1.9x10^{-3}$	Schwartz & White [1981]
	$1.9x10^{-3}$	Durham et. Al. [1981]
	$1.9x10^{-3}$	Dean [1992]
	$1.9x10^{-3}$	Lide & Frederikse [1995]
NO_2	$3.4x10^{-2}$	Berdnikov & Bazhin [1970]
	$7.0x10^{-3}$	Lee & Schwartz [1981]
	$4.0x10^{-2}$	Lee & Schwartz [1981]
	$2.4x10^{-2}$	Lee & Schwartz [1981]
	$1.2x10^{-2}$	Schwartz & White [1981]
	$4.1x10^{-2}$	Durham et. Al. [1981]
	$1.2x10^{-2}$	Chameides [1984]
N_2O_3	$6.0x10^{-1}$	Schwartz & White [1981]
	$2.6x10^{1}$	Durham et. Al. [1981]
N_2O_4	1.4	Schwartz & White [1981]
	1.6	Durham et. Al. [1981]

The most soluble NO_X species in Table 3.4 is N_2O_4, followed by N_2O_3, NO_2, and NO. Therefore, the design of a scrubber will be optimal when the conditions of the gas are altered in such a way that the equilibrium concentrations of N_2O_3 and N_2O_4 are maximized. Henry's Law coefficients vary with temperature according to Equation 3.1.

$$k_H = k_H^{\ominus} \times \left[\frac{-\Delta_{soln}H}{R}\left(\frac{1}{T} - \frac{1}{T^{\ominus}}\right)\right] \qquad \text{Equation 3.1}^{(22)}$$

The liquid phase saturation concentration of a gas in a liquid is defined by:

$$[A^*] = p_i \times k_H \qquad \text{Equation 3.2}^{(13)}$$

3.6.3 Gas Phase Equilibrium

The gas phase equilibrium constants for Reaction 3.2 and Reaction 3.3 are given by K_{G2} and K_{G3}, respectively.

$$K_{G2} = p_{N_2O_4}/p^2{}_{NO_2}$$ Equation 3.3

$$K_{G3} = p_{N_2O_3}/p_{NO}p_{NO_2}$$ Equation 3.4

The value of these equilibrium constants varies with temperature according to:

$$log_{10}K_{G2} = \frac{2293}{T} - 11.232$$ Equation 3.5

$$log_{10}K_{G3} = \frac{2072}{T} - 9.240$$ Equation 3.6

The units for the equilibrium constants are in kN/m^2 and the unit for T is Kelvin. Above high tetravalent oxide (N_2O_4 and NO_2) concentrations of 1000 ppm Reaction 3.8 dominates the absorption process, below 1000 ppm Reaction 3.6 dominates[13].

3.6.4 Tetravalent Nitrogen Oxides

As shown by Reaction 3.2, NO_2 and N_2O_4 exist in equilibrium with one another; their effective partial pressure may therefore be considered as a combination of the two species as according to:

$$p^*_{NO_2} = p_{NO_2} + 2p_{N_2O_4}$$ Equation 3.7[13]

The equilibrium partial pressure of the tetravalent nitrogen oxides varies with temperature and effective partial pressure according to Equation 3.3 and Equation 3.5. Table 3.5 displays this relationship.

Table 3.5: Variation of NO_2 and N_2O_4 Equilibrium with Temperature and Effective Partial Pressure

Temperature (°C)	Total Tetravalent Nitrogen Oxides Pressure (kPa)	Effective Partial Pressure, p*NO_2 (kPa)	Percent Species of Total Tetravalent Nitrogen Oxides (%)	
			NO_2	N_2O_4
0	100.00	187.280	12.720	87.280
	10.00	6.520	34.800	65.200
	1.00	.280	72.000	28.000
	.10	.005	95.000	5.000
	.01	.000	99.500	.500
25	100.00	168.680	32.320	68.680
	10.00	13.100	69.000	31.000
	1.00	1.058	94.200	5.800
	.10	.101	99.400	.600
	.01	.010	99.940	.060
50	100.00	139.550	60.450	39.550
	10.00	10.900	91.000	9.000
	1.00	1.011	98.900	1.100
	.10	.100	99.890	.110
	.01	.010	99.890	.011
75	100.00	118.370	83.630	5.530
	10.00	10.226	97.746	.600
	1.00	1.002	99.770	.800
	.10	.100	99.992	.008
100	100.00	105.530	94.470	5.530
	10.00	10.060	99.400	.600
	1.00	1.001	99.200	.080
	.10	.100	99.992	.008

In Table 3.5 it may be seen that the equilibrium concentration of N_2O_4 increases with a decrease in system temperature and increase in partial pressure of tetravalent nitrogen oxides. Therefore, a scrubber will be optimized when the temperature is as low as possible and the pressure is as high as possible.

3.6.5 Nitrogen Dioxide Absorption

The absorption of nitrogen dioxide into water occurs via two reactions; first by Reaction 3.9, followed by Reaction 3.6. The forward rate of Reaction 3.6 is second order with respect to NO_2 and zero order with respect to water; as water is in large excess.

$$NO_{2_{(g)}} \rightarrow NO_{2_{(l)}}$$ Reaction 3.9[21]

The overall mechanism for the absorption of NO_2 into water is dependent on temperature, the reaction rate constant, diffusivity, and the liquid side mass transfer coefficient. The absorption is controlled by the bulk liquid phase reaction if the following condition Equation 3.8 is satisfied:

$$k_L a \gg l\, k_{NO_2} k_{H,NO_2} p_{NO_2}$$ Equation 3.8[21]

When condition Equation 3.8 is satisfied, the absorption is kinetically controlled and the volumetric absorption rate is defined by Equation 3.9.

$$(Ra)_{NO_2} = k_{NO_2} l\, k_{H,NO_2}^2 p_{NO_2}^2$$ Equation 3.9[21]

The absorption of NO_2 into water is physically mass transfer controlled if the following condition, Equation 3.10 is satisfied.

$$k_L a \ll l\, k_{NO_2} k_{H,NO_2} p_{NO_2}$$ Equation 3.10[21]

In this case the volumetric absorption rate is defined by Equation 3.11 and all of the reaction occurs in the bulk phase. The concentration of NO_2 in the bulk of the liquid is virtually zero as the rate of reaction is very fast, consequently a term for the concentration of NO_2 in the liquid phase does not appear in the reaction rate equation.

$$(Ra)_{NO_2} = k_L a \cdot\ k_{H,NO_2} \cdot p_{NO_2}$$ Equation 3.11[21]

From the above rate equation it may be seen that increasing the partial pressure of NO_2 increases the rate of absorption, this occurs because the extent of reaction in the liquid film interface increases[13].

3.6.6 Dinitrogen Tetroxide Absorption

Like NO_2, the absorption of N_2O_4 occurs via two reactions; Reaction 3.10 and Reaction 3.8. Reaction 3.8 is first order with respect to dissolved N_2O_4 and zero order with respect to water.

$$N_2O_{4_{(g)}} \rightarrow N_2O_{4_{(l)}}$$ Reaction 3.10[13]

The rate of absorption of N_2O_4 is defined by Equation 3.12.

$$R_{N_2O_4} = p_{N_2O_4} k_{H,N_2O_4} \sqrt{D_{N_2O_4} k_{1,N_2O_4}}$$ Equation 3.12[13]

As the individual parameters for the absorption rate equation are difficult to measure, researchers often experimentally measure the combined term, $k_H\sqrt{Dk}$. Joshi[13] suggests an averaged value from various authors for this combined term of 7.4×10^{-9} kmole/m^{2}s at 25°C. Kameoka and Pigford[23] note that the reactions for the absorption of N_2O_4 into water occur more rapidly than those for NO_2.

3.6.7 Relative Rates of Absorption for Tetravalent Nitrogen Oxides

The equilibrium that exists between NO_2 and N_2O_4 causes the overall rate of absorption of tetravalent nitrogen oxides to be complex. The rates of absorption of NO_2 and N_2O_4 into water are chiefly dependent upon the total partial pressure of tetravalent nitrogen oxides. At the critical value of approximately 2000 ppm, the relative rates of absorption for NO_2 and N_2O_4 are the same. N_2O_4 absorption is relatively high above a total NO_X concentration of 2000 ppm. Conversely the absorption of NO_2 is relatively high below a total NO_X concentration of 2000 ppm.

3.6.8 Dinitrogen Trioxide Absorption

N_2O_3 is formed by an equilibrium reaction between NO and NO_2 according to Reaction 3.3 and equilibrium Equation 3.4 and Equation 3.6. It is absorbed into water via Reaction 3.11 followed by Reaction 3.8. At high N_2O_3 concentrations (above 2000ppm), N_2O_3 will react with water in the gas phase. Considering the temperature dependence of the equilibrium formation of N_2O_3 at high temperatures or low partial pressures, N_2O_3 will only react with water in the liquid phase. The overall rate of absorption is defined by Equation 3.13[13].

$$N_2O_{3(g)} \leftrightarrow N_2O_{3(l)}$$ Reaction 3.11[13]

$$R_{N_2O_3} = p_{N_2O_3} \sqrt{D_{N_2O_3} k_{N_2O_3}}$$ Equation 3.13[13]

The value of the combined term $k_H\sqrt{D_{N_2O_3} k_{N_2O_3}}$ for N_2O_3 is 1.57 at 25°C, twice that of N_2O_4. Limited information is provided in the literature about the absorption process of N_2O_3, especially with respect to the variation of absorption rate over a range of partial pressures, temperatures and into different reactive solvents[13].

3.6.9 Relative Rates of Absorption for Dinitrogen Trioxide and Dinitrogen Tetroxide

The relative rates of absorption of N_2O_3 and N_2O_4 may be calculated based on the equilibrium concentrations for a given temperature, NO partial pressure, and NO_2 partial pressure.

3.6.10 Nitrous Acid Decomposition

Nitrous acid formed during the NO_X absorption process is relatively unstable and readily decomposes in the liquid phase to form nitric acid and NO. Joshi[13] suggests that nitric acid decomposes according to Reaction 3.13. Following these liquid phase reactions, the NO and NO_2 generated is desorbed into the gas phase.

$$3HNO_2 \leftrightarrow HNO_3 + H_2O + 2NO \qquad \Delta H_R = \text{-7.17 kJ/mol} \qquad \text{Reaction 3.12}^{(17)}$$

$$2HNO_2 \leftrightarrow NO + H_2O + NO_2 \qquad \text{Reaction 3.13}^{(13)}$$

Depending on the operating conditions, the NO_2 that is desorbed from the decomposition of HNO_2 in Reaction 3.13 may be reabsorbed according to the following sequence of reactions: Reaction 3.2, Reaction 3.10, and Reaction 3.8. Research has shown that within a gas contactor the rate of NO_2 desorption from HNO_2 increases with the flow of inert gas[13].

3.6.11 Oxidation of Nitric Oxide

NO is substantially less soluble than other NO_X species, as shown in Table 3.4. In order to maximize NO_X absorption, it is therefore desirable to convert as much NO to NO_2 as possible. Typical designs of NO_X absorption systems consequently incorporate a NO oxidation step. Nitric oxide can be oxidized with oxygen however this occurs rather slowly, so sometimes a catalyst is employed to increase the rate of oxidation. Alternatively, chemical oxidation is used when the concentration of NO is low. Ozone, nitric acid, hydrogen peroxide, and chlorine dioxide are examples of commonly used oxidation agents.

3.7 Absorption into Different Liquors

Various solvents may be used to enhance the NO_X absorption process. This section introduces some of these solvents and discusses their effect on the absorption process. The diffusivities of gaseous species into liquids are inversely proportional to the viscosity of liquids. This phenomenon contributes the reduction of absorption rates of gaseous species into liquids with higher viscosities[23].

3.7.1 Nitric Acid

The rate of tetravalent nitrogen oxide absorption into nitric acid solutions decreases with an increase in nitric acid solution. This is primarily because of the decrease in the value of the term $H\sqrt{Dk}$, as the solubility and diffusivity of NO_X species decreases with an increase in acid concentration. Above a nitric acid concentration of 63% the absorption mechanism becomes completely physical mass transfer controlled[13]. For any given partial pressure of NO_X, there exists a limiting nitric acid concentration beyond which no NO_X absorption will occur. This concentration is the equilibrium partial pressure of the nitric acid vapor above a nitric acid solution. The rate of NO_X absorption substantially reduces as the concentration of the nitric acid approaches the limiting concentration value[20].

3.7.2 Sulfuric Acid

The rate of absorption of tetravalent nitrogen oxide into dilute solutions of sulfuric acid (0.09 M) is the same as that of water[23]. It is expected that this rate will decrease with an increase in acid concentration as the solubility and diffusivity of the NO_X gases will decrease[13]. Suchak[20] showed experimentally that NO_X absorption into sulfuric acid solutions of 40 wt% was significantly reduced when compared with absorption into water.

3.7.3 Sodium Hydroxide

In dilute solutions (0.2 M) of sodium hydroxide (NaOH), the rate of absorption of N_2O_4 is about 7% higher than the rate of absorption of N_2O_4 into water[23]. This is likely caused by the chemical reaction that occurs upon absorption[13]. When the concentration of sodium hydroxide is higher, the rate of N_2O_4 absorption is lower than that of water[24]. Indicating that there is an optimal concentration for which the rate of absorption of N_2O_4 is maximized. This phenomenon is known to occur for the absorption of carbon dioxide into solutions of sodium hydroxide[13].

3.7.4 Sodium Sulfite

The rate of absorption of N_2O_4 is increased in the presence of sodium sulfite, when compared with absorption into water or NaOH[21]. At sodium sulfite concentrations of 0.1 M the rate of absorption of N_2O_4 is about 2.5 times faster than that of water. Increasing the sulfite concentration increases the viscosity of this solution and should therefore reduce the rate of NO_X absorption[23]. The competing factors involved in NO_X absorption are therefore expected to result in an optimal sulfite concentration for NO_X absorption[13].

$$Na_2SO_3 + 2NO \rightarrow Na_2SO_3(NO)_2$$

$$R_A = \sqrt{(2/3)k_x D_{NO}\left(k_{H_{NO}} P_{NO}\right)^3}$$

Where k_x is 10^9 m^3/kmol.s at 25°C. The complex $Na_2SO_3(NO)_2$ decomposes in the presence of any acid to form a NO rich gaseous stream[25].

3.7.5 Sodium Chlorite and Sodium Hydroxide Solution

The absorption of NO_2 into solutions of sodium chlorite ($NaClO_2$) and NaOH occurs according to the Reaction 3.14. Reaction 3.14 is a combined overall chemical reaction that occurs between NO_2 and $NaClO_2$ as well as NO_2 and NaOH. The overall rate of absorption is defined by Equation 3.14.

$$4NO_2 + ClO_2^- + 4OH^- \rightarrow 4NO_3^- + Cl^- + 2H_2O$$ Reaction 3.14

$$R_A = \sqrt{\frac{2}{m+1} D_{NO_2}\left(k_{hyd} + k_{ClO_2}[ClO_2^-][NO_2]^2\right)}$$ Equation 3.14

The reaction between NO_2 and $NaClO_2$ is second order with respect to NO_2 and first order with respect to $NaClO_2$. The overall rate of absorption of NO_2 into these solutions is a function of NaOH concentration. Where the rate of absorption decreases over the concentration range of 0.15-0.4 kmol/m^3 and increases above concentrations of 0.4 kmol/m^3. This unusual behavior is a manifestation of the combined effect of the variation of solubility, diffusivity, and rate constant with NaOH concentration. Although the overall rate of tetravalent nitrogen oxides has not been investigated it is expected that the presence of N_2O_4 in the absorption process will dominate the overall rate of absorption as absorption will likely be a first order with respect to N_2O_4[21].

3.7.6 Calcium Hydroxide

The absorption of tetravalent nitrogen oxides into calcium hydroxide solutions occurs at about the same rate of that of water. In a NO_X concentration range of 600 - 2200 ppm the rate of absorption is first order with respect to N_2O_4 and 1.5 or second order with respect to NO_2, depending on whether NO_2 is the dominating species of the overall process[21].

3.7.7 Urea

Jenthi[25] suggests the use of urea solution liquor enhances the removal of NO_X from flue gas. This solvent is quite reactive with NO and NO_2 and it is relatively economical compared with other chemical reagents. Urea reacts with dissolved NO_X gas to produce carbon dioxide, water, and diatomic nitrogen. It is particularly important that the gas stream being treated with a urea solution contains equimolar quantities of NO and NO_2, as NO_X removal efficiency

is particularly sensitive to this factor and is at a maxima when these concentrations are equal. The chemical reactions that occur between urea and NO_X gas are presented by Reaction 3.15 and 2.16[25].

$$NO + NO_2 + H_2O \rightarrow 2HNO_2$$ Reaction 3.15[25]

$$NH_2CONH_2 + 2HNO_2 \rightarrow 2N_2 + CO_2 + 3H_2O$$ Reaction 3.16[25]

The effect of temperature on the absorption of NO_X into urea solutions has been investigated over a total system temperature range of 30-90°C. The optimal operating temperature range for the maximum rate of NO_X into urea solutions is 50-60°C. The volumetric rate of absorption of NO_X into urea solutions is defined by Equation 3.15.

$$R_{NO_x} = ap_{NO_x}\left(k_H\sqrt{kD}\right)_{NO_x}$$ Equation 3.15

The term $\left(k_H\sqrt{kD}\right)_{NO_x}$ for the absorption of NO_X into urea varies with temperature according to Equation 3.16.

$$\left(k_H\sqrt{kD}\right)_{NO_x} = 20.72\exp\left(\frac{-5600}{T}\right)$$ Equation 3.16

3.7.8 Fe(II)EDTA

Liquor solutions of Fe(II)EDTA are also suggested by Jenthi[25] as it is highly reactive with NO_X gas. The reaction between NO and Fe(II)EDTA is reversible and shown by Reaction 3.17; the rate of this reaction is quite high when compared with other liquid absorbents, even at low concentrations of Fe(II)EDTA.

$$NO + Fe(II)EDTA \leftrightarrow Fe(II)(NO)EDTA$$ Reaction 3.17

This chemical reagent is expensive and the process by-product requires special disposal. Destruction of the complex by-product, Fe(II)(NO)EDTA, yields a NO rich gas[25].

3.7.9 Hydrogen Peroxide

Using small quantities of hydrogen peroxide (H_2O_2) the scrubbing liquor can increase overall NO_X absorption and prevent the decomposition of the relatively unstable nitrous acid. The benefit of using H_2O_2 is that it reacts with species within the scrubber to from nitric acid; no other polluting by-products are generated, keeping disposal or destruction simple. Hydrogen peroxide reacts with NO and HNO_2 according to Reaction 3.18 and 2.19[19].

$$2NO + 3H_2O_2 \rightarrow 2HNO_3 + 2H_2O$$ Reaction 3.18

$$HNO_2 + H_2O_2 \rightarrow HNO_3 + H_2O$$ Reaction 3.19

Hydrogen peroxide also reacts with other NO_X species according to Reaction 3.20, Reaction 3.21, and Reaction 3.22. These reactions become the dominating liquid phase reactions when H_2O_2 is present. These reactions are effective even at low H_2O_2 concentrations of 0.2 M.

$$2NO_2 + H_2O_2 \rightarrow 2HNO_3$$ Reaction 3.20

$$N_2O_3 + 2H_2O_2 \rightarrow 2HNO_3 + H_2O$$ Reaction 3.21

$$N_2O_4 + H_2O_2 \rightarrow 2HNO_3$$ Reaction 3.22

These reactions are irreversible and occur faster than the rate of gas absorption. They are considered to occur directly after the steady state diffusion of NO_X species into the liquid film. When H_2O_2 is present for the NO_X absorption process only the more stable acid, nitric acid, is produced in the liquid phase[19].

3.7.9.1 Overall Kinetic Parameters

Thomas and Vanderschuren[19] suggest a new way of describing the kinetics of the NO_X absorption process by introducing the concept of overall kinetic parameters (OKPs). The use of OKPs is preferable to that of traditional parameters as it removes the uncertainty associated with Henry's law constants. They also do not contain mass transfer coefficients and are theoretically independent of absorber hydrodynamic conditions. The authors claim that using these OKPs yield less than a 5% average absolute error. The OKP expressions presented in Equations 3.17, 3.18, and 3.19 are for liquid solutions containing low concentrations of H_2O_2.

$$R_{NO_2} = \sqrt{\frac{2}{3}\frac{k_{2_{NO_2}} D_{NO_2}}{k_{H_{NO_2}}{}^3}} p_{NO_2}{}^{1.5} = OKP_{NO_2} p_{NO_2}{}^{1.5}$$ Equation 3.17

$$R_{N_2O_4} = \sqrt{\frac{k_{1_{N_2O_4}} D_{N_2O_4}}{k_{H_{N_2O_4}}}} p_{N_2O_4} = OKP_{N_2O_4} p_{N_2O_4}$$ Equation 3.18

$$R_{N_2O_3} = \sqrt{\frac{k_{1_{N_2O_3}} D_{N_2O_3}}{k_{H_{N_2O_3}}}} p_{N_2O_3} = OKP_{N_2O_3} p_{N_2O_3}$$ Equation 3.19

Calculating the volumetric rate of absorption using these OKPs requires only the surface area within a scrubber. Consequently maximizing the available surface area within a scrubber will maximize its NO_X absorption ability.

3.7.9.2 OKP Variation with Temperature

The temperature dependence of the OKPs in Equations 3.17, 3.18, and 3.19 are described by Equations 3.20, 3.21, and 3.22, respectively. These OKPs were developed over the temperature range of 10 through 30°C.

$$\ln OKP_{NO_2} = -7.156 - \frac{1847}{T} \quad \text{Equation 3.20}$$

$$\ln OKP_{N_2O_4} = -2.183 - \frac{2609}{T} \quad \text{Equation 3.21}$$

$$\ln OKP_{N_2O_3} = 3.104 - \frac{2609}{T} \quad \text{Equation 3.22}$$

The value of the OKPs for all three NO_X species increases with temperature. This is because reaction rate and diffusivity increase with temperature. It should be noted that the available interfacial area will decrease with increasing temperature, as the kinematic viscosity will decrease. Also increasing the temperature will reduce the presence of N_2O_3 and N_2O_4 because of their inverse equilibrium relationship with temperature[26].

3.8 Wet Scrubber Design Considerations

Wet scrubbers typically consist of the following components:

- Scrubber unit shell;
- Packing media;
- Liquor tank;
- Demister;
- Liquor pump;
- Liquor heat exchanger;
- Liquor distributor and nozzle(s)[12].

The configuration of these components is depicted in Figure 3.1. A scrubber typically operates by having the liquor pump draw the liquor from the liquor tank. The liquor is passed through the liquor heat exchanger to remove heat energy gained from the absorption process that occurs within the packed media. The liquor is then passed through the liquor distributor and nozzle(s), which distribute it on top of the packing media. The packing media increases the interfacial surface area between the liquor and gas streams as they pass counter currently through the packed bed section. The liquor re-enters the liquor tank at the base of the scrubber after it has passed though the packing media. The gas to be 'scrubbed' enters in the void section just below the packing media. It contacts with the liquor

as it passes through the packing media section of the scrubber. It then passes through the demister which reduces the quantity of vapor exiting the scrubber. The gas exits through the top of the scrubber[12].

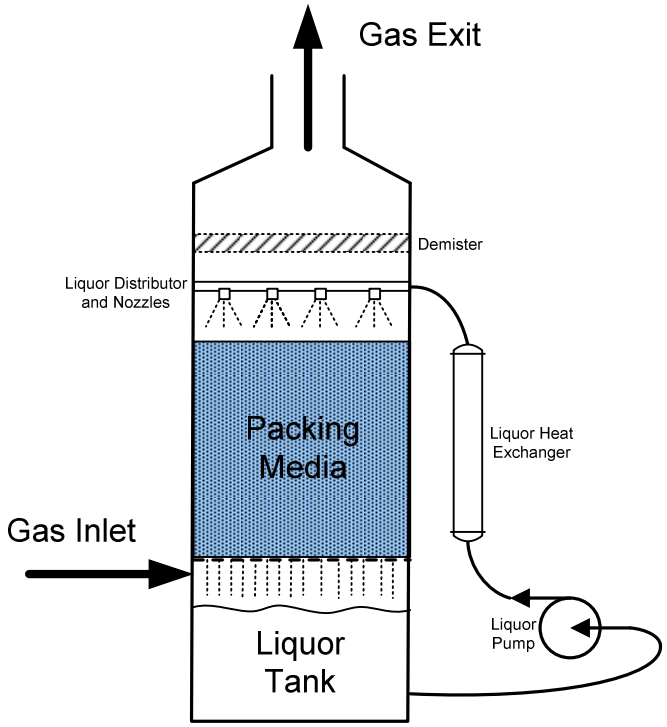

Figure 3.1: Packed Column Components

3.8.1 Interfacial Surface Area

The available area for gas absorption into a liquid is a key parameter in the overall absorption process. It is therefore important to estimate the available interfacial area for NO_X absorption. The higher the liquid flow rate, the more likely the packing surface is completely covered. The available interfacial surface area is generally determined experimentally. It is possible to create an environment within a scrubber where the phase interface area is greater than the surface area of the packing[27]. Thomas and Vanderschuren suggest that the effective interfacial area of a packing varies with temperature according to the relation in Equation 3.23[26].

$$a_{p_{HNO_3}}(T) = a_{p_{H_2O}}(293)\left(\frac{\upsilon_{HNO_3}(T)}{\upsilon_{H_2O}(293)}\right)^{0.7} \qquad \text{Equation 3.23}^{(13)}$$

Estimations of the volume of the interfacial gas film may be made based upon a_p, H, k_G, and D_G. Typically, the volume of the film within a packed column is estimated to be between 0.005-0.01 of the total packed volume[20].

3.8.2 Superficial Gas Velocity

The rate of absorption of tetravalent nitrogen oxides increases with increasing superficial liquid velocity. This is because the effective interfacial surface area increases with superficial liquid velocity as does the gas side mass transfer coefficient. The volume within the column decreases and load on the recirculation pump increases with an increase in superficial liquid velocity. Increasing the gas mass velocity through a packed tower increases the gas side transfer coefficient and therefore also increases the absorption rate of NO_X species[13].

3.8.3 Effect of Temperature

The variation of temperature affects multiple aspects of NO_X absorption and is therefore complex. The diffusivity and rate constants for the absorption of NO_X species increases with an increase in temperature. These phenomena are overcome by the increased formation of N_2O_3, formation of N_2O_4, and solubility with a decrease in temperature. The interaction of these factors with varying temperature results in a maxima for the overall rate of absorption; this point occurs at 10°C. The overall rate of the absorption of NO_X species is enhanced by reducing the operating temperature of a packed tower to 10°C. Reducing the temperature beyond 10°C reduces the rate of NO_X absorption, as the reduction in temperature results in a reduction in the term $k_H\sqrt{Dk}$ which begins to dominate the process at the maxima[13].

3.8.4 Effect of Nitric Acid Concentration

The overall rate of NO_X absorption decreases with increasing acid concentration. This occurs as diffusivity, solubility and the rate of NO_X species all decrease with an increase in acid concentration[13]. Figure 3.2 demonstrates how NO_X absorption varies with nitric acid concentration. Data for this figure were collected for NO_X partial pressures of 33 kPa, much higher than those in diesel exhaust however the trend of increased rate of decline of NO_X absorption with increase in acid concentration is maintained for lower partial pressures of NO_X[20].

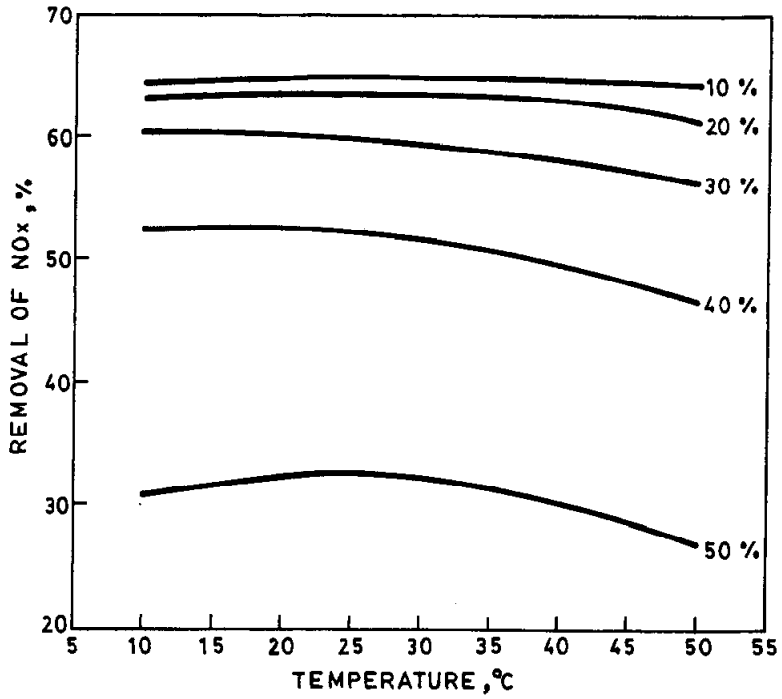

Figure 3.2 Variation of NO_X Absorption with Nitric Acid Concentration. Taken from Shuchak[20]

3.8.5 Packed Columns and Plate Columns

The design of liquid flow rate through packed columns needs to include consideration of having sufficient liquid to completely wet the packing and be able to have control over the liquid temperature rise per pass. The NO_X reduction ability of plate columns is virtually independent of the liquid flow rate. Plate columns generally have better mass transfer coefficients. The fixed costs of packed columns are generally lower as they are able to contain plastic packing and the tower itself may also be constructed out of plastic[13]. Plate columns have a longer liquid residence time due to the liquid hold-up that occurs over the trays[25]. They also have larger interfacial area, and heat transfer coefficients[25]. Packed columns have lower pressure drops across the column, the high pressure drop across plate columns is caused by the static head of the liquid[25]. Crushing of the packing can occur within large unsupported packed columns[25].

3.8.6 Optimal Liquid Flow Rate

Increasing the liquid flow rate decreases the volume within the scrubber and increases the load on the liquor recirculation pump. An optimum flow rate is selected by considering these factors. The flow must at least be enough to completely wet all of the packing. A heat exchanger may need to be used on the recycle liquid stream to remove the heat gained during contact with the gas stream and from the exothermic absorption process.

3.8.7 Liquid Hold-Up

The quantity of liquid entrained during scrubber operation depends on the gas and liquid flow rates and may be found using empirical correlations. The liquid hold-up is dependent upon operating conditions, packing type, and physical properties of the system. An estimation of the gas phase hold-up may also be calculated using the value of liquid phase hold-up[27]. Liquid phase hold-up can be quantified using Equation 3.24.

$$l = 2.2\frac{L\mu}{gd^2\rho} + 1.8\frac{L^2}{gd}$$ Equation 3.24[28]

Where L is the superficial liquid velocity through the scrubber (m/s), g is acceleration due to gravity (m/s^2), μ is the liquid viscosity (Pa.s), ρ is the liquid density (kg/m^3), and d is the diameter of the packing (m).

3.8.8 Minimum Liquid Wetting Rate

There exists a minimum liquid flow rate for all packing types; operating at a liquid flow rate above this minimum will ensure that the packing is completely covered with the liquid. The minimum liquid wetting rate ($m^3/h.m^2$) is found using Equation 3.25.

$$L_{min} = 0.079a_p$$ Equation 3.25

3.9 Absorption within a Scrubber

3.9.1 Physical Absorption

The term 'physical absorption' is used to describe the process of a gas solute dissolving into a liquid solvent without reacting, sometimes this is also referred to as 'pure absorption'. Under these circumstances the average rate of absorption of species A is defined by Equation 3.26.

$$\bar{R}a = k_L a(x_i - x)$$ Equation 3.26[28]

Where k_L is the liquid phase mass transfer coefficient, a is the interfacial mass transfer area, x_i is the average concentration of the dissolved solute at the interface and x is the concentration of the dissolved solute in the bulk of the liquid. The rate of absorption is known to fluctuate with time and location. It is difficult to measure the quantities 'k_L' and 'a' independently so often they are measured together as the term $k_L a$.

3.9.2 The Two Film Model

The film model may be used to predict physical mass transfer rates using first principles. It may also be used to determine the effect that chemical reactions have on the rate of absorption. This model proposes a stagnant film

layer on either side of the phase interface, one liquid film layer and one gas film layer. The composition of the bulk of the liquid adjacent to the liquid film and the composition of the bulk of the gas adjacent to the gas film is assumed to be constant (due to sufficient mixing). Mass transfer is assumed to occur entirely within the liquid and gas films. The liquid and gas film thicknesses δ, are theoretically dimensionless and physically very thin. Mass transport from the bulk of one phase through the films and interface into the bulk of the other phase is assumed to occur by steady-state molecular diffusion caused by the concentration gradient of the species. Convection is assumed to not be involved[27,28]. Mass transfer occurs according to Equation 3.27[28].

$$\bar{R} = \frac{D_A(x_i - x)}{\delta}$$ Equation 3.27[28]

Equation 3.26 and Equation 3.27 gives rise to Equation 3.28 for this model.

$$k_L = D_A/\delta$$ Equation 3.28[28]

The film thickness parameter δ, accounts for the hydrodynamic properties of the absorption system. It should be noted that $(k_L)^1$ varies with $(D_A)^1$ for the film model. Mass transfer is proportional to the interfacial area available for mass transfer and the concentration gradient over which the diffusion occurs. Mass transfer within the system is also dependent upon the equilibrium relationship between phases[29]. Film thickness and interfacial area for mass transfer are often determined by empirical correlations; these correlations allow for system scale-up[27].

3.9.3 Interphase Mass Transfer

When a gas species is being absorbed into a liquid a concentration gradient of that species forms across the liquid and gas films. At the interface the concentrations of that species are usually not equal in the liquid and gas phases but they are considered to be in thermodynamic equilibrium[30]. For systems where the solute concentration is dilute in both the liquid and gas phases, the rate of mass transfer may be described by Equation 3.29.

$$N_A = k_G(y - y_i) = k_L(x_i - x)$$ Equation 3.29[30]

Where N_A is the mass transfer rate, k_G is the gas phase mass transfer coefficient, y is the mole fraction of the solute in the bulk of the gas, y_i is the concentration of the solute in the gas at the interface, k_L is the liquid phase mass transfer coefficient, x is the concentration of the solute in the bulk of the liquid, x_i is the concentration of the solute in the liquid at the interface. The difference in solute concentration across the liquid phase or gas phase provides the driving force for mass transfer.

3.9.4 Gas Phase Mass Transfer Coefficient

When a soluble gas is mixed with an insoluble gas, the soluble gas must diffuse through the bulk of the gas and the gas film to reach the phase interface for absorption. A gas side mass transfer correlation has been developed for packed towers; it applies to all types of packing. This relationship is shown by Equation 3.30.

$$\frac{(k_G RT)l}{D_G} = 0.553\left\{\frac{(P_m l)^{1/3} l \rho_G}{\mu_G}\right\}^{0.62} (Sc_G)^{1/3}\left(\frac{P}{P_1}\right)$$ Equation 3.30[13]

Where l is dependent upon the packing used and P_m is the gas power consumption per unit mass. P_m is calculated from Equation 3.31.

$$P_m = \frac{f a_p}{6(\varepsilon - \varepsilon_L)^4} V_G^3$$ Equation 3.31[13]

Where ε_L is defined by Equation 3.32.

$$\varepsilon_L = \left[1.53 \times 10^{-4} + 2.9 \times 10^{-5} {Re_L}^{0.66}\left(\frac{\mu_L}{\mu_W}\right)^{0.75}\right] {d_p}^{-1.2}$$ Equation 3.32[13]

Where Reynolds number, Re_L, is defined by Equation 3.33.

$$Re_L = \frac{d_L V_L \rho_L}{\mu_L \varepsilon}$$ Equation 3.33[13]

The gas phase Schmidt number is defined by Equation 3.34.

$$Sc_G = \frac{\mu_G}{\rho_G D_G}$$ Equation 3.34[13]

The gas phase mass transfer coefficient is unaffected by the chemical reactions that occur in the liquid phase upon absorption. Given that the chemical reactions are fast and irreversible at low temperatures and concentrations, the gas phase mass transfer coefficient dominates the process as it is predominately controlled by the resistance to diffusion in the gas phase[30]. The gas phase mass transfer coefficient is independent of the total system pressure.

3.9.5 Liquid Phase Mass Transfer Coefficient

The liquid phase mass transfer coefficient for a packed column may be estimated using Equation 3.35.

$$Sh_L = a Re_{mL} Sc_L^{0.5}$$ Equation 3.35[25]

Where the Sh_L is Sherwood number and is defined by Equation 3.36, a is the effective interfacial area (m^2/m^3), Re_{mL} is the modified Reynolds number and is defined by Equation 3.38, and Sc_L is the Schmidt number and is defined by Equation 3.40.

$$Sh_L = \frac{k_L l}{D_L}$$ Equation 3.36[25]

Where l is the characteristic packing length and is defined by Equation 3.37, and D_L is the diffusion coefficient of the gas species in water (m^2/s)

$$l = l_c d$$ Equation 3.37[25]

Where l_c is a packing specific constant and d is the packing diameter (m).

$$Re_{mL} = \frac{(P_m l)^{1/3} l \rho_L}{\mu_L}$$ Equation 3.38[25]

Where P_m is the power consumption per unit weight of the liquid and defined by Equation 3.39, ρ_L is the density of the liquid, and μ_L is the viscosity of the liquid.

$$P_m = gV_L$$ Equation 3.39[25]

Where g is acceleration due to gravity (m^2/s), and V_L is the superficial liquid velocity (m/s).

$$Sc_L = \frac{\mu_L}{\rho_L D_w}$$ Equation 3.40[25]

3.9.6 Effect of Chemical Reactions on Mass Transfer

For absorption processes that involve chemical reactions in the liquid phase, the liquid-film absorption coefficient is increased as compared with absorption processes that do not involve chemical reactions[13]. Chemical reactions in the liquid phase generally increase the rate of the absorption process through converting the solute to a more soluble species; this is true for the NO_X absorption process[27]. When a chemical reaction is involved in the absorption process the typical considerations associated with physical absorption must be made, (i.e. gas solubility, diffusivity, and system hydrodynamics) along with new considerations for chemical reaction equilibrium and reaction kinetics. Gas phase resistance to mass transfer and interfacial area are not altered by the presence of a chemical reaction in the liquid phase[30]. Generally, k_L increases with increasing reaction rate[30].

The enhancement factor E, is often used to describe the effect of chemical reaction on the absorption process. E is the ratio of the average rate of absorption with a chemical reaction divided by the rate of absorption without the presence of a chemical reaction (physical absorption)[28]. The enhancement factor is defined by Equation 3.41.

$$E = \frac{\sqrt{D_A k_1}}{k_L}$$ Equation 3.41[28]

The Hatta number, presented by Equation 3.42, provides a measure of the rate of reaction relative to the diffusion rate and therefore the enhancement on the rate of absorption that a chemical reaction causes[30,31].

$$Ha = \frac{\overline{R_A}}{R_A^{phys}}$$ Equation 3.42[31]

Unlike pure physical absorption, when a chemical reaction occurs within the liquid film the flux of the solute at the liquid film/bulk boundary is different from that of the phase interface. In this case mass flux continuity is assumed to exist at the phase interface. The phase interface is therefore selected as the location at which to couple mass transfer equations and solve systems of equations[27], see Equation 3.43. The presence of a chemical reaction enhances the average rate of absorption by a factor of the Hatta number according to Equation 3.43[28].

$$\overline{R_A} = k_G(p - p_i) = Ek_L(x_i - x)$$ Equation 3.43[28]

The interfacial partial pressure of the gas solute p_i, will be at equilibrium with the interfacial concentration of the dissolved gas, x_i. M is a measure of dissolved solute that reacts in the liquid film. It is defined by Equation 3.44.

$$M = D_A k_1 / k_L^2 = E^2$$ Equation 3.44[28]

When $\sqrt{M} \gg 1$, all of the dissolved solute reacts within the liquid film and does not diffuse into the bulk of the liquid. The liquid side resistance is then considered negligible and k_L does not appear in the equation for the average rate of absorption, Equation 3.45.

$$\overline{R_A} = A^* \sqrt{D_A k_1}$$ Equation 3.45[28]

3.9.7 Controlling Mechanism

The controlling mechanism ratio φ, is used to define which mass transfer mechanism controls the absorption process. φ is presented in Equation 3.46.

$$\frac{k_G}{mk_L} = \varphi$$ Equation 3.46[31]

The controlling mechanism ratio can be used to define the following three cases:

Case 1:	$\varphi \ll 1$	The system is liquid phase controlled
Case 2:	$\varphi \gg 1$	The system is gas phase controlled
Case 3:	$0.1 < \varphi < 10$	The interactions of the two phases should be considered when describing the system.

It can seen here, that there is not a sharp dividing line between the different controlling mechanisms of an absorption process[30]. Often systems are limited by both the resistance to diffusion and the rate of reaction. Generally, systems that contain sparingly soluble solutes or have high liquid viscosities are liquid phase controlled[31]. Systems that contain a fast irreversible reaction in the liquid phase are generally gas phase controlled and typical physical absorption design methods may be used for system design. If the reaction takes place entirely in the liquid film then the process is physically controlled[30].

Perry[30] suggests that when the rate of the chemical reaction is fast and the reaction is irreversible that the process is governed by the gas phase resistance and that it may be assumed that the ratio in Equation 3.47 is true everywhere in the system. The system may therefore be designed based on k_G.

$$\frac{y_i}{y} < 0.05$$ Equation 3.47[30]

The chemical reactions that occur upon solute absorption during the NO_X absorption process, enhance the overall rate of absorption[27]. When the liquid phase chemical reactions are fast, as in the NO_X absorption process, a high liquid-film coefficient is generated as the gas molecules do not have to diffuse far compared with those involved with in simple absorption processes. The gas-film resistance therefore becomes the controlling factor in the process[28].

At high NO_X partial pressures (33 kPa) Joshi[13] shows that the NO_X absorption process is physically controlled and that nitric acid concentration (10-20%) and temperature (10-30°C) have a limited affect on the rate of absorption[13].

3.9.8 Overall Mass Transfer Rate

For cases of physical absorption or when the chemical reaction has a negligible effect on the rate of absorption the liquid and gas side resistances may be combined according to Equation 3.48, Equation 3.49, and Equation 3.50.

$$\overline{R_A} = K_G(p - k_H A^0) = K_L\left(\frac{p}{k_H} - A^0\right) = K_G(y_b - y_e) = K_L(x_e - x_b)$$ Equation 3.48[28,31]

$$\frac{1}{K_G} = \frac{1}{k_G} + \frac{k_H}{k_L}$$ Equation 3.49[28]

$$\frac{1}{K_L} = \frac{1}{k_L} + \frac{1}{k_H k_G}$$ Equation 3.50[28]

Where the overall resistance, either ($1/K_G$) or ($1/K_L$), is the sum of the liquid and gas film resistances. K_G is the overall mass transfer resistance based on the liquid phase and K_L is the overall mass transfer resistance based on the gas phase. The gas phase composition of the solute at the interface y_i, is in equilibrium with the liquid phase composition of the solute at the interface, x_i[28,31]. The rate of absorption may be found experimentally per unit area of phase interface and be used for process design without knowledge of reaction kinetics[28].

3.9.9 Describing the NO_X Absorption Process

The NO_X absorption process is one of the most complex known absorption processes[13]. Kenig[27] asserts that the equilibrium concept is inadequate to describe this process because it does not occur at thermodynamic equilibrium. Often the simplified concepts used for binary mixtures, like theoretical stage height equivalent, cannot be applied to multi-component absorption systems. Rate based models containing process kinetics much more accurately describe the NO_X absorption process. These models integrate reaction kinetics into the mass and energy balances typically used for pure absorption processes. Rate based models are often derived from the two-film model for gas absorption and assume that equilibrium is achieved at the phase interface. System equation coupling occurs at the phase interface as mass and energy fluxes between the film and bulk of a phase are altered by chemical reactions. Rate based models can predict scrubber exit NO_X concentrations within 5% and stream temperatures within 1%[27].

3.9.10 Effect of temperature on Mass Transfer

The variation of k_G with temperature arises principally from changes in gas viscosity. For typical system temperatures these variations are usually low. The gas phase mass transfer coefficient is therefore generally considered independent of temperature. The variation of the interfacial area a, with temperature may also be neglected over a temperature range of 10-50°C. The effect of temperature on k_La can be explained entirely by the variation of liquid viscosity and diffusion with temperature. The effect of temperature on k_L can be great and therefore should be carefully considered. The general form of the correlation between temperature and k_L is defined in Equation 3.51.

$$H_L = bN_{Re}^{a} N_{Sc}^{0.5}$$ Equation 3.51[30]

Where b is a proportionality constant that ranges from 0.2-0.5 depending on the packing. The Einstein relation can be used to alter H_L with temperature according to Equation 3.52.

$$H_{L2} = H_{L1}(T_1/T_2)^{0.5}(\rho_1/\rho_2)^{0.5}(\mu_2/\mu_1)^{1-a}$$ Equation 3.52[30]

When the liquid flow rates are maintained, H_L varies with k_La according to Equation 3.53.

$$\frac{H_{L2}}{H_{L1}} = \frac{(k_La)_1}{(k_La)_2}$$ Equation 3.53[30]

3.9.11 Process Optimization

The optimization of the NO_X absorption process can be achieved by utilizing rate based modeling to investigate the effects of scrubber operating conditions and overall scrubber configuration. Operating conditions that may be investigated include heating and cooling of liquid and gas streams, liquor flow rate, and the use of multiple recycle streams. Scrubber configuration variables include packed height, packing material, location of stream heating or cooling, and location of feed streams[27].

4 Scrubber System Development

This chapter discusses the design aspects of the scrubbing system. The complete absorber system consisted of a catalyzed particulate filter for particulate matter (PM) removal and NO oxidation, DOC for additional NO oxidation, an exhaust heat exchanger for temperature reduction, scrubber unit, and scrubbing liquor pump. Figure 4.1 presents a schematic the complete system showing the pathway of the engine exhaust. The design of the system focused on optimizing the experimental system NO_X reduction ability, although some considerations were made for the final in-use system during the design stage.

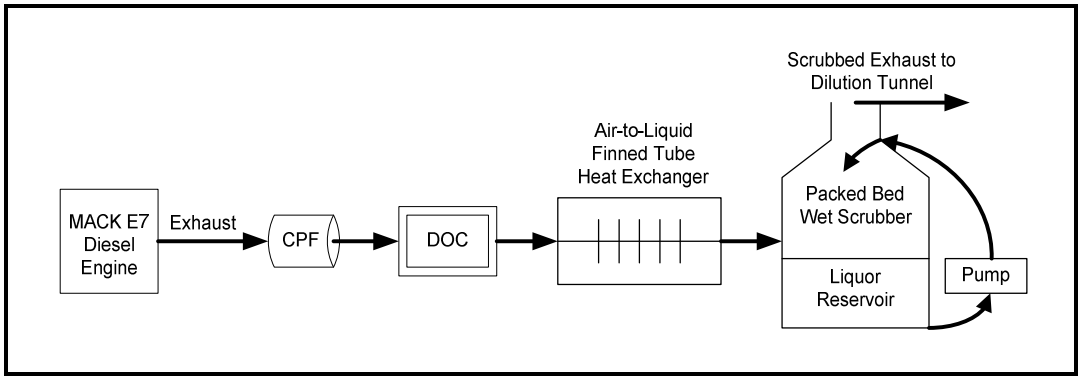

Figure 4.1: Schematic of Scrubber System Components

Figure 4.2 presents the NO_X absorption pathways for a H_2O_2 liquor solution used to design and model the scrubber system.

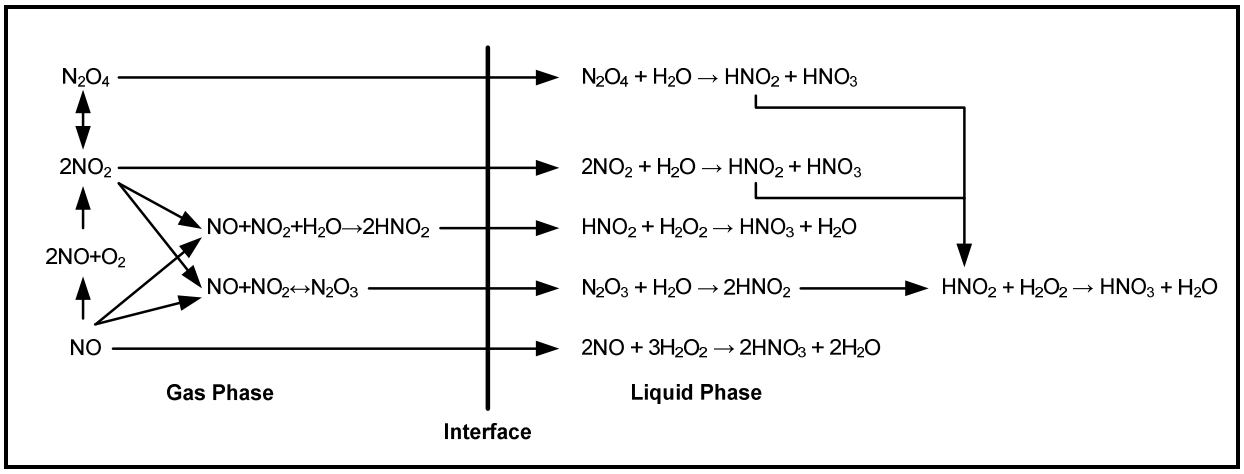

Figure 4.2: Reaction Pathways for NO_X Absorption into Solutions Containing Hydrogen Peroxide. Recreated from Thomas and Vanderschuren[19].

4.1 Temperature Control

Diesel exhaust temperature is too high for the absorption of NO_X gas into a liquid, so a heat exchanger unit was included in the design. The maximum rate of NO_X absorption occurs at a system temperature of 10°C, therefore the scrubber would have the greatest NO_X reduction ability if it were able to operate at this temperature. The temperature of diesel exhaust is typically greater than 300°C and must therefore be cooled for any NO_X absorption to occur within a scrubber. For this particular scrubber system application the Houston/Galveston area water is expected to be used as the cold sink for cooling the exhaust. The average temperature of the surface water in this area is 21.9°C[32]. This temperature represents the lower design limit of the scrubber operating temperature for this application.

The rate of heat transfer required to reduce the diesel engine exhaust temperature from 300°C to 22°C was calculated. Three stainless steel finned tube heat exchanger units were selected and purchased, Figure 4.3. The units were of a single stream, multi-pass cross flow deign; each with a heat transfer area of 11 m^2. They were placed in series in a single stainless steel housing and operated directly upstream of the scrubber, Figure 4.4. During operation of the marine scrubber system water passed through each of the units at a rate of 0.57-0.63 L/s.

Figure 4.3: Three Heat Exchanger Units

Figure 4.4: Heat Exchanger Housing

4.2 Nitric Oxide Oxidation

The solubility of NO_2 is one order of magnitude higher than the solubility of NO. Oxidizing NO to NO_2 can therefore significantly increase the rate of absorption that occurs within a scrubber and its overall NO_X absorption efficiency. Converting NO to NO_2 at low temperatures also results in the formation of N_2O_4 which exists in equilibrium with

NO_2 and has and solubility three orders of magnitude greater than that of NO. As the majority of diesel out NO_X is comprised of NO, the scrubber system needed to incorporate a NO to NO_2 conversion unit.

The scrubber system utilized two catalyst units to convert the exhaust NO to NO_2. The first catalyst was a continuously regenerating diesel particulate filter, referred to as the CPF. It was produced by Johnson Matthey, model number CCRT 2143. The CPF contained a diesel oxidation catalyst followed by a catalyzed particulate filter. The second catalyst used was a ceramic foam diesel oxidation catalyst, referred to as the DOC. This DOC was specially produced by Airflow Catalyst Systems, Inc. (Rochester, NY) for this project and it does not have a model number. The DOC was located downstream of the CPF, upstream of the heat exchanger. In addition to oxidizing the NO in the exhaust gas stream, the CPF had the additional benefit of reducing particulate matter, carbon monoxide, and hydrocarbon emissions. This in turn allowed for the scrubber by-product to be cleaner than what might be expected from simply passing raw diesel exhaust through a liquor solution. The CPF and DOC are depicted in Figure 4.5.

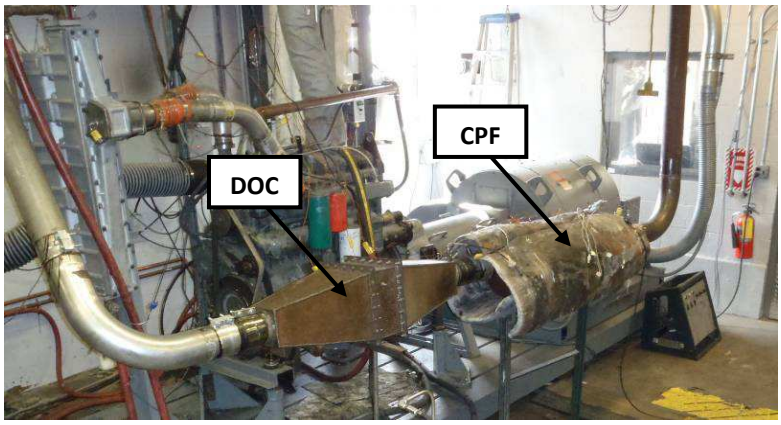

Figure 4.5: CPF and DOC

5 Scrubber Design

5.1 NO_X Absorption Column Type

A packed bed absorption column was selected and designed for the removal of NO_X gas from diesel exhaust. This type of equipment was selected over a plate/bubble column because the higher pressure drop across this type of equipment would cause significant loss in engine efficiency due to an increase in engine backpressure, packed beds require less maintenance than tray columns, and tray columns that are smaller than one meter in diameter are difficult to access. Further to this, the nitric acid generated in the NO_X absorption process is highly corrosive to many metals. It is difficult to construct trays from chemically resistant materials for corrosive systems, packed columns may be simply constructed from economical, light, chemically resistant plastic packing[30]. These qualities are preferable for the final in-use system.

5.1.1 Liquor Solution Selection

Numerous absorbents were reviewed for use as the liquor solution in the scrubber. It was determined that H_2O_2 was the best choice for two key reasons. The first being that only small concentrations are required for NO_X absorption to be enhanced when compared with absorption into water. Secondly the use of this liquor results in a simple by-product, a nitric acid solution. The scrubber system was tested with a water and hydrogen peroxide solution liquor. The water for both liquors was filtered 'tap' water. The hydrogen peroxide solution liquor contained 1.08 wt% hydrogen peroxide.

5.1.2 Packing Selection

When the packing for the scrubber was selected, three key factors were considered:

- Maximizing the interfacial surface area. The overall rate of NO_X absorption is directly related to the available surface area per unit volume within the scrubber and therefore should be as high as possible.
- Maximizing the void space. The higher the void space the lower the resistance to upward gas flow and therefore the lower the pressure drop. Keeping the pressure drop across the scrubber low is important as increased backpressure on the engine will reduce its operating performance.
- Chemical Resistance. The nitric acid produced during the NO_X absorption process is highly reactive; the packing used in the scrubber must be chemically resistant to this acid.

Polypropylene was selected as the material to be used in the scrubber. It is a commonly used material of commercially available packing. Polypropylene is chemically resistant to nitric acid and has the additional benefits of being light weight and economical when compared with ceramic and metal packing. Table 5.1 presents a sample of various commercially available polypropylene packing.

Table 5.1: Commercially Available Polypropylene Packing[30]

Packing Name	Size (mm)	Bed Density (kg/m^3)	Area (m^2/m^3)	Void Fraction (%)
Tri-Pack	25	99	279	90
	32	90	230	92
Pall Rings	25	71	206	90
	40	70	131	91
Super Intalox	25	83	207	90
	50	60	108	93
Nor-Pac	25	72	180	92
	38	61	144	93
Hiflow	25	63	192	92
	50	59	110	93

Optimizing the absorption rate by maximizing the available area was considered to be the most important factor in selecting the packing. Polypropylene 25mm Tri-Pasks (highlighted in green in Table 5.1) produced by Jager Products Inc. were selected as the packing for the scrubber. This packing has a surface area of 279 m^2/m^3 and void fraction of 90%. Figure 5.1 depicts the selected packing.

Figure 5.1: Jaeger 25mm Tri-Pack Packing

5.2 Scrubber Sizing

The scrubber label configuration used in this section is presented in Figure 5.2.

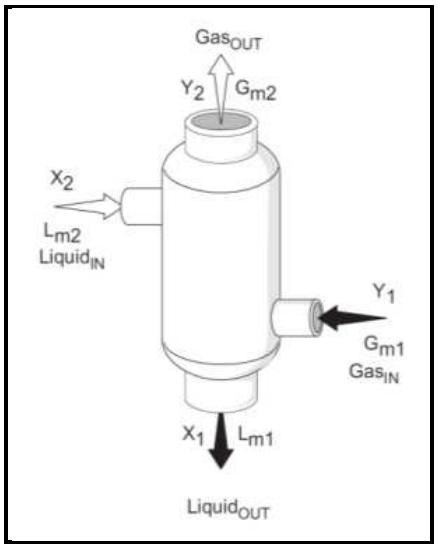

Figure 5.2: Scrubber Label Configuration, Taken from Richards[33]

The sizing of a scrubber usually begins with the determination of the required liquid to gas ratio for the desired removal efficiency. Difficulties arise however in determining the required liquid to gas ratio for NO_X absorption processes for several reasons:

- Several species that exist in equilibrium with one another;
- The NO_X species are being simultaneously absorbed;
- Henry's law constant for some of these species is uncertain.

This design method is further complicated by the chemical reactions that occur in the liquid phase once the NO_X species are dissolved. Very limited information exists in the literature regarding the determination of the liquid flow rate for practical experiments.

5.2.1 Exhaust Gas Characterization

The scrubber exhaust gas was characterized to adequately size the scrubber. The scrubber was tested over two steady state cycles; termed the High Flow and Low Flow cycle. These test cycles are covered in more detail in the Test Cycles section, Section 6.10. Table 5.2 presents exhaust gas data for the two test cycles after it has been produced by the engine and passed through the CPF and DOC.

Table 5.2: Exhaust Gas Characterization at Scrubber Inlet

			Exhaust Parameter			
Test Cycle	Engine Speed (RPM)	Engine Torque (N-m)	Standardized Flow Rate (L/s)	NO_X Concentration (ppm)	Temperature Entering Scrubber (°C)	% NO_2 of Total NO_X (-)
High Flow	1750	1624	386.0	788	23	NA
	1531	1109	228.3	1415	39	60
	1314	765	151.7	2203	40	69
	1090	442	105.7	2117	40	73
Low Flow	1210	1028	155.0	2009	24	58
	604	743	60.0	2070	27	70
	706	690	70.5	2512	28	74
	806	244	72.5	1890	22	82

5.2.2 Minimum Liquid to Gas Ratio

At the minimum liquid flow rate the concentration of NO_X in the liquid phase will be in equilibrium with concentration of the NO_X in the gas phase according to Henry's law, Equation 5.1.

$$Y_1 = k_H X_1 \qquad \text{Equation 5.1}^{(33)}$$

Where Y_1 is the mole fraction of the NO_X entering the base of the scrubber, X_1 is the mole fraction of NO_X dissolved in the liquid exiting the base of the scrubber, and H is Henry's law constant for the NO_X. Having calculated Y_1 the minimum liquid to gas ratio (L_m/G_m) may be calculated using Equation 5.2.

$$Y_1 - Y_2 = \frac{L_m}{G_m}(X_1 - X_2) \qquad \text{Equation 5.2}^{(33)}$$

The minimum liquid to gas ratio is dependent upon the Henry's law constant used and the desired NO_X reduction percentage. The liquid to gas ratio was calculated based upon a 90% NO_X reduction. Calculations used Henry's law coefficient for N_2O_4 and NO_2 to demonstrate a range and an averaged Henry's law coefficient for NO_2, N_2O_3, and N_2O_4. The values obtained from this calculation are presented in Table 5.3. It should be noted that this method does not account for the reactions that occur upon NO_X absorption. It is expected that the minimum liquid to gas ratio should be lower than the ones presented here because of these reactions.

Table 5.3: Minimum Liquid to Gas Ratio

Henry's Law Coefficient Used	Minimum Liquid to Gas Ratio (molar basis)
N_2O_4	3.32E+00
NO_2	2.04E+03
Average	7.65E+01

5.2.3 Scrubber Diameter

The diameter of a scrubber is typically designed such that the scrubber will be operating at a percent of flooding, often between 50% and 80%[33]. The point of flooding may be determined by using the generalized Eckert pressure drop curves for random packings, Figure 5.3. Flooding occurs when, at a fixed gas flow rate, the liquor flow rate is increased to a point where the liquor is unable to pass through the packed section faster than or at the same rate as it enters though the nozzle(s). At this point the liquor will begin backing up within the packed section. If the scrubber continues to operate under these conditions, the packed section of the scrubber will 'flood'.

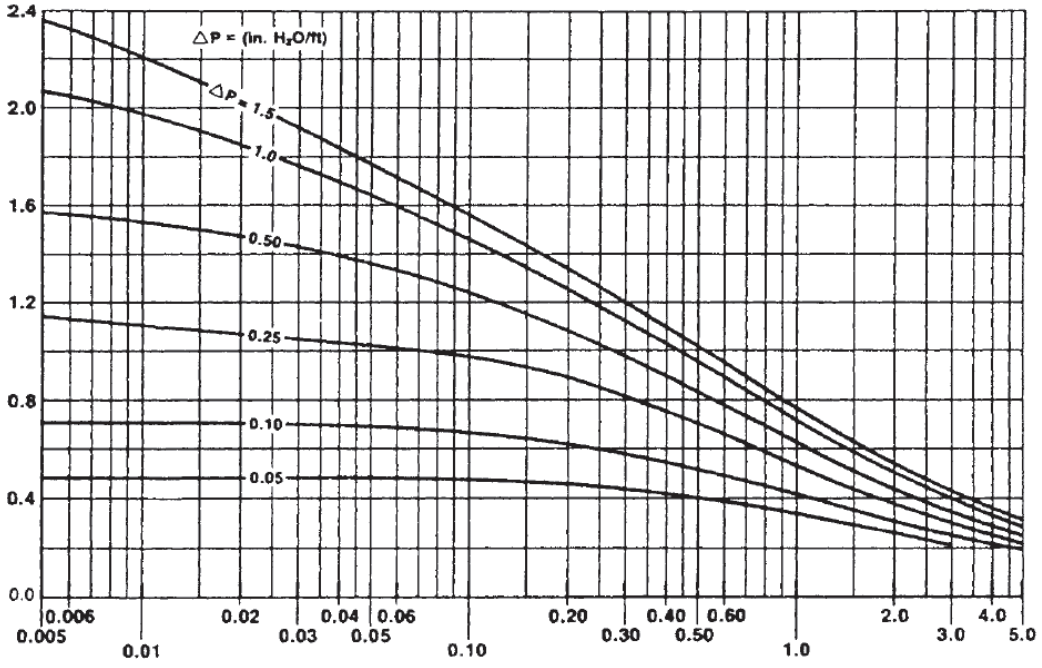

Figure 5.3: Generalized Eckert Pressure Drop Correlation[13]

The x-axis of Figure 5.3 is defined by Equation 5.3.

$$Abscissa = \left(\frac{L_m}{G_m}\right)\left(\frac{\rho_g}{\rho_l}\right)^{0.5}$$ Equation 5.3[30]

Where ρ_g is the gas density and ρ_l is the liquid density.

Pressure Drop

When using Figure 5.3 selecting the appropriate curve is achieved by estimating the pressure drop across the packed section per unit height at flooding. Pressure drop across the packed section of a scrubber is caused by resistance to flow. Liquid hold-up and phase equilibrium are both influenced by the scrubber pressure drop[27]. The pressure drop across the column at flooding is defined by the Kister and Gill equation, Equation 5.4.

$$\Delta P_{flood} = 0.12 F_p^{0.7}$$ Equation 5.4[30]

Where F_p is the packing factor (m^{-1}), specific to the type of packing used in the scrubber. F_p for the packing used in this research was 91.9 m^{-1}[34].

Using the calculated values of the abscissa and ΔP_{flood} the y-axis value, γ, of Figure 5.3 may be determined and used to calculate the volumetric gas flow rate at flooding according to Equation 5.5.

$$\gamma = C_S {F_p}^{0.5} \nu^{0.05}$$ Equation 5.5[30]

Where C_S is the C-factor defined by Equation 5.6 and ν is the kinematic viscosity of the liquid (cS). The C-factor is a gas loading term and is related to droplet entrainment.

$$C_S = G^* \sqrt{\frac{\rho_G}{\rho_L - \rho_G}}$$ Equation 5.6[30]

Where G* is the superficial velocity of the gas (in unit length per unit time) at flooding. The operational gas flow rate is calculated to be a fraction of the flooding gas flow rate according to Equation 5.7.

$$G_{op} = G^* f$$ Equation 5.7[33]

Where G_{op} is the actual gas flow rate per unit area, f is operational flooding coefficient (0.75 was used for this design). The gas flow rate per unit area determines the diameter of the packed bed as shown by Equation 5.8.

$$D = \left(\frac{4}{\pi}\frac{total\ gas\ flow\ rate}{G_{op}}\right)^{0.5}$$ Equation 5.8[33]

The minimum scrubber diameter was calculated according to the gas flow rates, with the scrubber operating at 80% of flooding for the High Flow and Low Flow cycles. The calculations were based on the Henry's law constant for NO_2 and N_2O_4, to show the range of acceptable diameters; as well as an average of Henry's law constants for the species NO_2, N_2O_3, and N_2O_4. Table 5.4 presents the calculated minimum scrubber diameter in meters using Henry's law constants for different species for the two test cycles.

Table 5.4: Calculated Minimum Packed Scrubber Diameter

		Henry's Law Constant Used		
Test Cycle	**Mode**	**N_2O_4 (m)**	**NO_2 (m)**	**Average of N_2O_4, N_2O_3, & NO_2 (m)**
High Flow	1	0.318	3.177	0.475
	2	0.247	2.466	0.369
	3	0.201	2.013	0.301
	4	0.169	1.689	0.253
Low Flow	1	0.206	2.061	0.308
	2	0.129	1.289	0.193
	3	0.139	1.395	0.209
	4	0.140	1.402	0.210

The scrubber diameter was selected to be 0.457 m; this was the diameter of the 0.114 m^3 stainless steel drums used to create the shell of the packed bed section. This diameter allowed for the minimum diameter to be observed over all modes of both test cycles using the average Henry's law constant in the calculations; except for mode 1 of the High Flow cycle which had a required minimum diameter 0.018 m greater than the selected diameter. The manufacturers of the packing used in the scrubber, Jaeger Environmental Inc., suggested that the optimum scrubber diameter to packing ratio was 12:1. Given that the packing size is 0.025 m the scrubber diameter was 1.5 times the suggested optimal size. Perry[30] suggests that the scrubber diameter to packing ratio remains between 10:1 and 40:1, the scrubber ratio of this work was within this range. Increasing the scrubber diameter decreases the required scrubber height for a given reduction percentage, provided that adequate liquor distribution is maintained[30].

5.2.4 Packed Bed Height

The overall NO_X absorption increases with packed bed height; the increase in height allows for an increase in residence time and available area for absorption. The rate of NO_X absorption decreases with height as the partial pressure of the NO_X species reduces, which corresponds to a decrease in the driving force for absorption[20]. The height of the packed bed was determined by modeling the scrubber in Simulink.

Model Development

A model of the NO_X absorption process that was expected to occur within the scrubber was developed in Simulink. The model was based upon the work of Thomas and Vanderschuren[19]. These authors developed OKPs that describe the NO_X absorption process when using a H_2O_2 liquor for temperatures ranging from 10 to 30 °C. The model required the following inputs: volumetric gas flow rate, system temperature, partial pressure of the NO_X gas, oxidation ratio of the NO_X gas, diameter of the packed column, surface area of the packing, and void fraction of the packing. The model determined the superficial gas velocity using the volumetric gas flow rate, void fraction of the packing, and packed column diameter. The model considered a fixed volume of exhaust gas as it passed up through the packed bed. The model divided the height of the packed bed into 0.01m increments. For each increment, the model used all of the model inputs in conjunction with the OKPs to determine the fraction of NO_X in the gas that would be absorbed from the fixed volume of gas into the liquid phase and re-calculated the partial pressure of the NO_X gas that would enter the next increment. The model accounted for the equilibrium concentrations of N_2O_3 and N_2O_4 that would be present at the inlet gas temperatures defined by the user. It used three absorption pathways (OKPs), one each for the NO_2, N_2O_3, and N_2O_4 species of NO_X gas. The N_2O_3 pathway accounted for NO, N_2O_3, and HNO_3 absorption[19]. The model was designed to stop running once the desired NO_X reduction was achieved. The explicit nature of the model solution meant that no convergence criteria were required. The number of iterations that the model ran through would reveal the required packed bed height according Equation 5.9.

$$0.01 * n = h_{PB} \qquad \text{Equation 5.9}$$

Where n is the number of iterations and h_{PB} is the required height of the packed bed for a given NO_X reduction in meters. The model did not account for variations in the liquor flow rate as previous calculations had already determined the liquor flow was adequate. The model assumed a constant system temperature. It did not consider heat transfer or the evolution of heat energy from the chemical reactions that occur during the NO_X absorption process.

The model demonstrated that a packed bed height of 0.864m would reduce the NO_X in the engine exhaust by an average of 11% over the High Flow test cycle. Three scrubber packed heights were tested, 0.864m, 1.804m, and 2.794m. These heights and their abbreviations are presented in Table 5.5. Heights 2 and 3 were two and three

times taller than Height 1 to simplify the identification of absorption trends and for easy modeling of the system. Figure 5.4 presents images of the three scrubber heights.

Table 5.5: Packed Bed Heights

Name	Abbreviation	Packed Bed Height (m)
Height 1	H1	0.864
Height 2	H2	1.804
Height 3	H3	2.794

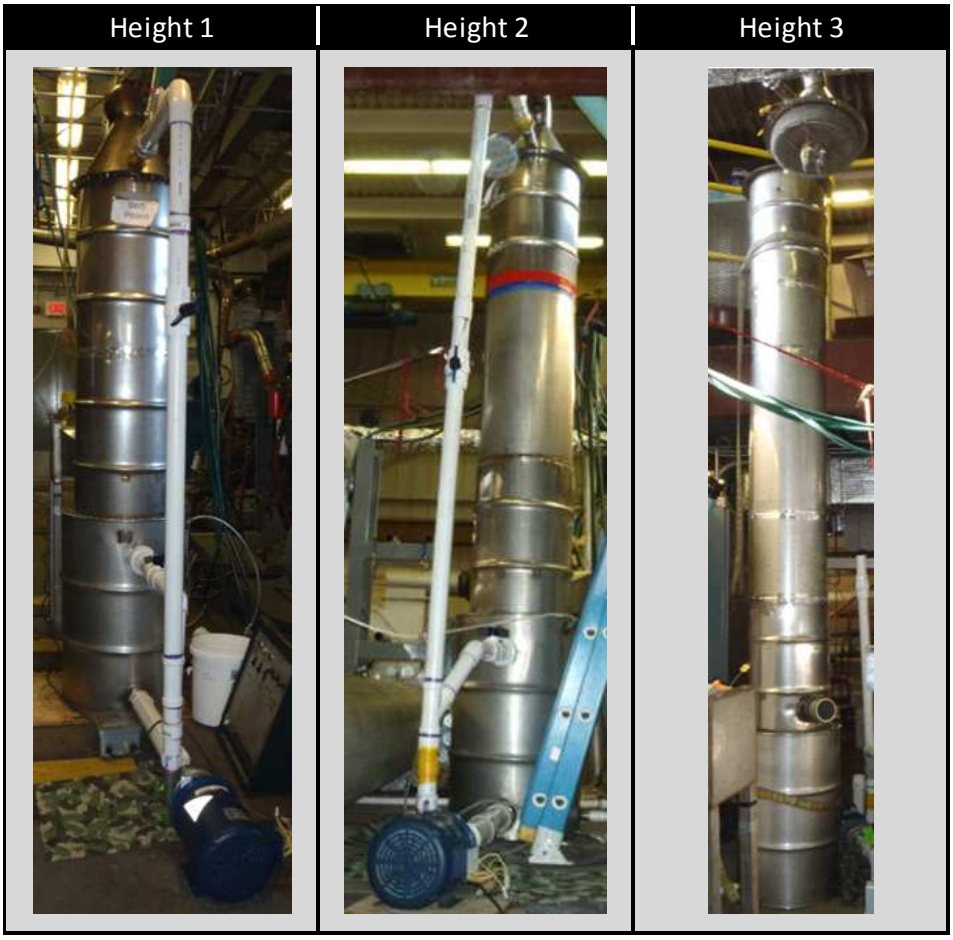

Figure 5.4: Three Scrubber Heights: Height 1, Height 2, and Height 3

5.2.5 Liquor Recirculation

Liquor flow rate determination methods are seldom mentioned in the literature for NO_X absorption systems. Complications arise when using traditional gas absorption liquor flow rate determination methods for the NO_X absorption process as multiple species are being absorbed within the system, these species exist in equilibrium

with one another, Henry's law constant is uncertain for some of these species, and as a chemical reaction follows the absorption of NO_X species converting them into more soluble liquid phase species. Further to this an engine has an unusually high turndown ratio as compared with a chemical or power plant that employs the NO_X absorption process. This means that the liquor flow rate needs to be adjustable to accommodate the wide range of gas flow rates produced by the engine. Some authors have claimed that the absorption of NO_X species is not significantly dependent upon the liquid flow rate; rather it is dependent upon gas residence time and available surface area[13].

The operating liquor flow rates were determined using a generalized flooding curve provided by the packing manufacturer. Flooding flow rates for the liquor were only able to be determined for the High Flow cycle. The conditions of the Low Flow cycle did not fit the data provided by the packing manufacturer and the flooding liquid flow rates were unable to be determined for this cycle. Table 5.6 provides the flooding and operating liquid flow rates for the High Flow cycle calculated using Jaeger's flooding curves. The operating flow rate was selected to be 75% of the flooding flow rate. A 3.7 kW Liquiflo pump was acquired and operated at the flow rates shown in Table 5.6. This pump was capable of flow rates up to 10.1 L/s, it is depicted in Figure 5.5.

Table 5.6: Flooding and Operating Liquor Flow Rates

Test Cycle	Mode	Flooding (L/s)	Operating (L/s)
High Flow	1	2.48	1.86
	2	5.02	3.76
	3	7.80	5.85
	4	11.15	8.36

Figure 5.5: LiquiFlo 3.7 kW Pump

Four stainless steel nozzles were used to distribute the liquor inside the top of the scrubbing unit (below the demister). They were selected for their full conical shape spray pattern, resistance to nitric acid, and ability to withstand high liquor flow rates. Figure 5.6 shows these nozzles attached to a liquid distributor before installation. Geometry dictated the distance between nozzle tips and the top of the packing to be approximately 0.05 m to minimize wall impingement.

Figure 5.6: Stainless Steel Nozzles attached to Liquor Distributor

5.2.6 Demister

Demisters are regularly used in scrubber and other applications. A demister was included in the design for this research to reduce the chances of water droplets or acid droplets escaping the packed section of the scrubber and entering the testing tunnel. The demister was supplied for this application from Jaeger Environmental Inc. The demister was a stainless steel mesh, 0.102 m thick and 0.451 m in diameter. It fitted snugly in the scrubber above the packed bed and was attached to the cone (top) of the scrubber. Figure 5.7 presents the demister with the stainless steel nozzles attached, in this picture the demister is also attached to the cone of the scrubber.

Figure 5.7: Demister with Nozzles Attached

5.2.7 Scrubbing Liquor Tank Design

The NO_X scrubbing process generates nitric and nitrous acid. Maintaining the concentration of the acid below 10 wt% will aid in achieving a maximal absorption rate and therefore overall scrubber NO_X removal efficiency. It was determined that a scrubbing liquor tank 0.2 m^3 in size would be required for the scrubber. With a tank of this size, the engine would be able to operate for a 12 hour day, in mode 2 of the High Flow cycle, and absorb all of the NO_X that the engine produced without the concentration of the acid in the liquor going above 10 wt%.

For Height 1 a 0.208 m^3 drum was used to hold the scrubbing liquor. The drum was constructed from stainless steel, which is chemically resistant to nitric acid, nitrous acid, and hydrogen peroxide. Aside from chemical resistance a stainless steel drum was selected for ease of fabrication; plumbing and other connections were welded to the tank. This tank was located directly beneath the scrubber.

For the scrubber Heights 2 and 3 a secondary tank was added to the system. This was done because with the pump operating at such high liquid flow rates the amount of liquid entrained in the scrubber would be so great that it would potentially empty the single 0.208 m^3 tank for these two heights. The secondary tank was also constructed from stainless steel and had a total volume of 0.104 m^3. Figure 5.8 shows the primary and secondary tanks used to hold the scrubbing liquor.

Figure 5.8: Primary and Secondary Liquor Tanks

5.2.8 Hydrogen Peroxide

For tests including H_2O_2 in the scrubbing liquor, the H_2O_2 was added to the scrubbing liquor in molar excess of the amount of NO_X expected to pass though the scrubber. This equated to 2 liters of 35 wt% H_2O_2. Given that the secondary tank was half the size of the first, when the secondary tank was used (for tests on Height 2 and Height 3), this amount was increased to 3 liters. This allowed the concentration of H_2O_2 in the scrubbing liquor to be the same for all H_2O_2 tests. The concentration of H_2O_2 in the liquor for all H_2O_2 tests was 1.08 wt%.

5.2.9 Water Condensation

Cooling the engine exhaust was expected to cause condensation in the heat exchanger, as the exhaust carries water vapor produced during combustion and water vapor contained in the engine intake air. The scrubber system was designed such that the water condensed out of the exhaust stream in the heat exchanger would drain into the primary scrubbing liquor tank.

It is important to quantify the amount of water condensed in the heat exchanger to ensure that the system does not begin to flood while operating and to determine at what point (if any), some of the scrubbing liquor will need to be removed from the system. Table 5.7 presents the rate at which water will condense in the heat exchanger and drain into the primary scrubbing liquor tank if the exhaust leaves the heat exchanger at 100% humidity and 21.9°C for all modes of the High Flow Cycle. It was assumed that air entering the engine was at 0% relative

humidity and the stream leaving the scrubber demister was 100% relative humidity air. The intake air humidity assumption is low so the actual condensation rate may have been higher than the values presented in Table 5.7.

Table 5.7: Condensation Rate by Mode for the High Flow Cycle

Mode	1	2	3	4	Cycle Average
Condensation Rate (L/s)	1.45×10^{-2}	7.84×10^{-3}	4.56×10^{-3}	2.11×10^{-3}	7.25×10^{-3}

6 Experimental Apparatus

The marine scrubber system was tested in the Engine and Emissions Research Laboratory at West Virginia University. Testing occurred periodically over the dates of 1/27/2011 and 3/3/2011. The system was tested for its NO_X reduction ability over two steady state test cycles using two types of scrubbing liquor.

6.1 Engine

The diesel engine used to demonstrate the NO_X reduction ability of the scrubber system was a 1992 Mack model E7-350. This engine was selected because its age, power output, and NO_X production levels were representative of the diesel marine engines for which the scrubber system was intended. The engine had a displacement of 12 L and a factory rated power of 261 kW. The fuel injection system of the engine was mechanically controlled. The fuel pump timing of the engine was advanced to increase the NO_X emissions levels closer to that of diesel marine engines. With the advanced timing, the engine's maximum rated power was 298 kW. Figure 6.1 presents an engine performance map created from engine test data. Figure 6.2 shows the engine used for system testing.

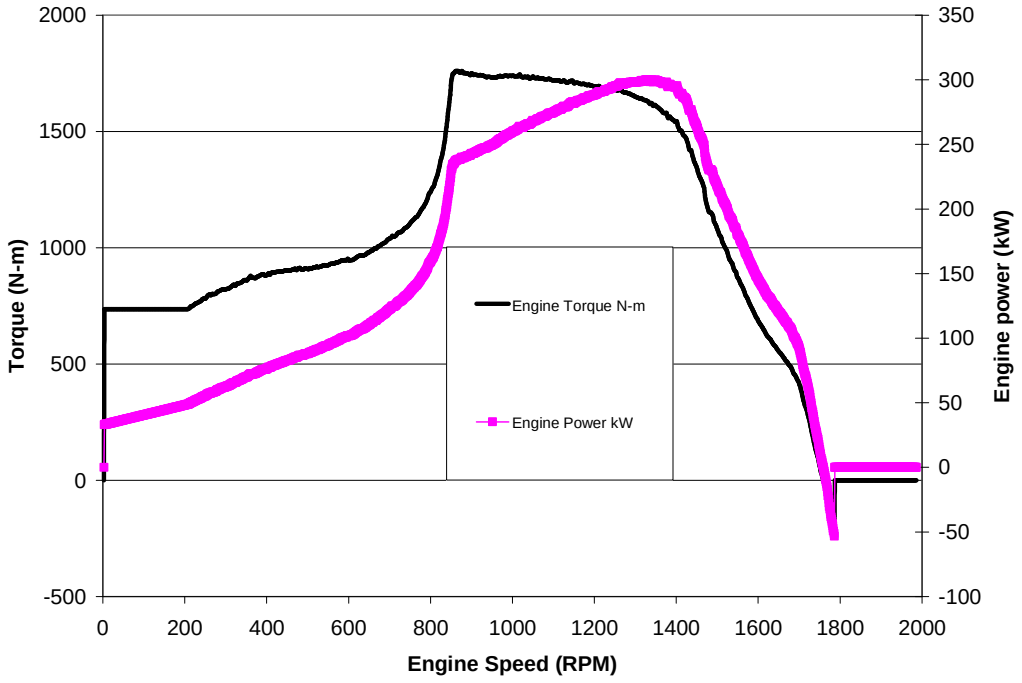

Figure 6.1: Engine Performance Map for 1992 Mack with Fully Advanced Timing

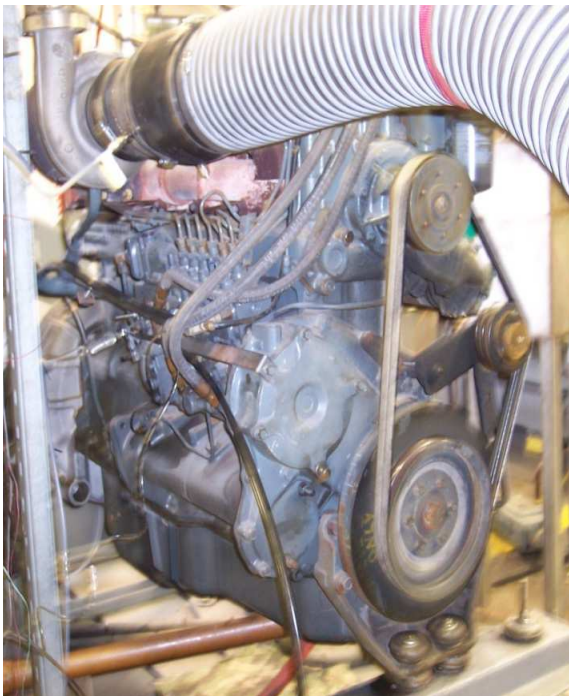

Figure 6.2: 1992 Mack E7 Diesel Engine

The intake air flow rate of the engine was determined by measuring the differential pressure with a laminar flow element and the intake air temperature. The humidity of the intake air was measured and used to correct NO_X concentration measurements. The engine's turbocharger outlet was connected to the marine scrubber system followed by the dilution tunnel via 0.127 m exhaust pipe, so that the exhaust gas would pass from the engine into the aftertreatment system and into the dilution tunnel.

6.2 Dynamometer

The engine was connected to a General Electric DYC243 direct current engine dynamometer via a Vulkan coupling and a driveshaft. The Vulkan coupling is a flexible coupling that dampens out vibrations that occur between the engine flywheel and driveshaft. This avoids possible mechanical failure of driveshaft components or the engine. The dynamometer was capable of producing 373 kW and absorbing 410 kW. The dynamometer speed was controlled electronically. An engine torque set point was attained by adjusting the engine throttle position which was as controlled by an electronic servo motor. Figure 6.3 presents the dynamometer used during system testing.

Figure 6.3: GE Dynamometer

6.3 Dilution Tunnel

After passing through the marine scrubber system the engine exhaust was passed though the dilution tunnel. The dilution tunnel was a full-scale constant volume sampling dilution tunnel. This tunnel complies with the 40 CFR §86.110-90 and was designed for testing the emissions of engines constructed before 2007. The dilution tunnel was 0.457 m in diameter and utilized three critical flow venturis to control the gas flow rate. A 56 kW blower was used to force air though the tunnel. Air conditioning units controlled the temperature and humidity levels of the air flowing through the tunnel. The standard flow rate through the dilution tunnel was 1.13 m^3/s.

6.4 Gas Analyzers

Gaseous emissions were analyzed for oxides of nitrogen NO_X (NO, NO_2+NO), carbon monoxide (CO), carbon dioxide (CO_2), and hydrocarbons (HC). Table 15 shows the analyzed gases, analyzer, measurement principal, and analyzer calibration measurement ranges. Since the CPF was utilized particulate matter was not collected for this testing.

Table 6.1: Gas Analyzers Used During Testing

Species	Analyzer	Measurement Method	Gas Range (ppm)
NO	Rosemount 955	Chemiluminescence	0-703
NO_X	Rosemount 955	Chemiluminescence	0-703
CO	Horiba AIA-220	Non-dispersive Infrared (NDIR)	0-251
CO_2	Horiba AIA-210	Non-dispersive Infrared (NDIR)	0-35,000
HC	Rosemount 402	Flame ionization detection	0-29.9

Two Rosemount 955 chemiluminescence gas analyzers were used to measure the concentration of NO_X in the exhaust. Both analyzers were calibrated, zeroed, and spanned with the same NO_X bottle. One analyzer was set in NO mode and the other was set in NO_X mode. This allowed for the concentration of both NO and NO_2 in the exhaust to be determined. For gas measurement in NO mode, the exhaust sample bypassed the Rosemount's internal converter and thus measured only NO. For gas measurement in NO_X mode, the exhaust sample ran through the Rosemount's internal converter that converted NO_2 within the sample to NO and then measured the total NO_X concentration. The NO_2 concentration was determined by the difference between the two analyzer readings. The internal converter efficiency for such low concentrations of NO_X was found to be 98-99%.

6.5 Fuel Measurement

The engine used ultra low sulfur diesel (ULSD) fuel, supplied by Guttman (Belle Vernon, PA), from a 0.061 m^3 barrel during testing. Fuel consumption was measured using two methods. The first method measured the weight of the barrel during the testing to yield an incremental mass flow rate of fuel into the engine. The second method involved using a carbon balance. The chemical reaction between the fuel and air was used along with knowledge of the chemical formula of the fuel, fuel molecular weight, and CO, CO_2, and HC emissions data to determine fuel consumption.

6.6 Temperature Measurement

The temperature of the exhaust gas is an important parameter in the NO_X absorption process; it was therefore measured during testing. K-type thermocouples (0.003m and 0.002m in diameter) were utilized to measure the exhaust gas temperature at various locations within the marine scrubber system. The thermocouples were connected to a data acquisition rack and data from this system was recorded during testing. Exhaust gas temperatures of the following locations were recorded: post-turbo, post DOC, pre-heat exchanger, post-heat exchanger, and post-scrubber exit.

6.7 Packed Bed Pressure Drop

It was important to maintain a relatively low gas pressure drop across the packed bed section of the scrubber. There exists, for every scrubber, a critical gas pressure drop for which if exceeded the bed will approach flooding. For this particular scrubber configuration and range of volumetric gas flow rates, the critical pressure drop was 2.5 kPa per meter of packing. This value was determined from the packing manufacturers generalized flooding curves for 25mm tri-pack packing. The gas pressure drop across the packed section of the scrubber was monitored and recorded continuously thought testing to ensure that the pressure drop did not approach the critical value. If the gas pressure drop approached this value during testing the liquor flow rate was reduced to avoid system flooding.

An Omega low differential pressure transducer, model PX2300, for 'wet' flows was used to measure the pressure drop across the scrubber packed bed. The device was powered with 24 volts and had a 4-20 mA output which corresponded to a 0 to 6.895 kPa range. The differential pressure transducer had an accuracy of 2% over the entire pressure range.

6.8 Scrubbing Liquor pH

The change in pH of the liquor solution provides an indication of how much NO_X was absorbed during a test. Liquor samples were taken before and after all tests to provide a secondary method of determining the quantity of NO_X absorbed (compared with the primary gas analyzer method). Liquor samples were collected before and after some tests. The pH of the samples were tested with an Oakton pH 110 meter. This pH meter automatically compensated for temperature when measuring pH. The pH range of this meter was -2.00 to 16 pH, accurate to within ±0.01 pH.

6.9 System Configurations

To characterize the gas entering the heat exchanger and scrubber a series of tests were conducted without these units. The system configuration for these tests consisted of the dynamometer, engine, DPF, DOC, and dilution tunnel. The tests conducted with this configuration are referred to as the baseline tests. Figure 6.4 presents a schematic of this arrangement. This configuration did not include the heat exchanger as the gas condensate would not have had a collection point. During the NO_X reduction testes the collection point was the scrubber liquor tank.

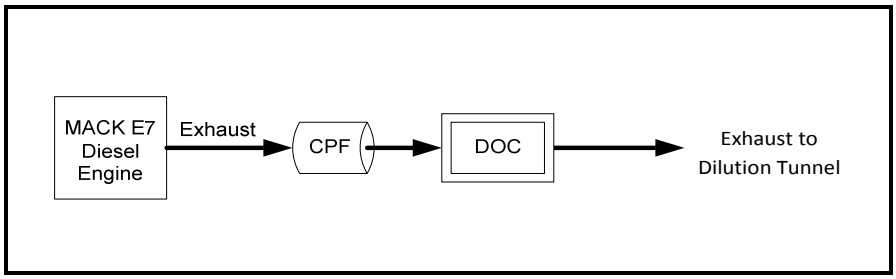

Figure 6.4: System Configuration for Baseline Tests

Tests that assessed the NO_X reduction ability of the scrubbing system were conducted with the configuration depicted in Figure 4.1. This configuration included the heat exchanger and scrubber unit. Not including the heat exchanger and additional plumbing in the baseline tests may have caused different exhaust gas conditions and account for some of the differences and contributed to error in results.

6.10 Test Cycles

Two different steady state engine test cycles were used to determine the NO_X reduction ability of the scrubber system; they are referred to as the High Flow cycle and Low Flow cycle. Steady state cycles are representative of the operation of diesel marine harbor craft engines.

6.10.1 High Flow Cycle

The High Flow cycle was employed as its NO_X concentration and power levels are representative of a typical marine cycle. The set points of the High Flow cycle are presented below in Table 6.2.

Table 6.2: Set Points of the High Flow Test Cycle

Mode	-	1	2	3	4
Engine Speed	RPM	1750	1531	1314	1090
Engine Torque	N-m	1591	1109	764	442
Engine Power	kW	292	178	105	51

6.10.2 Low Flow Cycle

The set points of the Low flow cycle were designed to have high NO_X emissions levels and low volumetric exhaust gas flow rates. This cycle was used to investigate the effect of exhaust gas flow rate on the NO_X reduction ability of the marine scrubber system. The set points of the Low Flow cycle are presented below in Table 6.3.

Table 6.3: Set Points of the Low Flow Test Cycle

Mode	-	1	2	3	4
Engine Speed	RPM	1210	605	707	806
Engine Torque	N-m	1025	745	686	245
Engine Power	kW	130	47	51	21

7 Results and Discussion

Baseline and marine scrubber system testing occurred periodically between the dates of 10/7/2010 and 3/3/2011. The system was tested for its NO_X reduction ability over two test cycles, at three different packed bed heights, and using two different liquors. Individual test data may be found in Appendix A. A number of background measurements deviated from typical values, these deviations and their impact on results are discussed below.

Negative NO_X Background Values

Some of the background NO_X concentration values in Appendix A are negative. This was likely caused by the calibration curve fit offset of the gas analyzers used. The negative background NO_X concentration values were set to zero during data processing.

CO Background Values

The background CO concentration values are slightly above atmospheric levels. This was likely caused by the calibration curve fit offset of the gas analyzer used. This data were not altered for calculations as they were expected to be neutralized by the measured values of the engine exhaust during data processing. This deviation was not expected to impact the results of this work.

Test 7

The value for the background CO concentration of test 7 in Appendix A was negative. Given that the background CO concentration values for other tests completed on the same day were positive, it was likely that this was caused by an error in data collection during background sampling (for example turning the valve to zero-air gas on the analyzer bench rather than to background sample). The background CO concentration is used in the calculation for brake specific fuel consumption. When the brake specific fuel consumption of test 7 was compared with the average fuel consumption of the other tests with the same test configuration (tests 6, 8, and 9), it was shown to vary by 0.13%, 0.31%, 0.13%, and 0.30%. This demonstrates that the negative background CO concentration had a negligible impact on the results.

Tests 22 and 23

Tests 22 and 23 in Appendix A had CO_2 and NO_X background levels an order of magnitude larger than other tests completed on the same day. This was likely caused by the background sample being collected too early, before the gas from testing had a chance to be evacuated from the analyzers.

The background CO_2 concentration is used in the calculation for brake specific fuel consumption. The brake specific fuel consumption of tests 22 and 23 were compared with the average brake specific fuel consumption of the other tests with the same test configuration (tests 24, 25, and 26). Test 22 varied by 3.31%, 5.68%, 8.11%, and 19.48%

for modes 1, 2, 3, and 4 respectively. Test 23 varied by 8.04%, 10.59%, 18.34, and 33.54% modes 1, 2, 3, and 4 respectively. These deviations are significant; these two tests were therefore not included in calculations and results that involved the brake specific fuel consumption of the engine.

The background NO_X concentration is used in the calculation for brake specific NO_X . The brake specific NO_X emissions of tests 22 and 23 were compared with the average brake specific NO_X emissions of the other tests with the same test configuration. Test 22 varied by 3.57%, 3.85%, 3.66%, and 11.16% for modes 1, 2, 3, and 4 respectively. Test 23 varied by 0.00%, 0.74%, 3.50%, and 5.18% for modes 1, 2, 3, and 4 respectively. These deviations indicated a minimal impact of variation of background NO_X concentration on brake specific NO_X emissions and results.

Tests 30 and 31

The background HC concentration values for Tests 30 and 31 in Appendix A were negative. This was again likely caused by an error in test method. The background HC concentration is used in the calculation for brake specific fuel consumption. The brake specific fuel consumption of tests 30 and 31 were compared with the average brake specific fuel consumption of the other tests with the same test configuration (tests 27, 28, 29, and 32). The brake specific fuel consumption for both tests varied by less than 1.2% for all modes. This indicates that the variation in background HC concentration had a negligible impact on the brake specific fuel consumption of the engine for these tests.

7.1 Mode One Baseline Data

During Mode 1 of the baseline testing the engine was unable to reach the power and torque set points of the High Flow test cycle. The engine power, torque, and NO_X emissions data recorded during this testing are presented in the row labeled 'original baseline' of Table 7.1 below. To avoid inaccuracies in the system baseline NO_X emissions and therefore inaccuracies in evaluation of system NO_X reduction ability, NO_X emissions from alternate testing were used as the baseline for Mode 1 of the High Flow cycle. The power, torque, and NO_X emissions that were produced by the engine during the alternate baseline testing are presented in the row labeled 'alternate baseline' of Table 7.1. The alternate baseline testing only included the DOC so the oxidation ratio and total NO emissions are not representative of the exhaust gas conditions entering the scrubber during the system testing of Heights 1, 2, and 3. Oxidation ratio data and NO emissions reduction data are therefore not presented for mode 1 of the High Flow cycle throughout this work.

Table 7.1 Original and Alternate Mode 1 Baseline Data

		Engine Data		Emissions Data			
	Test	Work (kW-hr)	Torque (kN.m)	Measured NO (ppm)	Measured NO_X (ppm)	NO (g/kWhr)	NO_X (g/kWhr)
Set Point	-	4.87	1.59	-	-	-	-
Original Baseline	1	3.54	1.16	109.38	245.05	3.57	7.91
	2	3.68	1.20	115.71	245.28	3.61	7.57
	3	3.92	1.28	117.02	246.64	3.41	7.12
Alternate Baseline	1	4.98	1.62	109.38	293.54	3.57	6.83
	2	4.98	1.63	115.71	291.51	3.61	6.80
	3	4.97	1.63	117.02	291.45	3.41	6.81

7.2 Variability between Tests

Changes in environmental and laboratory conditions between tests may have lead to variability in measurements taken from the marine scrubbing system. Table 7.2 demonstrates how measurements may have varied by presenting data collected from different tests of mode one of the High Flow test cycle. The coefficient of variation in Table 7.2 is the standard deviation divided by the average.

Table 7.2: Variation of Engine Data and Background Data between Tests

Test	Date	Engine Data				Background Data			
		Work (kW-hr)	Torque (kN.m)	Fuel Consumption (kg/kW-hr)	CO_2 (g/kW-hr)	CO (ppm)	CO_2 (ppm)	NO_X (ppm)	HC (ppm)
1	10/7/2010 and 2/10/2011	4.98	1.62	0.21	497.15	13.47	468.24	-0.67	2.60
2	10/7/2010 and 2/10/2012	4.98	1.63	0.21	495.81	13.44	460.61	-0.79	2.53
3	10/7/2010 and 2/10/2013	4.97	1.63	0.21	493.63	13.37	457.17	-0.70	2.48
6	2/10/2011	4.78	1.57	0.15	491.45	13.83	401.42	-0.90	2.63
7	2/10/2011	4.77	1.56	0.15	491.72	-0.24	424.52	-0.78	2.61
8	2/10/2011	4.58	1.50	0.15	492.00	13.83	436.18	-0.82	2.61
9	2/10/2011	4.70	1.54	0.16	493.17	14.02	439.35	-0.91	2.54
13	2/18/2011	4.94	1.62	0.16	498.85	15.35	469.37	-1.41	2.27
14	2/18/2011	4.93	1.61	0.16	495.30	13.06	440.79	-1.93	2.41
15	2/18/2011	4.93	1.61	0.16	496.41	12.60	445.49	-1.92	2.39
16	2/18/2011	4.94	1.62	0.16	496.97	14.17	446.81	-1.69	2.35
17	2/18/2011	4.94	1.62	0.16	493.93	13.93	449.08	-1.73	2.37
22	3/2/2011	4.94	1.62	0.14	454.06	12.92	1294.74	18.53	2.87
23	3/2/2011	4.94	1.62	0.14	432.53	12.88	2164.54	23.69	2.61
24	3/2/2011	4.91	1.61	0.15	469.12	12.70	394.27	0.53	2.48
25	3/2/2011	4.88	1.60	0.15	468.53	12.67	404.23	0.91	2.36
26	3/2/2011	4.86	1.59	0.15	473.15	14.31	376.57	0.40	2.52
Average		4.88	1.60	0.16	484.3	12.7	586.7	1.8	2.5
Coefficient of Variation		0.023	0.022	0.139	0.038	0.269	0.780	4.212	0.057

Table 7.2 shows that the work, torque, fuel consumption, CO_2 emissions, background CO concentration, and background HC concentration levels were relatively consistent. The main variations can be seen in the background CO, CO_2, and NO_X concentration levels. The CO background data for test 7 and the CO_2 and NO_X background data for tests 22 and 23 (highlighted in green) are statistical outliers that cause the CO, CO_2, and NO_X coefficient of variation values to be high. Given that the tests immediately following tests 7, 22, and 23 had background emissions data within the normal ranges, these outliers are indicative of errors in measurement caused by instrumentation failure or test procedure error.

7.3 NO_X Humidity Correction

Adjustments for engine intake air humidity were made to NO_X concentration data (measured in ppm). This was done according to Equation 7.1. This equation was developed from the 40 CFR Part 86. Calculations were completed on a modal basis.

$$[NO_X]_{adj} = [NO_X]\frac{k_{H_{MT}}}{k_{H_{AvgBase}}} \quad \text{Equation 7.1}$$

Where $[NO_X]_{adj}$ is the adjusted NO_X concentration in ppm, $[NO_X]$ is the NO_X concentration recorded during the test, $k_{H,MT}$ is the NO_X humidity correction factor specific to the test and mode, and $k_{H,AvgBase}$ is the average baseline NO_X humidity correction factor for the mode.

7.4 Oxidation Ratio

The oxidation ratio, OxR, is the percent NO_2 of total NO_X. It is calculated on a concentration basis according to Equation 7.2.

$$OxR = \frac{[NO_X]_{ppm} - [NO]_{ppm}}{[NO_X]_{ppm}} * 100 \quad \text{Equation 7.2}$$

7.5 Baseline Tests

Baseline tests were conducted so that the exhaust gas could be characterized. Knowing the exhaust NO_X concentration and composition allowed the scrubber unit to be adequately sized. These tests demonstrated the combined ability of the CPF and DOC to oxidize the NO to NO_2 over the four modes of the High Flow and Low Flow cycles. The ability of these catalysts to oxidize NO is primarily dependent upon gas flow rate or residence time, exhaust temperature, and catalyst platinum loading. Table 7.3 presents the results of the baseline tests for the exhaust gas after it had passed thought the CPF and DOC. The exhaust gas NO_X concentration and oxidation ratio are presented. The coefficient of variation in Table 7.3 is the standard deviation divided by the average

Table 7.3: Baseline NO_X Concentration and Oxidation Ratio

Mode	Low Flow Cycle				High Flow Cycle			
	NO_X		OxR		NO_X		OxR	
	Average (ppm)	Coefficient of Variation (-)	Average (%)	Coefficient of Variation (-)	Average (ppm)	Coefficient of Variation (-)	Average (%)	Coefficient of Variation (-)
1	2009	1.50E-03	66	1.09E-02	788	1.43E-03	NA	NA
2	2070	1.69E-02	68	2.42E-02	1394	1.41E-02	68	3.14E-03
3	2512	3.05E-02	75	3.39E-03	2186	1.19E-02	72	1.24E-03
4	1890	1.58E-02	85	7.89E-04	2128	1.00E-02	78	9.13E-03

7.6 Average System Results

The scrubber system was evaluated over the High Flow cycle for Height 1, Height 2, and Height 3. The system was evaluated over the Low Flow cycle for Height 3 only. The average results for all testing are presented in this section. All NO_X reduction results are presented in percent and based on NO_X emissions in g/kW-hr. Table 7.4 presents the average NO_X reduction results for the High Flow cycle, for all packing heights when the scrubbing system used a water liquor. Please refer to Appendix A for mass based NO_X emissions.

Table 7.4: Average NO_X Reduction Results for the High Flow Cycle – Water Liquor

	Reduction (%) - Water Liquor					
	Height 1		Height 2		Height 3	
Mode	NO_X	NO	NO_X	NO	NO_X	NO
1	12.6	NA	20.8	NA	28.3	13.2
2	3.2	2.3	10.6	8.1	21.4	12.9
3	12.2	0.0	24.1	6.2	36.0	11.4
4	24.3	7.1	33.6	25.9	45.5	23.9
Average	16.0	1.4	25.6	12.7	36.8	15.0

It may be seen in Table 7.4 that the average cycle NO_X reduction for Heights 1, 2, and 3 are 16.0%, 25.6%, and 36.8%, respectively. The NO_X reduction of the scrubber with a water liquor appears to increase almost linearly with height.

Table 7.5 presents the average NO_X reduction results for the High Flow cycle, for all packing heights when the scrubbing system used a hydrogen peroxide liquor.

Table 7.5: Average NO_X Reduction Results for the High Flow Cycle – Hydrogen Peroxide Liquor

	Reduction (%) - Hydrogen Peroxide Liquor					
	Height 1		Height 2		Height 3	
Mode	NO_X	NO	NO_X	NO	NO_X	NO
1	24.6	NA	24.8	NA	30.5	NA
2	8.6	9.0	15.5	5.3	22.3	13.1
3	21.6	9.4	33.5	11.4	40.8	19.1
4	38.6	28.4	41.4	39.8	50.4	43.5
Average	26.1	15.2	33.0	19.7	40.7	25.9

It may be seen in Table 7.5 that the average cycle NO_X reduction for Heights 1, 2, and 3 are 26.1%, 33.0%, and 40.7%, respectively. Using a hydrogen peroxide liquor with the scrubber appears to result in diminishing returns with an increase in height. When the scrubber utilizes a hydrogen peroxide liquor the NO_X absorption is increased as compared with the use of a water liquor. At Height 3 using a hydrogen peroxide liquor the project goal of reducing the NO_X emissions by greater than 40% was achieved with a test cycle average NO_X reduction of 40.7%.

The average modal NO_X reduction results for modes 2, 3, and 4 increases in series as expected. This was expected because the volumetric gas flow rate decreases with each mode and the oxidation ratio increases with each mode. According to NO_X absorption theory this will increase the overall NO_X absorption. Mode 1 however has a significantly higher NO_X reduction than mode 2. This is unexpected as it has a higher volumetric flow rate, lower NO_X concentration, and lower oxidation ratio than mode 2. The rational for this result is presented in Section 7.6.5.

Table 7.6 presents the average NO_X reduction results for the Low Flow cycle, for Height 3 when the scrubbing system used a hydrogen peroxide liquor.

Table 7.6: Average NO_X Reduction Results for the Low Flow Cycle – Hydrogen Peroxide Liquor

	Reduction (%) - Hydrogen Peroxide Liquor	
	Height 3	
Mode	NO_X	NO
1	45.5	31.2
2	60.1	34.2
3	65.8	43.8
4	62.0	38.6
Average	59.9	37.2

Over the Low Flow cycle, using a hydrogen peroxide liquor the scrubber was able to reduce the NO_X in the exhaust gas by an average of 59.9%. The NO_X reduction of this test cycle was likely higher than the High Flow cycle as the volumetric gas flow rates and inlet gas temperatures were lower.

7.7 Parameter Influence on NO_X Absorption

NO_X absorption literature indicates that multiple parameters influence the total NO_X absorption ability of scrubbers. This section investigates a number of these parameters and their respective influence on NO_X absorption within the marine scrubbing system.

7.7.1 Oxidation Ratio

Data collected from the marine scrubber system testing was analyzed to investigate the influence of the oxidation ratio on the scrubber performance. The oxidation ratio for all testing ranged from 66% - 85%. Due to the nature of the marine scrubber system, determining the influence of the oxidation ratio on the system performance was not possible as the oxidation ratio of the gas was shown by the test data to be too closely coupled with exhaust gas temperature. The test data collected did not allow for adequate separation of variables to sufficiently investigate the effect of the oxidation ratio on the absorption of NO_X species within the scrubber. It should be noted that NO_X absorption literature consistently ascertains that increasing the oxidation ratio increases the overall rate of the NO_X absorption process, for both water and hydrogen peroxide solution liquors. This is primarily because NO_2 is more soluble than NO[13].

7.7.2 Liquor Flow Rate

The influence of the liquor flow rate on scrubber performance was investigated. The total pressure drop over the packed bed section of the scrubber was used for this analysis as this parameter is directly related to the liquor flow rate through the packed bed. An increase in pressure drop indicates an increase in the liquor flow rate through the scrubber.

Test data of the same mode and height was selected for this analysis when the average liquor and inlet gas temperatures were within one degree Celsius of each other. Data from the water liquor test were collected and are presented in Figure 7.1. This figure is a plot of the pressure drop against the NO_X reduction, (presented as a percentage and based on g/kW-hr), for an individual mode. Figure 7.1 indicates that there is a positive relationship between pressure drop and NO_X reduction for the scrubber when using a water liquor. Not enough data exits to adequately define this relationship. The same data for a hydrogen peroxide liquor indicated that a relationship between pressure drop and NO_X reduction did not exist for the pressure drop (or liquor flow rate) range tested.

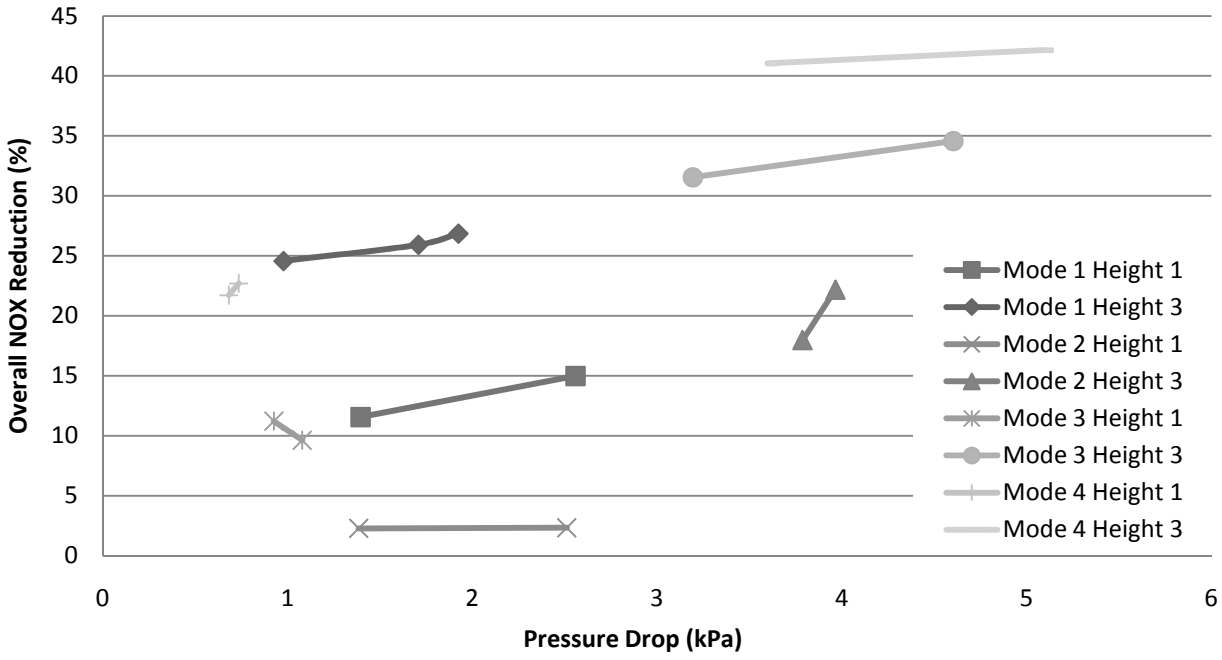

Figure 7.1: Influence of Pressure Drop on NO_X Absorption - Water Liquor

It is suggested that increasing the pressure drop across the column has two possible effects. The first being that the corresponding increased volume of liquid in the scrubber decreases the space available for the gas, reducing the gas residence time and therefore reducing the overall NO_X reduction ability of the scrubber. The second being that the increased pressure within the scrubber raises the partial pressure of the gaseous NO_X species therefore increasing the mass transfer driving force and hence the overall NO_X reduction ability of the scrubber. It should be noted that adequate liquor needs to be available for NO_X absorption to avoid increasing the liquid side resistance to mass transfer across the liquid film. Adequate liquor flow is usually calculated based upon Henry's law coefficient for the solute. It is difficult to calculate the required liquid flow rate for maximized NO_X absorption as multiple species are being absorbed simultaneously and Henry's law coefficient is not well defined for some of these species.

7.7.3 Gas Flow Rate

The influence of gas flow rate on total NO_X reduction was investigated. This was accomplished by determining the exhaust gas residence time for each mode for each packed height of the scrubber; as the gas residence time is directly proportional to the gas flow rate. The scrubber outlet concentration of NO_X for each mode and packing height was plotted against the gas residence time. A zero point (gas residence time) was also included in this analysis which represented the baseline NO_X emissions of the engine. Figure 7.2 and Figure 7.3 present the averaged modal data for a water liquor and hydrogen peroxide solution liquor, respectively. The error bars represent the upper and lower bounds of the averaged data for individual tests.

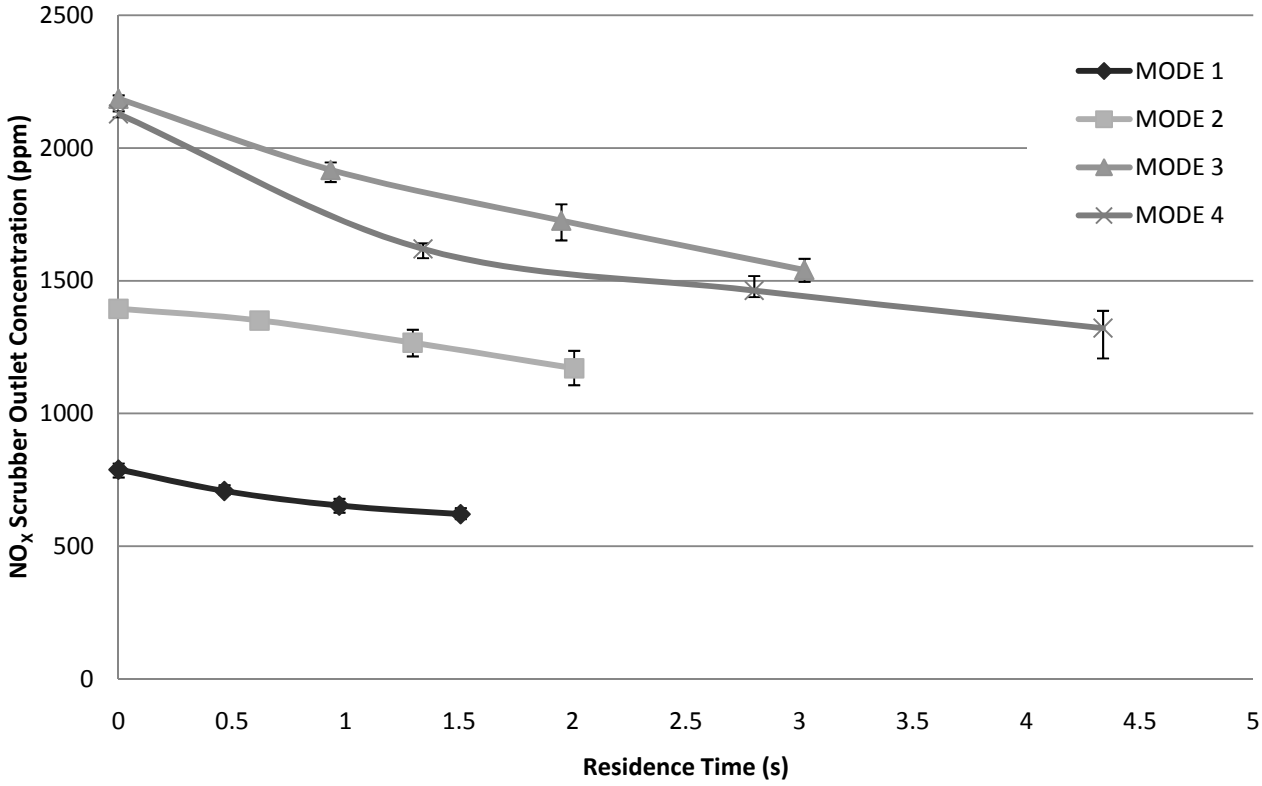

Figure 7.2: Influence of Residence Time on NO_X Scrubber Outlet Concentration - Water Liquor

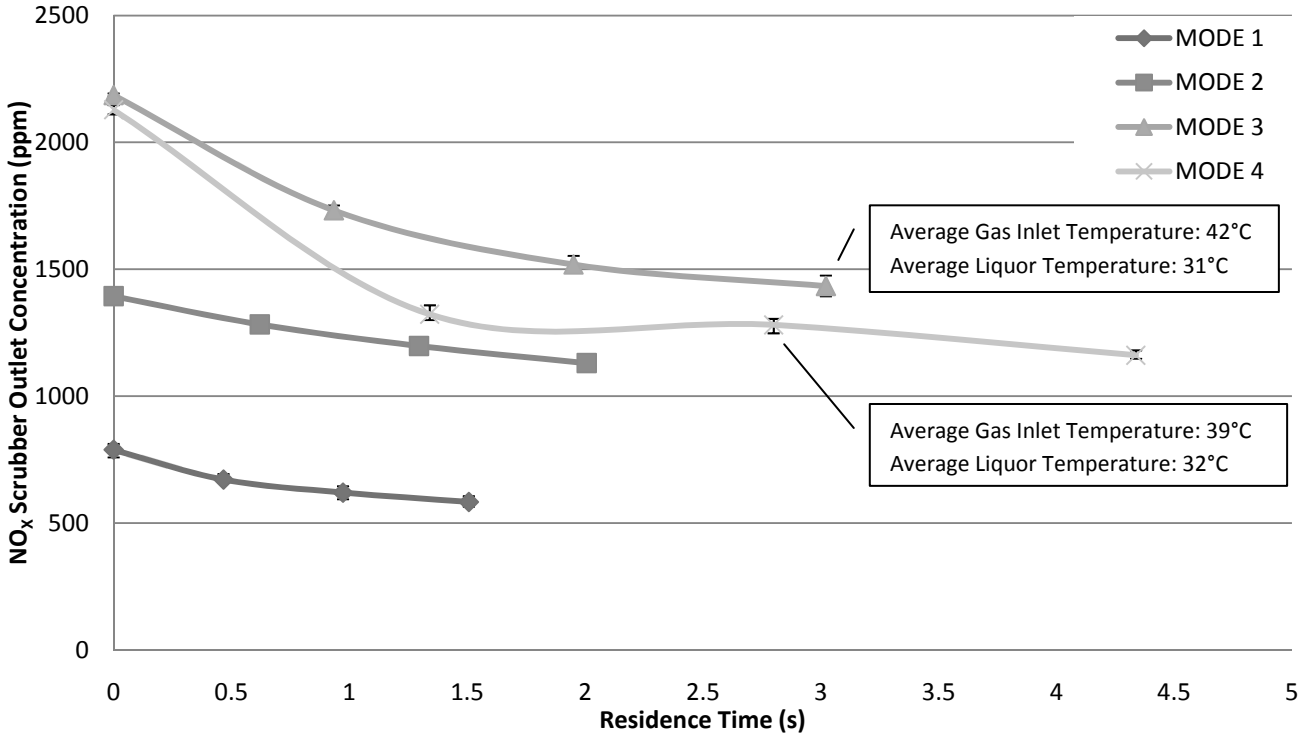

Figure 7.3: Influence of Residence Time on NO_X Scrubber Outlet Concentration - Hydrogen Peroxide Liquor

Figure 7.2 and Figure 7.3 show that the gas residence time has a significant impact on the scrubber's ability to reduce the exhaust gas NO_X concentration. The average modal NO_X reduction increases with an increase in gas residence time. According to NO_X absorption literature this phenomenon is expected. Modes 1, 3, and 4 indicate diminishing returns with increasing scrubber height (or gas residence time), for both liquor types.

7.7.4 Liquor Solution Type

The influence of type of scrubbing liquor on NO_X reduction was investigated. Figure 7.4 presents averaged, modal data for the reduction of NO and NO_X for the two different liquors used, water and hydrogen peroxide solution. The NO and NO_X reduction data are presented as a percentage of the baseline data and are based on g/kW-hr for NO or NO_X. In Figure 7.4, WA indicates a water liquor and PE indicates a hydrogen peroxide liquor. Table 7.7 presents the average percentage by which using hydrogen peroxide as a liquor enhanced total NO_X reduction for the four modes and three packing heights as compared with using a water liquor.

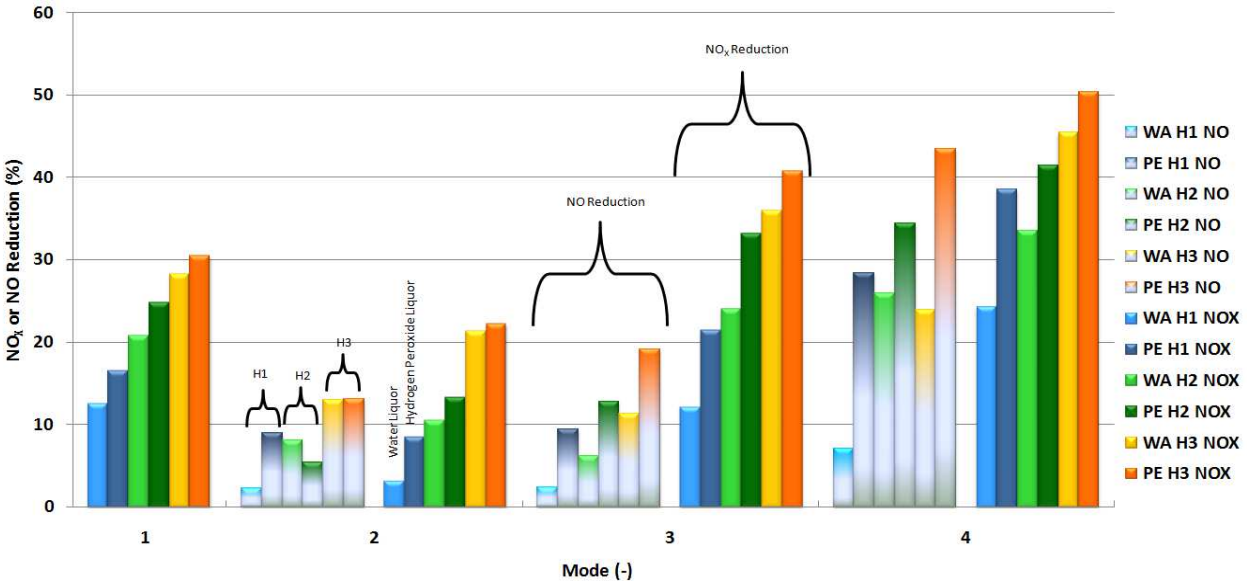

Figure 7.4: NO_X and NO Reduction Comparison for Water and Hydrogen Peroxide Solution Scrubbing Liquors

Table 7.7: Increase in NO_X Reduction from using a Hydrogen Peroxide Liquor Compared with a Water Liquor

	Increase in NO_X Reduction (%)			
	Mode 1	Mode 2	Mode 3	Mode 4
H1	4.1	5.3	9.4	14.2
H2	4.0	2.8	9.2	7.8
H3	2.2	0.9	4.8	4.9

It may be seen in Figure 7.4 that for all heights and modes, both NO and NO_X were reduced by a greater amount when a hydrogen peroxide solution was used; with the single exception of NO reduction for mode two at height

two. In most instances the total NO_X reduction was greater than the NO reduction indicating that a greater percentage of the total NO_2 was absorbed than NO. This is expected as NO_2 is more soluble and present in greater concentrations than NO. Table 7.7 shows that the benefit of using hydrogen peroxide as a liquor diminishes with an increase in packing height.

7.7.5 Gas and Liquor Temperature

The influence of inlet exhaust gas temperature and liquor temperature on the NO_X reduction ability of the scrubber was investigated. The liquor temperature has an influence on the exhaust gas exhaust temperature as the exhaust gas temperature was always that of the liquor temperature at the scrubber exhaust gas exit. The temperature analysis was achieved by selecting test modes that had similar inlet gas NO_X concentrations and residence times and comparing their modal NO_X reduction (in percent, based on g/kW-hr) with their inlet exhaust gas and liquor temperature. Table 7.8 and Table 7.9 present individual test data for the modes used for the temperature analysis for the scrubber when water and hydrogen peroxide liquor, respectively. The inlet NO_X concentrations in Table 7.8 and Table 7.9 are the average value of the baseline tests for each mode point for a given test cycle. Figure 7.5 presents the influence of inlet exhaust gas temperature on NO_X reduction when the scrubber used a hydrogen peroxide liquor.

Table 7.8: Temperature Correlation Data - Hydrogen Peroxide Liquor

Packing Height	Mode (#)	Inlet NO_X Concentration (ppm)	Residence Time (s)	Reduction (%)	Gas Temperature (°C)	Liquor Temperature (°C)
H3	High Flow Mode 3	2192.7	3.0	42.4	38.8	28.7
	High Flow Mode 3	2192.7	3.0	42.1	39.1	28.8
	High Flow Mode 3	2192.7	3.0	44.0	38.5	29.3
	High Flow Mode 3	2192.7	3.0	38.5	41.9	32.1
	High Flow Mode 3	2192.7	3.0	40.9	38.7	31.1
	High Flow Mode 3	2192.7	3.0	37.4	44.6	30.5
H2	High Flow Mode 4	2123.5	2.8	42.1	42.7	33.6
	High Flow Mode 4	2123.5	2.8	42.5	41.8	32.1
	High Flow Mode 4	2123.5	2.8	40.3	32.8	29.8
	High Flow Mode 4	2123.5	2.8	41.6	42.0	31.9
H3	Low Flow Mode 1	2009.1	3.0	45.3	23.9	26.1
	Low Flow Mode 1	2009.1	3.0	45.7	24.8	27.2

Table 7.9: Temperature Correlation Data - Water Liquor

Packing Height	Mode (#)	Inlet NO_X Concentration (ppm)	Residence Time (s)	Reduction (%)	Gas Temperature (°C)	Liquor Temperature (°C)
H3	High Flow Mode 3	2192.7	3.0	38.9	37.3	27.2
	High Flow Mode 3	2192.7	3.0	41.2	39.3	28.4
	High Flow Mode 3	2192.7	3.0	34.1	37.1	29.7
	High Flow Mode 3	2192.7	3.0	31.5	39.1	30.9
	High Flow Mode 3	2192.7	3.0	34.6	37.7	30.5
H2	High Flow Mode 4	2123.5	2.8	34.5	49.6	33.0
	High Flow Mode 4	2123.5	2.8	33.8	41.0	32.9
	High Flow Mode 4	2123.5	2.8	33.9	42.2	33.4
	High Flow Mode 4	2123.5	2.8	33.1	39.6	29.8

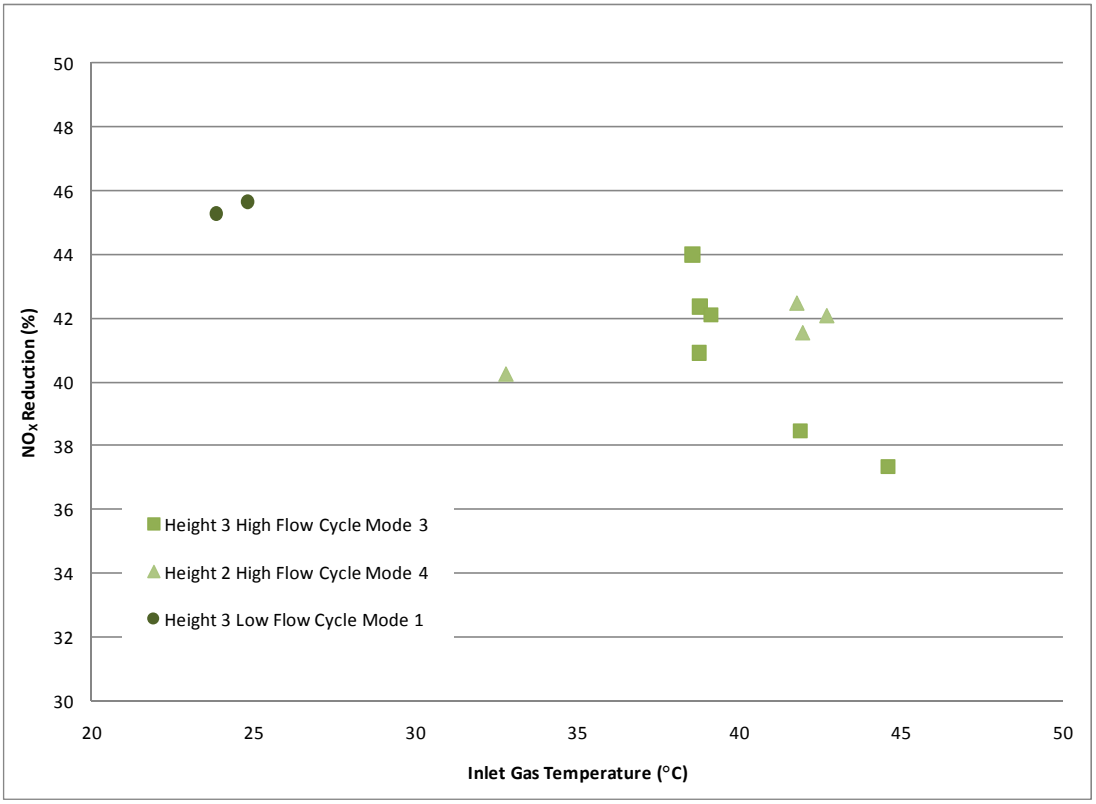

Figure 7.5: Influence of Inlet Gas Temperature on NO_X Reduction – Hydrogen Peroxide Liquor

Figure 7.5 shows that an inverse relationship exists between the inlet gas temperature and NO_X reduction ability of the scrubber. According to NO_X absorption literature this is expected. When the exhaust gas entered the scrubber at 44.6°C a modal NO_X reduction of 37.4% was seen. Under similar conditions with a reduced exhaust gas inlet temperature of 24.8°C the modal NO_X reduction was increased to 45.7%.

Generally the liquor temperature would vary by less than two degrees Celsius over a single mode. Figure 7.6 and Figure 7.7 present the influence of liquor temperature on NO_X absorption for a water only and hydrogen peroxide liquor, respectively. NO_X absorption is presented as a percentage and is based on NO_X in g/kW-hr. Figure 7.5, Figure 7.6, and Figure 7.7 are presented with the same axis range for comparison.

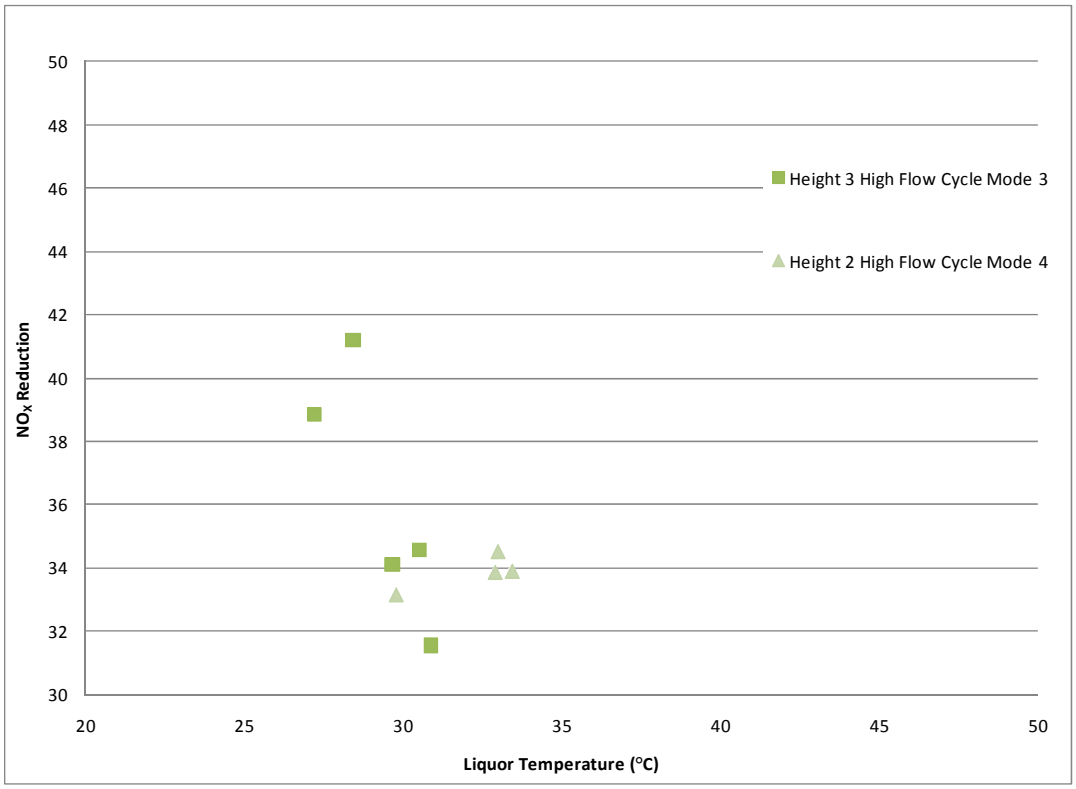

Figure 7.6: Influence of Liquor Temperature on NO_X Reduction – Water Liquor

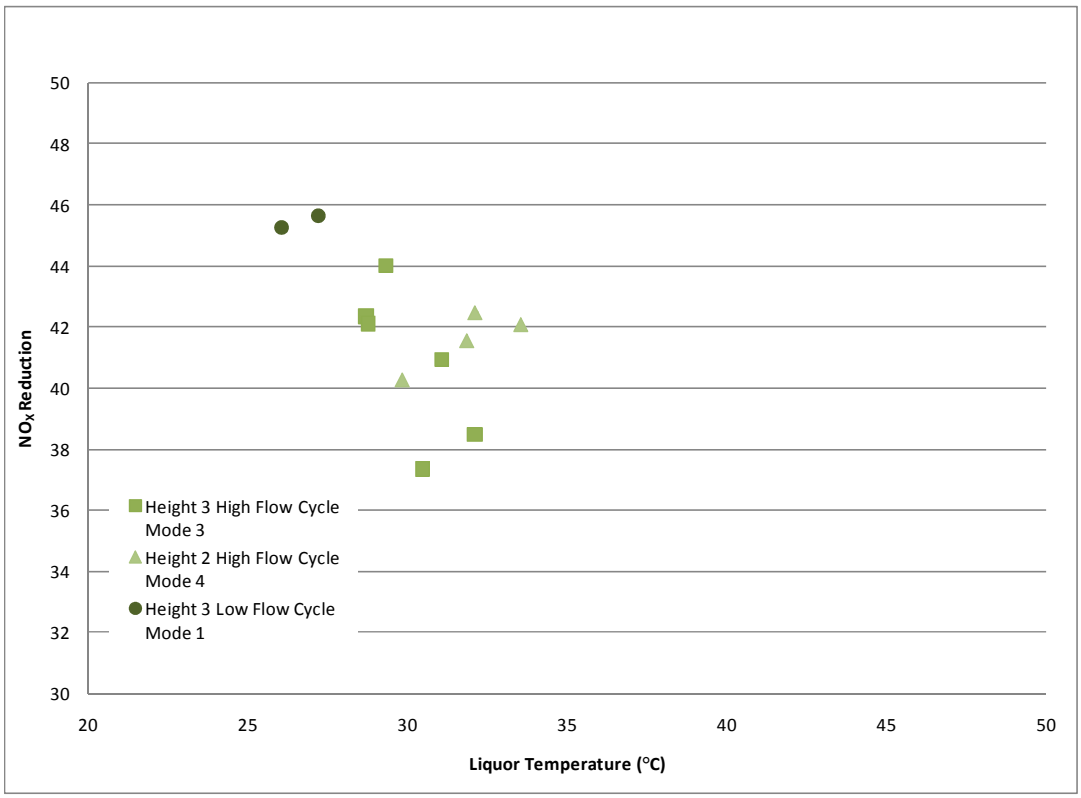

Figure 7.7: Influence of Liquor Temperature on NO_X Reduction – Hydrogen Peroxide Liquor

Figure 7.6 and Figure 7.7 demonstrate that a decrease in liquor temperature results in a higher overall NO_X absorption. This appears to be a loose correlation as the data in these figures are scattered. Applying a linear trendline produces an R-squared value of 0.39 and 0.34 for Figure 7.6 and Figure 7.7, respectively.

Modes One and Two

Modes 1 and 2 provide an example of how significantly the exhaust gas temperature can negatively impact the NO_X absorption process when using either water or hydrogen peroxide liquors. Modes 1 and 2 had a scrubber inlet NO_X concentration of 788 and 1394 ppm, respectively. Mode 1 had an approximated oxidation ratio of 57% and mode 2 had an oxidation ratio 69%. Mode 1 had an exhaust gas flow rate of 0.30 m^3/s and mode 2 had an exhaust gas flow rate of 0.23 m^3/s. According to the literature, given these three parameters (inlet NO_X concentration, oxidation ratio, and gas flow rate) mode 2 should have a higher NO_X reduction than mode 1, however scrubber system testing revealed that the system was better at reducing the exhaust gas NO_X concentration during mode 1 rather than during mode 2. Table 7.10 presents averaged modal data for modes 1 and 2 for Height 1.

Table 7.10: Influence of Gas Temperature on NO_X Reduction for Modes 1 and 2

	Water Liquor		Hydrogen Peroxide Liquor	
	Mode 1	Mode 2	Mode 1	Mode 2
NO_X Reduction (%)	12.57	3.25	24.62	8.57
Inlet Gas Temperature (°C)	23.93	41.90	23.26	40.30
Liquor Temperature (°C)	31.37	33.94	32.00	33.51

It may be seen in Table 7.10 that the NO_X reduction of mode 1 was about triple that of mode 2. The temperature of the scrubbing liquor varied by only a few degrees Celsius; while the inlet temperature of the exhaust gas was around 17°C higher for mode 2. This indicates that the inlet gas temperature for the scrubbing system has a significant effect on its NO_X reduction ability.

7.8 System Operation

7.8.1 Fuel Consumption

Attaching the heat exchanger and scrubber to the engine exhaust increased the exhaust backpressure. This caused an increase in the fuel consumption and therefore a reduction in its overall power generating efficiency. Table 7.11 presents the average modal fuel consumption for the baseline and each scrubber packing height tested. It also includes the average percentage increase in fuel consumption for each mode and scrubber packing height.

Table 7.11: Fuel Consumption Data

		Mode 1	Mode 2	Mode 3	Mode 4	Cycle Average
Baseline	Average Fuel Consumption (g/s)	12.36	9.55	5.73	2.97	7.65
	Standard Deviation (g/s)	0.65	0.08	0.03	0.02	0.19
Height 1	Average Fuel Consumption (g/s)	16.20	9.58	5.74	3.03	8.64
	Standard Deviation (g/s)	0.39	0.05	0.03	0.04	0.13
	Average Increase (%)	31.00	0.30	0.21	1.85	12.83
Height 2	Average Fuel Consumption (g/s)	17.45	9.58	5.81	3.02	8.97
	Standard Deviation (g/s)	0.05	0.09	0.02	0.06	0.05
	Average Increase (%)	41.17	0.34	1.34	1.74	17.15
Height 3	Average Fuel Consumption (g/s)	17.39	9.62	5.87	3.10	8.99
	Standard Deviation (g/s)	0.10	0.07	0.04	0.07	0.07
	Average Increase (%)	40.68	0.69	2.33	4.21	17.48

It may be seen that modes 2, 3, and 4 did not significantly impact the fuel consumption of the engine. The increase in fuel consumption for these modes, for all heights, ranged between 0.03% - 4.21%. The increase in fuel consumption for mode 1 was significant, an order of magnitude greater than the other modes. It is suggested that this was caused by an increase in backpressure on the engine at high exhaust flow rates. This may be alleviated by increasing the diameter of the scrubber or reducing the liquor flow rate. The cycle average increase in fuel consumption increased non-linearly with height from 12.83% to 17.48%. These values have the potential to be significantly reduced if the fuel consumption issue for mode one is addressed.

7.8.2 Hydrogen Peroxide Consumption

The hydrogen peroxide present in the scrubbing liquor was consumed according to Equations 2.15 through 2.19. The hydrogen peroxide consumption for different heights and the two test cycles was calculated. These calculations were based on the additional NO_X reduction seen between the tests with water only and water-hydrogen peroxide scrubbing liquors. Hydrogen peroxide consumption is presented in Table 7.12.

Table 7.12: Hydrogen Peroxide Consumption

Cycle and Height	Peroxide Consumption (g/hr)				
	Mode 1	Mode 2	Mode 3	Mode 4	Cycle Average
High Flow - Height 1	91.20	121.78	231.12	229.07	168.29
High Flow - Height 2	86.86	111.19	231.12	127.43	139.15
High Flow - Height 3	56.46	10.59	70.27	74.33	52.91
Low Flow - Height 3	1042.1	556.4	880.6	590.9	767.5

Hydrogen peroxide consumption was also calculated on a fuel consumption basis. The hydrogen peroxide consumption rates, (shown in Table 7.12), were divided by the actual fuel consumption of the engine. This data is presented in Table 7.13.

Table 7.13: Hydrogen Peroxide Consumption on Fuel Consumption Basis

Cycle and Height	Peroxide Consumption (g H_2O_2/g Fuel)				
	Mode 1	Mode 2	Mode 3	Mode 4	Cycle Average
High Flow - Height 1	2.36E-03	3.64E-03	1.16E-02	2.27E-02	1.01E-02
High Flow - Height 2	2.02E-03	4.07E-03	1.11E-02	1.23E-02	7.38E-03
High Flow - Height 3	1.31E-03	3.87E-04	3.38E-03	7.17E-03	3.06E-03
Low Flow - Height 3	2.42E-02	2.04E-02	4.24E-02	5.70E-02	3.60E-02

It may be seen in Table 7.12 and Table 7.13 that total hydrogen peroxide consumption decreases with scrubber height. It is suggested that this is because the scrubber itself is able to achieve greater NO_X reduction levels with increased height and therefore has a reduced requirement for the hydrogen peroxide. The cycle average hydrogen peroxide consumption was higher for the Low Flow cycle than the High Flow test cycle. This was expected as the Low Flow cycle had significantly higher NO_X reduction.

7.8.3 Liquor Sample Analysis

A sample of the liquor was analyzed by the National Research Center for Coal and Energy at WVU. The sample was taken from the scrubber when it was at Height 3 and after it had been using a hydrogen peroxide liquor. Table 7.14 presents the results of the sample analysis.

Table 7.14: Sample Analysis Results

Analyte	Unit	Value
pH	-	1.91
Acidity	mg/L	2893.1
Conductivity	uS/cm	2560
Total Dissolved Solids	mg/L	504
Total Kjeldahl Nitrogen	ppm	2.12
Aluminum	mg/L	0.45
Calcium	mg/L	31.4
Iron	mg/L	2.6
SO_4	mg/L	64.7
NO_2	mg/L	1.6
NO_3	mg/L	892.6

Analyte	Unit	Value
Boron	mg/L	0.16
Copper	mg/L	7.4
Magnesium	mg/L	3.4
Manganese	mg/L	0.039
Nickel	mg/L	0.19
Phosphorus	mg/L	1.21
Lead	mg/L	0.54
Sulfur	mg/L	9.66
Tin	mg/L	0.051
Strontium	mg/L	0.066
Zinc	mg/L	5.69

Manganese and iron are both present in 'tap' water and stainless steel, so the presence of these elements in the sample may have been caused by either source. The copper in the sample may have come from the copper in the pipes that 'tap' water travels though.

7.8.4 By-product Disposal

The NO_X emissions from the diesel engine are absorbed into the scrubbing liquor and stored in the form of nitric acid. Due to the negative impact of pH and nitrification on ocean water ecosystems, the liquor should not be discharged into ocean or bay area waters. Ultimately, most of the NO_X emitted by diesel marine engines reacts with atmospheric water vapor to form nitric acid. It is then precipitated into the surrounding ocean or bay area waters having the same effect as discharging scrubber liquor directly into the ocean or bay area waters[35]. The acid may have value as an input to other chemical processes like the production of fertilizer. Acid destruction methods were researched at WVU. It was shown that an acid boiler vessel design can successfully decompose greater than 99% of nitric acid (10 wt %) into water, oxygen, and nitrogen dioxide. This method incorporated the use of two three-way-catalysts and small amounts of diesel fuel (the optimal mass based acid-to-fuel ratio ranged between 1:49.8 and 1:58.9). A full report on this research is presented in a report submitted to M.J. Bradley & Associates, LLC[36].

7.9 Modeling

7.9.1 Packed Bed Height Prediction

The scrubber system design, using a hydrogen peroxide liquor, achieved the average cycle NO_X reduction project goal of greater than 40%. The average NO_X reduction for all of the test cycles with a water scrubbing liquor can be seen in Figure 7.8. The single black columns are baseline emissions. Each set of columns from left to right corresponds to the emissions for the Heights 1, 2, and 3, respectively.

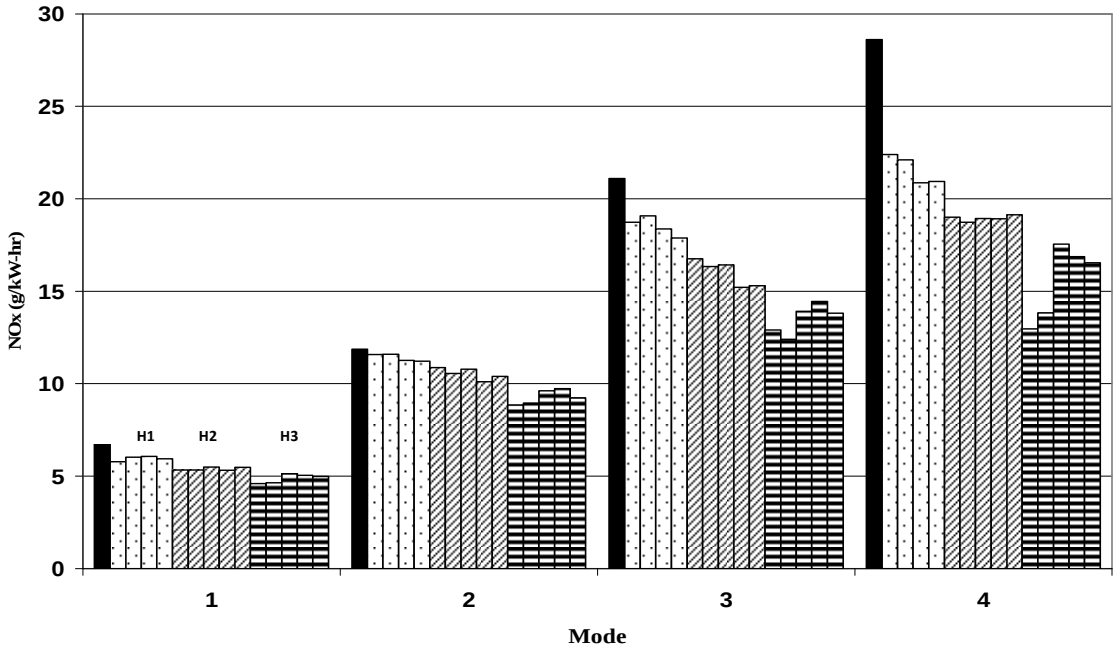

Figure 7.8: Average NO_X Reduction for All of the Test Cycles - Water Scrubbing Liquor

Figure 7.9 shows a plot of the average cycle NO_X reduction for the three scrubber packing heights, for both liquor types, for the high flow cycle. A best fit linear trendline was applied to each set of data. Table 7.15 presents the required scrubber heights for a desired average cycle NO_X reduction of 75% or 90% using the linear trendline for both liquors.

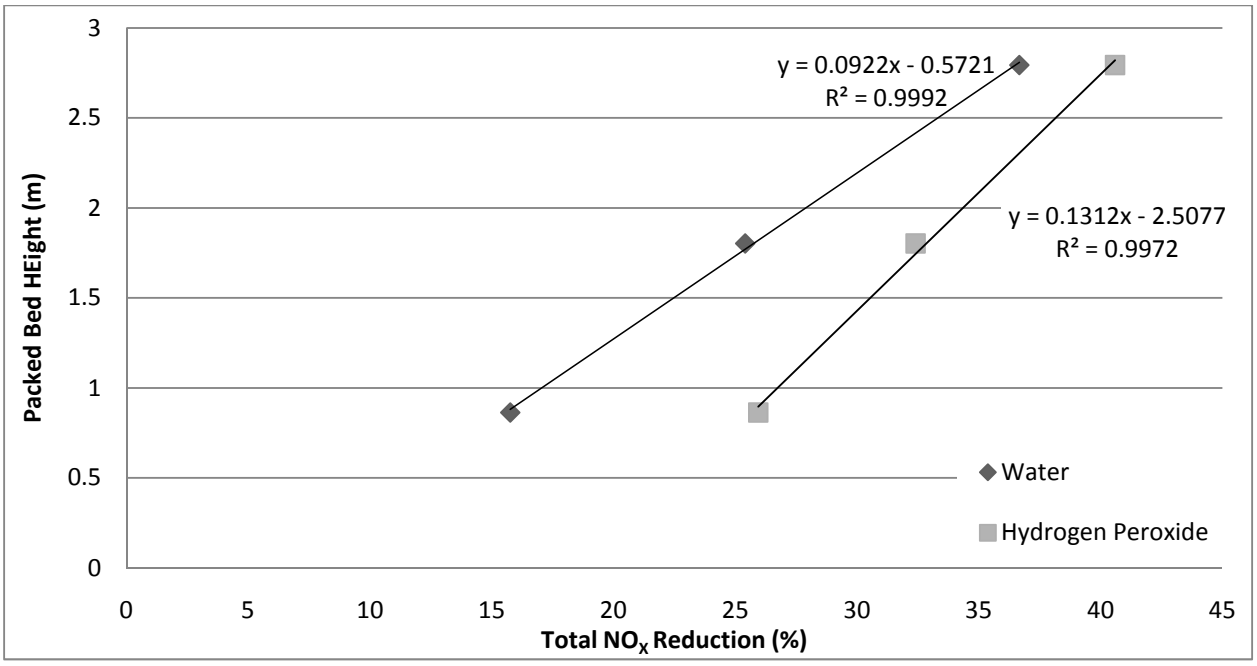

Figure 7.9: Average Cycle NO_X Reduction for the Three Scrubber Packing Heights

Table 7.15: Required Scrubber Heights for Desired Average Cycle NO_X Reduction of 75% or 90%

Liquor Type	Projected Required Scrubber Height (m)	
	90% Average NO_X Cycle Reduction	75% Average NO_X Cycle Reduction
Water	8.9	7.5
Hydrogen Peroxide	14.3	7.3

Interestingly, the trendlines predict that a smaller packed bed height is required for a water liquor than for a hydrogen peroxide liquor for a NO_X reduction of 90%. It is expected that this phenomena is unrelated to liquor type and dependent upon experimental conditions, for example liquor and inlet gas temperature. For an average High Flow cycle NO_X reduction of 90% the trendlines predict that a packed bed height of 8.9 m and 14.3 m are required for a water and hydrogen peroxide liquor, respectively.

7.9.2 Modeling Comparison

Two programs were used to model the results, Simulink and ProSimPlus HNO3. The simulink model was developed using correlations found in the literature. It included three reaction pathways, one each for NO_2, N_2O_3, and N_2O_4. The ProSimPlus HNO3 program was purchased and required only a description of absorber dimensions, packing parameters and flows. Both models used an available surface area packing factor; a value of 92 m^{-1} was provided by the manufacturer. Total NO_X reduction for the modeling comparison was based on NO_X concentration (in ppm).

Both models were steady state models and did not account for variations in inlet gas or liquor temperature over a mode. The Simulink model did not account for heat transfer between the phases or heat evolution from the chemical reactions. It is likely that the Simulink model could therefore be optimized in the future by accounting for heat energy transfer and heat of reactions. Table 7.16 presents the results of the modeling comparison.

Table 7.16: Modeling Comparison Data

		Total NO_X Reduction (%)		
Height	**Mode**	**Simulink Model**	**ProSim HNO3**	**Actual Results**
Height 1	1	2.96	16.27	24.62
	2	6.53	26.73	8.57
	3	14.52	39.54	21.57
	4	20.21	52.88	38.57
Height 2	1	5.97	28.27	24.81
	2	12.63	39.25	13.42
	3	26.03	52.29	33.26
	4	34.46	63.61	41.43
Height 3	1	8.88	36.11	30.50
	2	18.12	47.03	22.28
	3	34.98	59.51	40.81
	4	44.54	68.86	50.42

Mode 1 had higher absorption rates in than modes 2 and 3. This was unexpected because modes 2 and 3 had lower flow rates, higher oxidation ratios and higher initial NO_X concentrations than mode 1. The Simulink model was unable to account for the high NO_X absorption of mode 1. The Simulink model consistently produced results closer to actual results for modes 2, 3, and 4. While the ProSim model consistently produced results closer to the actual results for mode 1.

8 Conclusions

Oxides of nitrogen emissions have negative impact on human health and the environment. NO_X emissions from diesel marine engines are regulated by the EPA. Scrubber systems as a NO_X emissions reduction technology require little chemical additives, do not need to communicate with the engine, and can use gulf water as a cold sink for cooling the exhaust gas. Theory on the NO_X absorption process was presented. The absorption of NO_X gas into water is one of the most complex known absorption processes. Both the gas and liquid phase species exist in equilibrium with one another, chemical reactions proceed the desorption of NO_X species, and chemical reactions follow the absorption of NO_X species. Adding low concentrations of hydrogen peroxide to the scrubbing liquor can reduce the desorption of NO_X species and aid in overall NO_X absorption. Nitric acid is the generated by-product of the NO_X absorption process (less than 10 wt%).

A marine scrubber system for the removal of NO_X emissions from diesel marine engine exhaust was designed, fabricated, tested, and analyzed. Emissions for testing were generated by a 298 kW 1992 Mack E7 diesel engine. An optimized scrubbing system will have minimized exhaust temperatures, maximum oxidation of NO to NO_2 in the exhaust, and high interfacial surface area within packed bed of the scrubber. The final laboratory apparatus for the scrubber system consisted of a CPF, DOC, air-to-liquid heat exchanger, scrubbing unit, and scrubbing liquor pump.

Two cycles were tested on the system, the High Flow cycle and Low Flow cycle. The average cycle NO_X reduction increased with packed bed height. Using a water liquor the NO_X reduction increase appears to be linear with height. Using a hydrogen peroxide liquor, the increase in total NO_X reduction appears to have diminishing returns with an increase in packed bed height. At Height 3 using a hydrogen peroxide liquor the system was able to reduce an average of 62% of the NO_X emissions over the Low Flow cycle. Over the High Flow cycle NO_X emissions were reduced by 41%.

There appears to be a positive relationship between NO_X reduction and liquor flow rate when a water liquor was used, although there were insufficient data to quantify this relationship. The gas residence time had a significant impact on NO_X reduction ability of the scrubber. An increase in gas residence time resulted in an increase in NO_X reduction. Modes 1, 3, and 4 demonstrated diminishing returns for an increase in gas residence time, when either a water or hydrogen peroxide liquor was used.

The NO_X reduction for every mode and packed bed height was greater when hydrogen peroxide liquor was used, relative to that of a water liquor. When a hydrogen peroxide liquor was used, there was diminishing benefit to increasing the packed bed height. Hydrogen peroxide consumption within the scrubber unit decreased with an increase in height.

The absorption of NO_2 was almost always greater than that of NO; this indicated that increasing the oxidation ratio was beneficial to total NO_X absorption. The influence of inlet gas temperature on NO_X reduction appeared to be significant. NO_X reduction increased with a decrease in inlet gas temperature. A similar correlation between NO_X reduction and liquor temperature was also observed.

The scrubber system caused the fuel consumption for modes 2 through 4 to be increased by 0.03% to 4.21%. The fuel consumption was significantly increased for mode 1. The average cycle fuel consumption increased from the baseline by 12.83%, 17.15%, and 17.48% for packed bed heights 1, 2, and 3, respectively.

9 Recommendations

1. The marine scrubber system is particularly sensitive to temperature. Testing showed that NO_X reduction can be substantially enhanced by reducing the inlet gas temperature. While testing the system the inlet gas temperature was often significantly above the 21.9°C design minimum; the average modal temperature was 34.8°C, it ranged between 17.7°C and 50.0°C. Future design and testing should have the gas inlet temperature closer to 21.9°C.

2. Increasing the gas residence time of the exhaust gas was shown to increase the overall NO_X reduction ability of the scrubber system. It is therefore recommended that the packed bed size be increased. This may be achieved through either increasing the backed bed diameter or height. When increasing the packed bed size, the packing should be adequately supported and gas and liquid streams should not be allowed to become mal-distributed throughout the bed.

3. An investigation of the liquor flow rate, pressure drop, exhaust back pressure and consequently the power generating efficiency of the engine should be investigated. Particularly for mode 1, as fuel consumption increased significantly by ~41% for Heights 2 and 3.

4. Increasing the oxidation ratio of the exhaust gas is known to have a positive effect on NO_X absorption. The oxidation ratios of the exhaust gas during testing ranged from 59% to 78%. It is recommended that additional efforts be made to increase this ratio.

10 Cited Works

1. Pulkrfabek, W.W.; “Engineering Fundamentals of the Internal Combustion Engine,” Second Edition, Pearson Prentice Hall, Upper Saddle River, NJ, 2004.
2. Majewski, W.A.; “Diesel Emission Control,” DieselNet, 2007, Accessed April 24th 2011, <http://www.dieselnet.com/tech/engine_control.html>.
3. Yu, R., Cole, A., Strola, B., and Huang, S., “Development of Diesel Exhaust Aftertreatment System for Tier II Emissions,” SAE Paper No. 2002-01-1867, 2002.
4. Skalska, K., Miller, J., and Ledakowicz, S.; “Trends in NO_X Abatement: A Review,” Science of the Total Environment, 2010, Vol. 408, pp. 3976-3989.
5. Pohanish, R. P.; “HazMat Data - For First Response, Transportation, Storage, and Security,” Second Edition, 2004, John Wiley & Sons, Hoboken, NJ, USA.
6. United Nations Environment Programme; “Global Environment Outlook (GEO-4),” ISBN 978-92-807-2836-1, 2007.
7. United States Environmental Protection Agency; “Commercial Marine Emissions Inventory for EPA Category 2 and 3 Compression Ignition Marine Engines in the United States Continental and Inland Waterways,” Document No. EPA420-R-98-020, August 1998.
8. R. Henningsen, MARINTEK; “Study of Greenhouse Gas Emissions from Ships,” International Maritime Organization Issue 2-3, March 2000.
9. Charmley, W.J.; “The Federal Government’s Role in Reducing Heavy Duty Diesel Emissions,” SAE Paper No. 2004-01-2708, 2004.
10. United States Environmental Protection Agency; “National Ambient Air Quality Standards,” United States Environmental Protection Agency, Accessed 31 December 2009, <www.epa.gov>.
11. Dieselnet; “Emissions Standards, United States, Marine Diesel Engines,” Dieselnet, Accessed December 29 2009, <www.dieselnet.com/standards/us/marine.php>.
12. Schifftner K. and Hesketh H.; “Wet Scrubbers,” Second Edition, Technomic Publishing Co., Inc., Pennsylvania, 1996.
13. Joshi, J., Mahajani, V., and Juvekar, V.; “Invited Review, Absorption of NO_X Gases,” Chemical Engineering Communications, 1985, Vol. 33, pp. 1-92.
14. Krystallon, Ltd.; “Seawater Scrubbing: Technology and History,” Krystallon Ltd., Accessed July 2009. <http://www.krystallon.com/technology-history.html>.
15. An S. and Nishida. O.; “Marine Air Pollution Control System Development Applying Seawater and Electrolyte,” SAE Paper No. 2002-01-2295, 2002.
16. Suchak, N., Jethani, K., and Joshi, J.; “Modeling and Simulation of NO_X Absorption in Pilot-Scale Packed Columns,” AICHE Journal, 1991, Vol. 37, No. 3, pp. 323-339.

17. Kenig, E., Wiesner, U., and Gorak, A.; “Modeling of Reactive Absorption Using the Maxwell-Stefan Equations,” Journal of Industrial & Engineering Chemistry Research, 1997, Vol. 36, pp. 4325-4334.
18. Emig, G., Wohlfahrt, K., and Hoffmann, U.; “Absorption with Simultaneous Complex Reactions in Both Phases, Demonstrated By the Modeling and Calculation of a Countercurrent Flow Column for the Production of Nitric Acid,” Journal of Computers and Chemical Engineering, 1979, Vol. 3, pp. 143-150.
19. Thomas, D. and Vanderschuren, J.; “Modeling of NO_X Absorption into Nitric Acid Solutions Containing Hydrogen Peroxide,” Journal of Industrial & Engineering Chemistry Research, 1997, Vol. 36, pp. 3315-3322.
20. Suchak, N., Jethbani, K., and Joshi, J.; “Modeling and Simulation of NO_X Absorption in Pilot-Scale Packed Columns,” AIChE Journal, 1991, Vol. 37, no. 3, pp. 323-339.
21. Lee, Y. and Schwartz, S.; “Reaction Kinetics of Nitrogen Dioxide with Liquid Water at Low Partial Pressure,” Journal of Physical Chemistry, 1981, Vol. 85, pp. 840-848.
22. Sander, R.; “Compilation of Henry's Law Constants for Inorganic and Organic Species of Potential Importance in Environmental Chemistry (Version 3),” 1999, Accessed July 2009, <http://www.henrys-law.org>.
23. Kameoka, Y. and Pigford, R.; “Absorption of Nitrogen Dioxide into Water, Sulfuric Acid, Sodium Hydroxide and Alkaline Sodium Sulfite Aqueous Solutions,” Journal of Industrial and Engineering Chemistry Fundamentals, Vol. 16, No. 1,pp. 163-169, 1977.
24. Chambers, F. and Sherwood, T.; “Absorption of Nitrogen Dioxide by Aqueous Solutions,” Journal of Industrial and Engineering Chemistry Research, Vol. 29, pp. 1415-1422, 1937.
25. Jenthi, K., Suchak, N., and Joshi, J.; “Selection of Reactive Solvent for Pollution Abatement of NO_X,” Gas Separation and Purification, Vol. 4, pp. 8-28, 1990.
26. Thomas, D., and Vanderschuren, J.; “Effect of Temperature on NO_X Absorption into Nitric Acid Solutions Containing Hydrogen Peroxide,” Journal of Industrial and Engineering Chemistry Research, Vol. 37, pp. 4418-4423, 1998.
27. Kenig, E. and Seferlis, P.; “Modeling Reactive Absorption,” Chemical Engineering Progress, Vol. 105, No. 1, 2009.
28. Denckwerts, P.; “Gas-Liquid Reactions,” McGraw-Hill Chemical Engineering Series, 1970
29. Richardson, J., Harker, J., and Backhurst, J.; “Coulson and Richardson's Chemical Engineering Volume 2 - Particle Technology and Separation Processes,” 5^{th} Edition, Butterworth Heinmann, Oxford, United Kindom, 2007.
30. Perry, H. and Green, D.; “Perry’s Chemical Engineers’ Handbook,” 8^{th} Edition, McGraw-Hill Companies, China, 2008.
31. Bird, B., Stewart, W., and Lightfoot, E.; “Transport Phenomena,” Second Edition, John Wiley & Sons, USA, 2007.

32. National Oceanographic Data Center (NODC), NOAA, U.S. Department of Commerce, Accessed April 2011, <http://www.nodc.noaa.gov/dsdt/cwtg/wgof.html>.
33. Richards, J.; "Control of Gaseous Emissions, Student Manual," Third Edition, ICES Ltd., 2000, EPA Contract No. 68D99022.
34. Raschig Jaeger Technologies; "Jaeger Tri-Packs/Hacketten, Product Bulletin 600," Raschig Jaeger Technologies, Accessed December 2009, <http://www.jaeger.com/Brochure/Series600-09.pdf>.
35. Butler, T., Likens, G., Vermeylen, F., and Stunder, B.; "The Relation Between NO_X Emissions and Precipitation NO_3^- in the Eastern USA," Atmospheric Environment, Vol. 37, pp. 2093-2104, 2003.
36. Johnson, D., Ayre, L., and Clark, N.; "Marine Engine Sea Water Scrubber Report," Center for Alternative Fuels, Engines and Emissions, West Virginia University, 2011, Submitted to M.J. Bradley & Associates.

11 Appendix A

Baseline Test Data

Test Information			Background Data			
Test Name	Date	Test Description	CO (ppm)	CO_2 (ppm)	NO_X (ppm)	HC (ppm)
1	10/7/2010 and 2/10/2011	High Flow Test Cycle	13.4661	468.24	-0.665	2.5996
2	10/7/2010 and 2/10/2011		13.4414	460.61	-0.793	2.5267
3	10/7/2010 and 2/10/2011		13.3741	457.17	-0.699	2.4848
4	1/27/2011	Low Flow Test Cycle	11.5333	394.19	-1.622	3.0609
5	1/27/2011		11.1321	388.09	-1.737	2.8104

	Engine Data				Emissions Data			
Mode	Work (kW-hr)	Torque (kN.m)	Fuel Consump-tion (kg/kWhr)	CO_2 (g/kWhr)	Measured NO (ppm)	Measured NO_x (ppm)	NO (g/kWhr)	NO_x (g/kWhr)
1	4.98	1.623866	0.2071	497.148	109.384	293.54	3.571	6.827
2	2.94	1.099706	0.1948	619.661	99.792	312.84	3.882	12.006
3	1.74	0.759666	0.1994	634.546	90.817	323.64	6.085	21.341
4	0.82	0.426677	0.2183	694.463	46.774	215.07	6.383	28.411
1	4.98	1.630374	0.2077	495.81	115.712	291.51	3.61	6.799
2	3	1.120992	0.1926	612.912	99.971	309.78	3.822	11.683
3	1.73	0.755598	0.2002	636.981	88.832	317.91	5.994	21.104
4	0.82	0.430744	0.2215	704.797	50.083	218.08	6.754	28.528
1	4.97	1.626035	0.2064	493.631	117.019	291.45	3.41	6.809
2	2.96	1.107841	0.1937	616.25	98.892	306.5	3.825	11.71
3	1.74	0.760344	0.199	632.984	88.864	316.04	5.936	20.802
4	0.8	0.416643	0.2232	710.137	46.065	212.08	6.409	28.635
1	4.34	1.028118	0.197	626.936	101.177	297.91	5.423	15.88
2	1.58	0.746514	0.2305	733.209	37.816	115.53	5.834	17.543
3	1.65	0.668013	0.2205	701.488	43.501	169.6	6.362	24.402
4	0.72	0.254081	0.2562	815.053	19.546	131.76	6.316	40.706
1	4.33	1.024051	0.1979	629.62	104.032	297.43	5.618	15.966
2	1.57	0.744888	0.2297	730.599	35.995	118.44	5.571	17.964
3	1.71	0.692011	0.2208	702.412	41.587	164.43	5.913	22.928
4	0.68	0.242421	0.262	833.355	18.953	126.95	6.478	41.207

Height One Test Data (1 of 2)

Test Information			Background Data			
Test Name	Date	Test Description	CO (ppm)	CO_2 (ppm)	NO_X (ppm)	HC (ppm)
6	2/10/2011	Water Liquor High Flow Test Cycle Height One	13.8337	401.42	-0.899	2.6331
7	2/10/2011		-0.2422	424.52	-0.775	2.6062
8	2/10/2011		13.8307	436.18	-0.819	2.6093
9	2/10/2011		14.0234	439.35	-0.907	2.5449

	Engine Data				Emissions Data			
Mode	Work (kW-hr)	Torque (kN.m)	Fuel Consump-tion (kg/kWhr)	CO_2 (g/kWhr)	Measured NO (ppm)	Measured NO_X (ppm)	NO (g/kWhr)	NO_X (g/kWhr)
1	4.78	1.565023	0.1545	491.452	107.859	225.18	2.802	5.791
2	2.96	1.107298	0.1938	616.701	89.415	276.4	3.801	11.587
3	1.74	0.758988	0.2005	637.733	83.799	262.28	6.081	18.739
4	0.82	0.428846	0.2229	709.175	42.72	164.28	6.014	22.395
1	4.77	1.561905	0.1545	491.723	110.398	235.78	2.84	6.025
2	2.97	1.11001	0.1929	613.683	93.023	279.38	3.897	11.594
3	1.75	0.763462	0.1991	633.473	86.37	267.29	6.23	19.074
4	0.84	0.440777	0.2206	701.879	46.233	166.77	6.261	22.113
1	4.58	1.50035	0.1546	492.004	102.399	224.69	2.796	6.067
2	2.97	1.110823	0.1928	613.38	86.722	270.5	3.666	11.266
3	1.73	0.756141	0.1994	634.482	80.626	256.91	5.864	18.375
4	0.82	0.429117	0.217	690.321	42.336	153.42	5.954	20.869
1	4.7	1.5375	0.155	493.174	103.028	225.41	2.745	5.94
2	2.98	1.116382	0.1939	616.924	86.957	270.66	3.657	11.218
3	1.73	0.753022	0.1982	630.54	80.035	248.36	5.855	17.87
4	0.81	0.421931	0.2199	699.526	41.767	151.48	5.97	20.942

Height One Test Data (2 of 2)

Test Information			Background Data			
Test Name	Date	Test Description	CO (ppm)	CO_2 (ppm)	NO_x (ppm)	HC (ppm)
10	2/10/2011	Hydrogen Peroxide Solution Liquor High Flow Test Cycle Height One	13.8125	435.41	-1.052	2.4741
11	2/10/2011		14.0163	434.87	-0.799	2.3213
12	2/10/2011		13.7781	446.27	-0.779	2.2772

	Engine Data				Emissions Data			
Mode	Work (kW-hr)	Torque (kN.m)	Fuel Consump-tion (kg/kWhr)	CO_2 (g/kWhr)	Measured NO (ppm)	Measured NO_x (ppm)	NO (g/kWhr)	NO_x (g/kWhr)
1	4.66	1.526518	0.1546	491.751	102.816	211.21	2.766	5.617
2	2.97	1.111637	0.1927	613.066	79.063	260.33	3.376	10.925
3	1.73	0.755463	0.1985	631.576	72.548	229.47	5.36	16.622
4	0.83	0.432371	0.2142	681.281	33.532	130.82	4.742	17.682
1	4.58	1.499401	0.1532	487.321	99.316	211.67	2.728	5.733
2	2.97	1.112315	0.1932	614.803	84.918	255.56	3.625	10.714
3	1.73	0.753972	0.1968	626.008	75.468	227.56	5.603	16.54
4	0.81	0.422067	0.2148	683.446	31.118	124.44	4.536	17.187
1	4.62	1.510926	0.1536	488.735	98.164	211.78	2.66	5.682
2	2.98	1.11462	0.1933	614.927	82.327	256.3	3.492	10.728
3	1.74	0.760615	0.1972	627.393	73.17	227.96	5.359	16.441
4	0.81	0.423287	0.2171	690.623	33.021	128.66	4.71	17.699

Height Two Test Data (1 of 2)

Test Information			Background Data			
Test Name	Date	Test Description	CO (ppm)	CO_2 (ppm)	NO_x (ppm)	HC (ppm)
13	2/18/2011	Water Liquor High Flow Test Cycle Height Two	15.353	469.37	-1.409	2.2732
14	2/18/2011		13.0616	440.79	-1.931	2.4128
15	2/18/2011		12.6012	445.49	-1.923	2.3866
16	2/18/2011		14.1678	446.81	-1.689	2.354
17	2/18/2011		13.9348	449.08	-1.729	2.3727

	Engine Data				Emissions Data			
Mode	Work (kW-hr)	Torque (kN.m)	Fuel Consump-tion (kg/kWhr)	CO_2 (g/kWhr)	Measured NO (ppm)	Measured NO_x (ppm)	NO (g/kWhr)	NO_x (g/kWhr)
1	4.94	1.616273	0.1571	498.849	140.342	224.61	3.364	5.337
2	2.94	1.099434	0.1948	619.632	84.489	270.94	3.457	10.869
3	1.74	0.75709	0.1989	632.841	80.105	245.16	5.593	16.755
4	0.84	0.440777	0.2167	689.477	33.446	144.68	4.644	19.005
1	4.93	1.61451	0.1558	495.295	123.238	225.54	2.927	5.341
2	2.98	1.116111	0.1927	613.121	85.965	268.63	3.408	10.554
3	1.75	0.761022	0.1995	634.659	81.398	241.06	5.571	16.344
4	0.83	0.433862	0.2148	683.342	33.868	139.9	4.667	18.74
1	4.93	1.613561	0.156	496.408	100.545	231.83	2.386	5.482
2	2.96	1.107841	0.1932	614.632	93.881	272.68	3.736	10.789
3	1.75	0.764005	0.1981	630.309	86.838	244.69	5.867	16.429
4	0.81	0.423423	0.2195	698.237	35.004	137.94	4.904	18.927
1	4.94	1.6179	0.1563	496.968	120.559	231.74	2.777	5.323
2	3	1.121128	0.1913	608.643	88.184	265.82	3.378	10.11
3	1.75	0.76292	0.1971	627.072	83.197	232.82	5.474	15.204
4	0.8	0.415152	0.2228	708.748	34.417	135.28	4.925	18.917
1	4.94	1.616273	0.1552	493.931	104.999	241.94	2.387	5.478
2	2.96	1.105807	0.1933	614.911	96.333	274.07	3.68	10.404
3	1.74	0.758852	0.1969	626.406	87.04	236.42	5.671	15.299
4	0.81	0.422609	0.2124	675.8	35.585	139.21	5	19.129

Height Two Test Data (2 of 2)

Test Information			Background Data			
Test Name	Date	Test Description	CO (ppm)	CO_2 (ppm)	NO_X (ppm)	HC (ppm)
18	2/18/2011	Hydrogen Peroxide Solution Liquor High Flow Test Cycle Height Two	13.6852	426.78	-1.83	2.3535
19	2/18/2011		13.047	426.01	-1.686	2.4031
20	2/18/2011		12.8095	420.61	-1.676	2.4009
21	2/18/2011		12.9215	407.11	-1.69	2.4574

	Engine Data				Emissions Data			
Mode	Work (kW-hr)	Torque (kN.m)	Fuel Consump-tion (kg/kWhr)	CO_2 (g/kWhr)	Measured NO (ppm)	Measured NO_X (ppm)	NO (g/kWhr)	NO_X (g/kWhr)
1	2.41	0.787731	0.1531	487.191	132.871	201.95	6.142	9.309
2	2.59	0.968869	0.1942	617.989	84.128	257.02	3.622	10.949
3	1.72	0.749768	0.1965	625.024	76.667	220.54	4.993	14.198
4	0.84	0.440099	0.2135	679.3	39.087	125.91	5.321	16.718
1	4.96	1.624408	0.1547	492.161	108.413	235.9	2.396	5.182
2	2.93	1.096858	0.1923	611.712	100.902	270.05	3.793	10.073
3	1.73	0.754514	0.1977	628.855	85.512	226.87	5.482	14.404
4	0.79	0.413796	0.2162	687.775	27.565	120.95	4.049	17.09
1	4.95	1.620883	0.1552	493.881	104.309	232.7	2.293	5.096
2	2.96	1.106349	0.1936	615.957	94.186	267.88	3.49	9.867
3	1.74	0.757632	0.1969	626.521	81.897	218.35	5.194	13.753
4	0.82	0.42749	0.2148	683.139	27.371	119.99	3.864	16.452
1	4.95	1.620476	0.1558	495.812	104.078	232.89	2.279	5.087
2	2.94	1.098214	0.1915	609.267	97.47	268.96	3.63	9.976
3	1.73	0.75587	0.197	626.82	83.217	220.33	5.285	13.93
4	0.79	0.412983	0.2184	694.693	26.521	116.62	3.858	16.564

Height Three Test Data (1 of 3)

Test Information			Background Data			
Test Name	Date	Test Description	CO (ppm)	CO_2 (ppm)	NO_x (ppm)	HC (ppm)
22	3/2/2011	Water Liquor High Flow Test Cycle Height Three	12.919	1294.74	18.533	2.8727
23	3/2/2011		12.8751	2164.54	23.688	2.6057
24	3/2/2011		12.6984	394.27	0.532	2.4791
25	3/2/2011		12.6695	404.23	0.909	2.364
26	3/2/2011		14.3085	376.57	0.397	2.5248

	Engine Data				Emissions Data			
Mode	Work (kW-hr)	Torque (kN.m)	Fuel Consump-tion (kg/kWhr)	CO_2 (g/kWhr)	Measured NO (ppm)	Measured NO_x (ppm)	NO (g/kWhr)	NO_x (g/kWhr)
1	4.94	1.61668	0.1431	454.06	143.752	215.98	3.245	4.597
2	2.96	1.106214	0.1787	568.609	87.651	246.14	3.275	8.846
3	1.73	0.75248	0.1779	566.034	82.277	212.97	5.243	12.905
4	0.83	0.4321	0.1695	539.254	33.905	115.03	4.142	12.97
1	4.94	1.616409	0.1361	432.53	127.794	223.98	2.801	4.643
2	2.94	1.098757	0.1694	538.933	90.531	254.09	3.281	8.956
3	1.74	0.760615	0.1581	503.038	85.626	213.33	5.205	12.412
4	0.8	0.416508	0.1399	445.141	38.797	122.78	4.59	13.828
1	4.91	1.606918	0.1477	469.119	137.493	227.84	3.152	5.139
2	2.97	1.110281	0.19	604.481	90.586	256.82	3.472	9.612
3	1.74	0.759937	0.1946	619.01	82.514	217.91	5.413	13.909
4	0.83	0.433049	0.2137	679.921	39.281	132.32	5.52	17.555
1	4.88	1.595936	0.1473	468.531	122.456	224.02	2.795	5.047
2	2.97	1.111772	0.1893	602.259	91.943	263.36	3.453	9.731
3	1.74	0.759395	0.1932	614.745	84.886	226.07	5.526	14.447
4	0.84	0.437523	0.2081	662.047	39.746	128.68	5.417	16.866
1	4.86	1.591055	0.149	473.151	145.172	220.09	3.333	4.983
2	2.97	1.109468	0.1891	601.61	85.141	247.81	3.246	9.232
3	1.75	0.764005	0.193	614.096	80.845	219.22	5.225	13.81
4	0.85	0.442404	0.2097	667.081	37.199	127.45	5.108	16.548

Height Three Test Data (2 of 3)

Test Information			Background Data			
Test Name	Date	Test Description	CO (ppm)	CO_2 (ppm)	NO_x (ppm)	HC (ppm)
27	3/2/2011	Hydrogen Peroxide Solution Liquor High Flow Test Cycle Height Three	13.8132	411.09	0.531	2.2966
28	3/2/2011		13.7488	409.65	0.593	2.3743
29	3/2/2011		13.7614	419.22	0.634	2.325
30	3/3/2011		13.6246	367.73	0.692	-1.0661
31	3/3/2011		13.1975	379.26	0.37	-1.4181
32	3/3/2011		13.1427	385.56	0.469	2.4854

	Engine Data				Emissions Data			
Mode	Work (kW-hr)	Torque (kN.m)	Fuel Consump-tion (kg/kWhr)	CO_2 (g/kWhr)	Measured NO (ppm)	Measured NO_x (ppm)	NO (g/kWhr)	NO_x (g/kWhr)
1	4.93	1.611934	0.1470	467.877	100.266	218.33	2.285	4.862
2	2.95	1.104722	0.1899	604.119	97.974	255.68	3.752	9.561
3	1.75	0.764547	0.1921	611.257	81.759	208.83	5.333	13.22
4	0.85	0.442268	0.2031	646.132	26.233	110.07	3.732	14.306
1	4.86	1.590106	0.1479	470.409	112.209	201.21	2.593	4.555
2	2.98	1.115298	0.1887	600.363	82.99	245.25	3.164	9.096
3	1.77	0.772275	0.1898	603.953	72.381	199.05	4.687	12.468
4	0.85	0.444845	0.2068	657.856	25.467	111.2	3.614	14.398
1	4.89	1.60163	0.1483	471.948	105.505	209.58	2.416	4.716
2	2.96	1.107841	0.1881	598.437	93.815	241.38	3.571	9.012
3	1.76	0.769157	0.1913	608.694	82.905	205.67	5.356	12.985
4	0.85	0.443895	0.2058	654.803	27.806	108.06	3.852	14.006
1	4.94	1.618713	0.1495	475.35	128.965	218.08	2.84	4.755
2	2.97	1.110552	0.1891	601.712	86.767	254.77	3.215	9.315
3	1.77	0.771597	0.1927	613.039	72.076	191.91	4.515	11.818
4	0.83	0.435083	0.2088	664.302	26.528	103.7	3.71	13.869
1	4.95	1.619663	0.1496	475.648	116.607	218.76	2.585	4.791
2	2.96	1.10879	0.1891	601.743	84.127	246.92	3.122	9.016
3	1.74	0.758446	0.1913	608.677	71.956	194.64	4.609	12.218
4	0.81	0.4241	0.2095	666.428	24.516	102.24	3.568	14.041
1	4.92	1.610307	0.1483	471.694	117.031	215.97	2.588	4.724
2	2.94	1.101468	0.1893	602.181	85.527	244.14	3.208	9.024
3	1.74	0.758581	0.1915	609.116	72.649	194.02	4.639	12.165
4	0.79	0.413661	0.2165	688.621	24.446	101.6	3.612	14.242

Height Three Test Data (3 of 3)

Test Information			Background Data			
Test Name	Date	Test Description	CO (ppm)	CO_2 (ppm)	NO_x (ppm)	HC (ppm)
33	3/3/2011	Hydrogen Peroxide Solution Liquor Low Flow Test Cycle Height Three	13.17	380.94	0.325	2.4911
34	3/3/2011		12.8933	386.8	0.187	2.4973

	Engine Data				Emissions Data			
Mode	Work (kW-hr)	Torque (kN.m)	Fuel Consump-tion (kg/kWhr)	CO_2 (g/kWhr)	Measured NO (ppm)	Measured NO_x (ppm)	NO (g/kWhr)	NO_x (g/kWhr)
1	4.34	1.027305	0.1891	0.012	73.811	172.84	3.769	8.653
2	1.57	0.742311	0.2139	0.007	25.948	52.36	3.832	7.294
3	1.7	0.690384	0.2055	0.005	27.153	65.29	3.673	8.36
4	0.69	0.243505	0.2392	-0.001	11.94	49.24	4.39	16.077
1	4.34	1.027983	0.1909	607.166	74.796	173.82	3.832	8.714
2	1.58	0.748684	0.2125	675.739	24.83	49.74	3.669	6.873
3	1.69	0.687265	0.2043	649.715	23.3	60.81	3.226	7.845
4	0.69	0.24581	0.2423	770.422	8.97	46.46	3.461	15.076